VILLE KUJALA

Human Pluripotent Stem Cell Derived Cardiomyocytes

Differentiation, analysis and disease modeling

ACADEMIC DISSERTATION
To be presented, with the permission of
the board of Institute of Biomedical Technology of the University of Tampere,
for public discussion in the Jarmo Visakorpi Auditorium,
of the Arvo Building, Lääkärinkatu 1, Tampere,
on March 23rd, 2012, at 12 o'clock.

UNIVERSITY OF TAMPERE

UNIVERSITY
OF TAMPERE

ACADEMIC DISSERTATION
University of Tampere, Institute of Biomedical Technology
BioMediTech
Tampere University Hospital, Heart Center
Tampere Graduate Program in Biomedicine and Biotechnology (TGPBB)
Finland

Supervised by
Docent Katriina Aalto-Setälä
University of Tampere
Finland
FT Erja Kerkelä
University of Tampere
Finland

Reviewed by
Docent Mika Laine
University of Helsinki
Finland
Associate Professor Robert Passier
Leiden University
The Netherlands

Distribution
Bookshop TAJU
P.O. Box 617
33014 University of Tampere
Finland

Tel. +358 40 190 9800
Fax +358 3 3551 7685
taju@uta.fi
www.uta.fi/taju
http://granum.uta.fi

Cover design by
Mikko Reinikka

Acta Universitatis Tamperensis 1710
ISBN 978-951-44-8745-3 (print)
ISSN-L 1455-1616
ISSN 1455-1616

Acta Electronica Universitatis Tamperensis 1179
ISBN 978-951-44-8746-0 (pdf)
ISSN 1456-954X
http://acta.uta.fi

Tampereen Yliopistopaino Oy – Juvenes Print
Tampere 2012

To Maria with love

Abstract

Stem cell technology is an area of research that will hopefully bring new treatment options to the currently available traditional medical therapies, drug therapies and surgeries. In particular, this field brings hope of new disease and drug testing models and the potential for human spare parts. New disease models would allow for the more accurate study of major illnesses at the cellular and tissue level using cells of human origin. Pharmaceutical testing models could, in turn, provide more detailed information on the pharmacodynamic effects of medicines that are not able to be investigated using current cellular and animal models. A particularly important application area of stem cell technology are the heart muscle cells cardiomyocytes, for which there has been no human cell model, as genetic heart diseases can be fatal and because a large number of drugs cause serious cardiac side effects. Pluripotent stem cell-derived cardiomyocytes bring hope to these medical challenges.

This thesis describes the differentiation of human pluripotent stem cells into cardiomyocytes. The molecular biology of these cardiomyocytes was analyzed using several methods. The electrophysiological properties of these cells were recorded with a microelectrode array (MEA) platform, in addition to other methods, and analyzed using in-house developed software. The responses of the cardiomyocytes to various drugs were also studied using the MEA platform. Using hiPSC technology, we investigated the properties of a genetic cardiac disease, the long QT syndrome, in human cells.

This research demonstrates that human pluripotent stem cells can differentiate towards multiple cell lineages, including functional cardiomyocytes, which have spontaneous beating activity. Moreover, these cells express cardiac-specific markers, exhibit the typical electrophysiological profiles of cardiomyocytes, and respond to different pharmacological substances in a way that is characteristic of cardiomyocytes. The electrophysiological properties that were recorded with the MEA platform were robustly analyzed for different cardiac parametes using software that we developed. Correct phenotypic characteristics of the long QT syndrome could also be recapitulated in the laboratory, paving way for more in-depth future studies.

Tiivistelmä

Kantasoluteknologia on tieteenala, jonka toivotaan tuovan uusia hoitomuotoja perinteisen lääkehoidon, kirurgian ja muiden lääketieteellisten hoitomuotojen rinnalle. Erityisesti alan toivotaan tuottavan tulevaisuudessa soluperäisiä tauti- ja lääketestausmalleja sekä ihmisen varaosia. Uudet tautimallit mahdollistaisivat vaikeiden sairauksien tutkimisen solu- ja kudostasolla entistä tarkemmin ihmisperäisissä soluissa. Lääketestausmallit puolestaan voivat mahdollisesti antaa tarkempaa farmakodynaamista tietoa lääkkeiden vaikutuksista ihmisen eri solutyyppeihin, mitä ei voida tutkia nykyisillä solu- ja eläinmalleilla. Erityisen tärkeä sovelluskohde kantasolutekniikalle on sydänlihassolut eli kardiomyosyytit, joille ei ole ollut ihmisperäistä solumallia, koska geneettiset sydänsairaudet ovat pahimmillaan kuolemaan johtavia ja suuri määrä eri lääkeaineita aiheuttaa vakavia sydänperäisiä sivuoireita. Kaikkiin näihin lääketieteellisiin haasteisiin pluripotenteista kantasoluista erilaistetut kardiomyosyytit tuovat oman toivonsa.

Väitöskirjatutkimuksessani kuvataan ihmisen erittäin monikykyisten kantasolujen erilaistuminen sekä näiden rakenteiden ominaisuudet. Tutkimme myös sydänlihassolujen erilaistumista ihmisen alkion ja uudelleenohjelmoiduista kantasoluista sekä niiden molekyylibiologisia ominaisuuksia. Mikroelektrodi arraylla (MEA) nauhoitettujen kardiomyosyyttien elektrofysiologisten ominaisuuksien analysoimiseksi kehitimme oman tietokoneohjelman. Tutkimme myös kardiomyosyyttien vasteita eri lääkeaineille käyttäen hyödyksi MEA teknologiaa. Ihmisen uudelleenohjelmoituja kantasoluja käyttäen kykenimme myös tutkimaan geneettisen sydänsairauden, nimeltään pitkä QT oireyhtymä, ominaisuuksia ihmisperäisissä kardiomyosyyteissä.

Väitöskirjatutkimukseni osoittavat, että ihmisen erittäin monikykyiset kantasolut kykenevät erilaistumaan useiksi solutyypeiksi, mukaan lukien toimiviksi kardiomyosyyteiksi, jotka sykkivät spontaanisti, ilmentävät niille ominaisia merkkiaineita, omaavat niille tyypillisen elektrofysiologisen profiilin ja reagoivat niille ominaisella tavalla erilaisille lääkeaineille. Näiden kardiomyosyyttien elektrofysiologisia ominaisuuksia pystyttiin tarkaan analysoimaan hyödyntäen kehittämäämme tietokoneohjelmaa. Kykenimme myös laboratorio-oloissa onnistuneesti mallintamaan pitkä QT oireyhtymää uudelleenohjelmoiduista

kantasoluista erilaistamissamme kardiomyosyyteissä. Osoitimme, että oireyhtymän fenotyyppi on mahdollista tuottaa soluviljelyolosuhteissa.

Table of contents

List of abbreviations

α-MHC	α-myosin heavy chain
β-MHC	β-myosin heavy chain
ΔcFPD	Relative rate-corrected field potential duration
AFP	Alphafetoprotein
ANP	Atrial natriuretic peptide
ALP	Alkaline phosphatase
AP	Action potential
APD	Action potential duration
bFGF	Basic fibroblast growth factor
BMP4	Bone morphogenetic protein 4
BR	Beating rate
BSA	Bovine serum albumin
CHD	Congenital heart defect
c-MYC	c-myc myelocytomatosis viral oncogene homolog
cTNT	Cardiac troponin T
dB	Decibel
DKK1	Dickkopf homolog 1
DMSO	Dimethyl sulphoxide
EB	Embryoid body
ECG	Electrocardiogram
eGFP	Enhanced green fluorescent protein
END-2	mouse visceral endoderm –like
END-2-CM	END2 –conditioned medium
ESC	Embryonic stem cell
$ETCP_{unbound}$	Unbound effective therapeutic plasma concentration
FA	Forced aggregation
FBS	Fetal bovine serum
FHF	First heart field
Flk	Fetal liver kinase
FP	Field potential
FPD	Field potential duration
GF	Growth factor
GMP	Good manufacturing practice
HCN	Hyperpolarization activated cyclic nucleotide-gated potassium channel
hERG	Human ether-a-go-go related gene
hESC	Human embryonic stem cell
HFH	Human fetal heart
hiPSC	Human embryonic stem cell
HOP	Homeobox-only protein
hPSC	Human pluripotent stem cell
$I_{Ca,L}$	Voltage-dependent Ca^{2+} current

ICC	Immunocytochemistry
iCM	Induced cardiomyocyte
I_f	Funny current
ISH	In situ hybridization
I_{Kr}	Rapid delayed rectifier current
I_{Ks}	Slow delayed rectifier current
I_{K1}	Inward rectifying potassium current
Isl1	Islet-1
I_{to}	Transient outward potassium current
KLF4	Kruppel-like factor 4
LIN28	RNA-binding protein LIN-28
LQTS	Long QT syndrome
LQT1	Long QT syndrome type 1
LQT2	Long QT syndrome type 2
MDP	Maximum diastolic potential
MEA	Microelectrode array
MEF2	Myocyte enhancing factor 2
mESC	Mouse embryonic stem cell
MESP1	Mesoderm posterior 1 homolog
MI	Myocardial infarction
MINK	Misshapen-like kinase
miPSC	Mouse induced pluripotent stem cell
MiRP	MINK-related peptide
mRNA	Messenger ribonucleic acid
MSE	Mean square error
NANOG	Nanog homeobox
NCE	New chemical entity
NCX1	Sodium-calcium exchanger 1
NIH	United States National Institutes of Health
Nkx2.5	NK2 transcription factor related, locus 5
NRC	Neonatal rat cardiomyocyte
OCT4	Octamer-4
PBS	Phosphate-buffered saline
PFA	Paraformaldehyde
POU5F1	POU class 5 homeobox 1
PPI	Peak-to-peak interval
QTc	Heart rate –corrected QT interval
qPCR	Quantitative polymerase chain reaction
qRT-PCR	Quantitative reverse-transcriptase polymerase chain reaction
REX1	RNA exonuclease 1
RiPSC	RNA-induced pluripotent stem cell
RNA	Ribonucleic acid
ROCK	Rho-associated, coiled-coil containing protein kinase
RT	Room temperature
RT-PCR	Reverse-transcriptase polymerase chain reaction
RyR	Ryanodine receptor
SERCA	Sarcoplasmic-endoplasmic reticulum Ca^{2+} -ATPase
SSEA	Stage-specific embryonic antigen
SC	Stem cell
SCNT	Somatic cell nuclear transplantation

SD	Standard deviation
SHF	Second heart field
SNR	Signal-to-noise ratio
SNS	Secondary neurospheres
SOX2	SRY (sex determining region Y)-box 2
SRF	Serum response factor
Tbx	T-box
TdP	Torsade de pointes
TF	Transcription factor
TRA	Tumor-related antigen
VEGF	Vascular endothelial growth factor
WT	Wild-type

List of original publications

The present study is based on the following original publications, which are referred to in the text by their Roman numerals (I-IV):

I Pekkanen-Mattila M, Pelto-Huikko M, **Kujala V**, Suuronen R, Skottman H, Aalto-Setälä K, Kerkelä E. Spatial and temporal expression pattern of germ layer markers during human embryonic stem cell differentiation in embryoid bodies. Histochemistry and Cell Biology. 2010. 133 (5): 595-606.

II **Ville J. Kujala***, Zaida C. Jimenez*, Juho Väisänen, Jarno M.A. Tanskanen, Erja Kerkelä, Jari Hyttinen, Katriina Aalto-Setälä. Averaging in vitro cardiac field potential recordings obtained with microelectode arrays. Computer Methods and Programs in Biomedicine. 2011. 104 (2): 199-205. *equal contribution

III Anna L. Lahti*, **Ville J. Kujala***, Hugh Chapman, Ari-Pekka Koivisto, Mari Pekkanen-Mattila, Jari Hyttinen, Kimmo Kontula, Heikki Swan, Bruce R. Conclin, Shinya Yamanaka, Olli Silvennoinen, Katriina Aalto-Setälä. Human Disease Model for Long QT Syndrome Type 2 Using iPS Cells Demonstrates Arrhythmogenic Characteristics in Cell Culture. Disease Models and Mechanisms. 2011. First posted online November 3, 2011, doi:10.1424/dmm.008409. *equal contribution

IV **Ville J. Kujala**, Anna Lahti, Marisa Ojala, Heikki Swan, Kimmo Kontula, Katriina Aalto-Setälä. Effects of cardioactive drugs on human iPSC-derived long QT syndrome cardiomyocytes. *Submitted*.

1. Introduction

Human embryonic stem cells (hESCs) (Thomson et al., 1998) and human-induced pluripotent stem cells (hiPSCs) (Takahashi et al., 2007), collectively known as human pluripotent stem cells (hPSCs), offer an abundant source of cells that can be differentiated into multiple cell types, including cardiac cell types such as cardiomyocytes (Kehat et al., 2001; Zhang et al., 2009). This has created much hope for new therapeutic possibilities, disease modeling, and drug-testing platforms in the cardiac context. These are important issues that the current field of biomedicine is focused on resolving. Therapeutic cardiac applications of pluripotent stem cells are currently at an experimental level, but some promising advancements have been made in cardiac disease modeling (Itzhaki et al., 2011; Moretti et al., 2010b; Yazawa et al., 2011) and drug testing (Braam et al., 2010; Caspi et al., 2009; Tanaka et al., 2009; Yokoo et al., 2009) with cardiomyocytes derived from pluripotent stem cells, including some results presented in this thesis. These hPSC-derived cardiomyocytes can also serve as a valuable tool to study the developmental stages of cardiomyocyte lineage commitment and maturation (Bu et al., 2009; Moretti et al., 2010a; Pekkanen-Mattila et al., 2010b; Yang et al., 2008).

Disease modeling using hPSC-derived cardiomyocytes is important because these cells provide, for the first time, a tool to study the mechanisms of different diseases in an appropriate cellular context. Currently, other cell and animal models fail to recapitulate the relevant physiology. Primary cells obtained from heart biopsies also dedifferentiate *ex vivo*. Drug testing of new chemical entities (NCEs) during pharmacological development and preclinical testing is usually performed in animal models and with cells using heterologous expression of ion channels (ICH, 2005b). hPSC-derived cardiomyocytes offer an advantage over these systems in that they provide a proper human cellular milieu and other possible regulatory mechanisms that may modulate the response to disease and drugs.

The objective of this thesis was to investigate the embryoid body and cardiac differentiation of human embryonic stem cells and the electrophysiological properties and field potential analysis of the derived cardiomyocytes. We also sought to develop an *in vitro* cell model for long QT syndrome. Additionally, we investigated long QT syndrome type 2 (LQT2)-specific cardiomyocytes in depth as well as the drug responses of LQT1- and 2-specific cardiomyocytes.

2. Review of literature

2.1 Stem cells

2.1.1 Definition, sources and potency of stem cells

By definition, stem cells are able to self-renew and differentiate into specialized cell types. Self-renewal means that a stem cell can produce a copy of itself in a process called symmetrical division. Stem cells are also able to produce daughter cells that begin to differentiate down a specific pathway towards a certain lineage or cell type. This is called asymmetrical division (Mountford, 2008).

Stem cells can be broadly divided into four different categories according to their differentiation potency: toti-, pluri-, multi-, and unipotent stem cells (SC). Totipotent SCs are able to form all the cell types of a developing organism, including extraembryonic (i.e., placental) tissue. Totipotent cells are found during mammalian development from the fertilized zygote stage up to the eight-cell stage (Yamanaka et al., 2008). Pluripotent SCs are able to form an entire living organism, but not extraembryonic tissue. In other words, these SCs can differentiate into the cells of the three germ layers: the ecto-, meso-, and endoderm. Pluripotent SCs (PSCs) can be derived from a 4-7-day-old blastocyst-stage embryo (Thomson et al., 1998), or they can be induced from somatic cells (Takahashi and Yamanaka, 2006; Takahashi et al., 2007; Yu et al., 2007). Multipotent SCs are also called tissue-specific stem cells, meaning that these SCs reside in specific tissues and can only differentiate into cells found in that particular tissue (Yamanaka et al., 2008). Unipotent SCs can only differentiate into a single cell type; for example, germline SCs can only differentiate into germline cells (Yuan and Yamashita, 2010).

2.1.2 Human embryonic stem cells

Mouse embryonic stem cell (mESC) lines were derived 30 years ago (Evans and Kaufman, 1981; Martin, 1981), and the inner cell mass of human blastocysts was first derived and cultured *in vitro* in 1994 (Bongso et al., 1994). However, the

derivation of the first stable hESC lines in 1998 brought real hope for clinical applications when Thomson and colleagues described the derivation of five human embryonic stem cell lines from 14 isolated inner cell masses from five separate donated embryos. These cells had high telomerase activity, expressed distinct cell surface markers and retained pluripotency after 4-5 months of continuous culture (Thomson et al., 1998). The derivation of hESCs from a human blastocyst is illustrated in figure 1. hESCs are characterized mainly by the following properties: the ability to proliferate extensively *in vitro*; their expression of the pluripotency markers POU class 5 homeobox 1 (POU5F1, also known as octamer-4 [OCT3/4]), RNA exonuclease 1 (REX1), Nanog homeobox (NANOG), stage-specific embryonic antigen 3 and 4 (SSEA3 and SSEA4), tumor-related antigen (TRA)-1-60, TRA-1-81, and alkaline phosphatase (ALP); the ability to differentiate into cell types of all three germ layers; and the ability to form teratomas (Klimanskaya et al., 2008; Thomson et al., 1998). hESCs also have a high nucleus-to-cytoplasm ratio, prominent nucleoli, and high telomerase activity (Thomson et al., 1998).

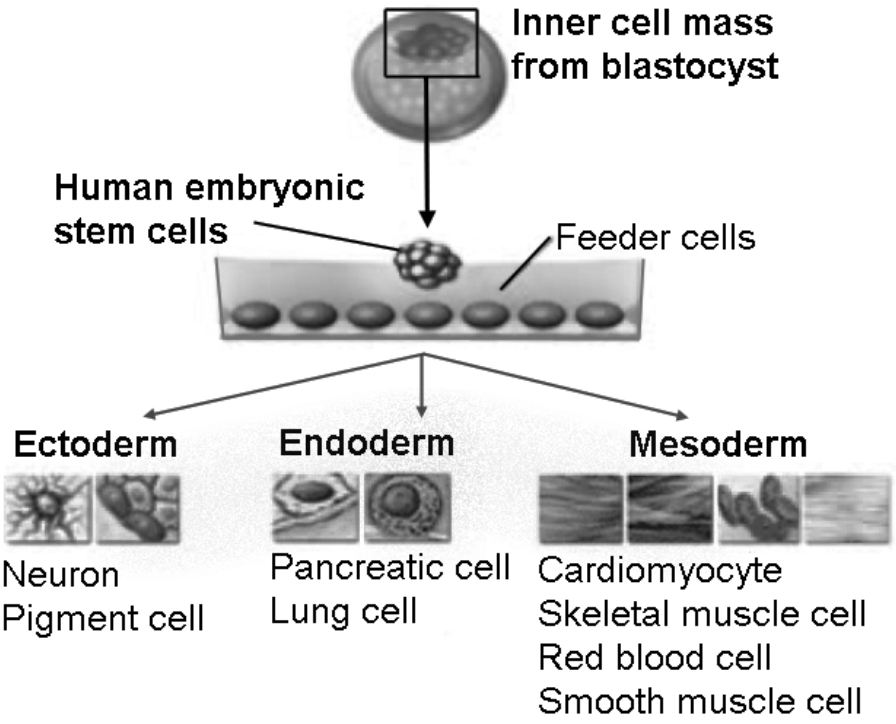

Figure 1. Derivation of pluripotent human embryonic stem cell (hESC) lines from the isolated inner cell mass (box on top). The derived hESC lines are able to differentiate into cells of all the three germ layers: the ectoderm, endoderm, and mesoderm. Figure modified from (Mountford, 2008).

2.1.3 Human induced pluripotent stem cells

The emergence of iPSC technology (figure 2) was preceded by many techniques and observations to which it owes, in part, its success. Some of the key steps include somatic cell nuclear transplantation (SCNT) (Briggs and King, 1952), the derivation of human embryonic stem cells (Thomson et al., 1998) and the observation that some transcription factors are able to change the identity of somatic cell types, which was first demonstrated by the conversion of fibroblast cells into myofibers by the retroviral expression of MyoD (Davis et al., 1987).

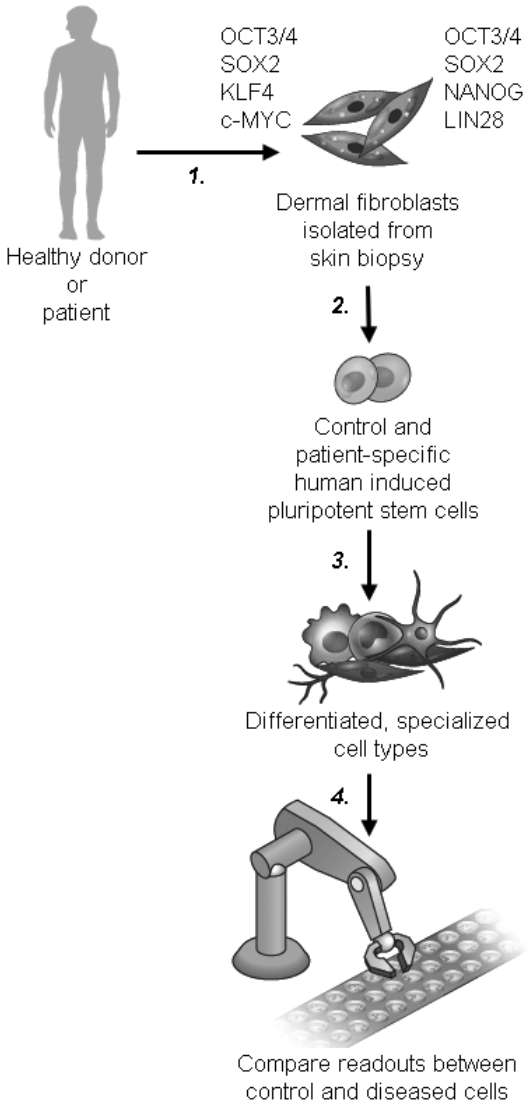

Figure 2. Somatic cell reprogramming into a pluripotent state. Two common sets of viral reprogramming factors are the "Yamanaka combination" (OCT3/4, SOX2, KLF4, and c-MYC) and the "Thomson combination" (OCT3/4, SOX2, NANOG, and LIN28), of which the former is probably more widely used. These transgenes convert differentiated somatic cells back into a pluripotent embryonic-like state. The human induced pluripotent stem cells can then differentiate into specialized cell types. This method enables the comparison of cell types between healthy individuals and patients carrying a monogenic disease, for example. Figure modified from (Passier et al., 2008).

The first cells to be successfully reprogrammed back into a pluripotent state were mouse embryonic and adult fibroblasts. This was achieved by retroviral transfection of four distinct transcription factors, namely, *Oct3/4*, SRY (sex determining region Y)-box 2 (*Sox2*), c-myc myelocytomatosis viral oncogene homolog (*c-Myc*), and Kruppel-like factor 4 (*Klf4*) (Takahashi and Yamanaka, 2006). Later, iPS cells were also generated from adult human fibroblasts using the same method (Takahashi et al., 2007) and from adult mouse liver and stomach cells. The liver and stomach cells do not appear to require retroviral integration to specific sites, which could lower the risk of tumorigenicity after transplantation to patients (Aoi et al., 2008). At the same time, human fibroblasts were also reprogrammed using another cocktail of transcription factors: *OCT3/4*, *SOX2*, *NANOG*, and the RNA-binding protein LIN-28 (*LIN28*) (Yu et al., 2007). These current iPS cell lines generated by retroviral transfection are not applicable for clinical use, however, due to potentially harmful genetic modifications. Reprogramming with excisable transposons, lentiviral vectors, transient adenoviral, episomal, plasmid vectors or recombinant proteins with cell-penetrating moieties all represent efforts to develop different reprogramming strategies (Chang et al., 2009; Kaji et al., 2009; Kim et al., 2009b; Okita et al., 2008; Stadtfeld et al., 2008; Woltjen et al., 2009; Yu et al., 2009; Zhou et al., 2009). The second major application for iPS cells after differentiation into the desired cell type is *in vitro* drug screening of drug candidates on healthy and diseased cells (Passier et al., 2008). These cells would be ideal to generate patient- and disease-specific stem cells, and the use of iPS cells circumvents the ethical issues that surround and hamper hESC research (Takahashi *et al*. 2007). The safety issues related to the reprogramming strategies do not hamper the *in vitro* disease model and drug testing development and the currently available lines can readily be used for such *in vitro* studies.

In addition, at least on one occasion, successful reprogramming has been reported without using *c-Myc*, which potentially has oncogenic properties (Nakagawa et al., 2008). However, another group has demonstrated the generation of iPS cells from adult mouse neural stem cells using only two exogenously introduced transcription factors (*OCT3/4* and either *Klf4* or *c-Myc*). This was possible because these neural stem cells already express higher endogenous levels of *Sox2* and *c-Myc* than embryonic stem cells (Kim et al., 2008). A new viral-free method of producing hiPSCs uses synthetic RNA, which can reprogram fibroblasts upon transfection (Warren et al., 2010; Yakubov et al., 2010). These reprogrammed cells are called RNA-iPSCs (RiPSCs) and can be generated using mRNAs for the OCT3/4, SOX2, NANOG, and LIN28 reprogramming factors (Yakubov et al.,

2010) or for the KLF4, c-MYC, OCT3/4, and SOX2 transcription factors (Warren et al., 2010).

2.1.3.1 Challenges with induced pluripotent stem cells

Although hiPSCs are a potential tool for pharmacological and toxicological testing and for regenerative medicine in the future, currently there are still many obstacles to overcome. For instance, the question of how similar hiPSCs truly are to hESCs still remains unanswered. Although hiPSCs pass the standards required of hPSCs (Takahashi et al., 2007; Yu et al., 2007), a recent study suggests that these cells have aberrant epigenetic reprogramming in specific genomic hotspots (Lister et al., 2011). Reprogrammed hiPSCs appear to retain some somatic cell DNA methylation patterns along with hiPSC-specific methylation patterns (Lister et al., 2011). Another study found that hiPSCs can harbor aneuploidies, especially the duplication of chromosome 12 (Mayshar et al., 2010). Guenther and colleagues compared the chromatin structure and gene expression pattern of hESCs to hiPSCs and found some variations between them; however, they concluded that these variations were not enough to distinguish between the two pluripotent cell types (Guenther et al., 2010). Cardiomyocytes, that are differentiated from hiPSCs and hESCs, however, appear to possess similar global transcriptomes (Gupta et al., 2010).

2.2 Cardiomyogenesis and pluripotent stem cells

2.2.1 Heart development and regulation

In spite of intensive research on the molecular mechanisms of the developing heart, the chamber-specific gene expression underlying the spatiotemporal regulation within the heart remains largely unclear, although considerable success has been made recently to identify key cardiac commitment steps in heart formation (Chien et al., 2008; Musunuru et al., 2010; Nemer, 2008).

The heart is the first organ to develop in vertebrates (Buckingham et al., 2005). The mesodermal cardiac progenitors arise from two distinct fields: the first and second heart fields (FHF and SHF, respectively). Studies in mice have shown that the FHF contributes to both atria, the ventricles, and the atrioventricular canal (Meilhac et al., 2004). The SHF contributes to the outflow tract and the right ventricle (Domian et al., 2009; Meilhac et al., 2004) as well as the atrio-ventricular

canal and both atria (Meilhac et al., 2004); this includes all regions except the left ventricle. Table I summarizes some of the key proteins regulating cardiac differentiation, which are discussed below.

Table I. Key proteins regulating cardiac differentiation and the cell types in which they are expressed.

Protein	*Class*	*Expressed in*	*Reference*
Nkx2.5	Homeobox transcription factor	Cardiac precursor cells	(Anton et al., 2007)
Isl1	T-box transcription factor	Transiently in secondary heart field precursors	(Kattman et al., 2007)
GATA4	GATA family of zinc-finger transcription factor	Cardiac precursor cells	(Nemer, 2008)
Mef2c	MADS-box transcription factor	Cardiac precursor cells	(Lin et al., 1997)
Tbx5	T-box transcription factor	Heart and upper limbs	(Bruneau et al., 2001)
Flk1 (Kdr)	Receptor tyrosine kinase	Mesodermal cell populations	(Anton et al., 2007)

One of the earliest markers expressed in developing cardiac cells is NK2 transcription factor-related, locus 5 (Nkx2.5) (Abu-Issa and Kirby, 2007; Anton et al., 2007; Chen and Fishman, 2000; Kattman et al., 2007; Musunuru et al., 2010; Zhou et al., 2008). Nkx2.5 is an NK-class homeodomain-containing protein, which binds DNA trough its homeodomain by forming a homodimer at its DNA binding sites. After Nkx2.5 is bound to DNA, it is phosphorylated by casein kinase II (CKII), thereby increasing its DNA binding affinity. Nkx2.5 interacts with many transcription factors (TFs), which include GATA-4, serum response factor (SRF), T-box 5, T-box 2, T-box 20, hand1/hand2, and Foxh1. Genes whose expression is regulated by Nkx2.5 include atrial natriuretic peptide (ANP), cardiac alpha actin, A1 adenosine receptor, calreticulin, connexin 40, sodium-calcium exchanger 1 (NCX1), endothelin-converting enzyme-1, homeobox-only protein (HOP), and myocardin (Abu-Issa and Kirby, 2007). Nkx2.5 is essential for appropriate heart formation (Kattman et al., 2007), and mutations in this gene can cause atrial and ventricular septal and outflow tract defects, cardiomyopathy, valvular abnormalities, tetralogy of Fallot, hypoplastic left heart, and arrhythmias (Musunuru et al., 2010). *Nkx2.5*-deficient mice die at embryonic day 9.5 (E9.5) due to an abnormal morphogenesis of the outflow and inflow components of the heart tube (Abu-Issa and Kirby, 2007). Heart formation in *Nkx2.5*-deficient mice is not necessarily compromised, however, because beating cardiomyocytes are still present and other NK2 homeobox

transcription factors may compensate for the lack of Nkx2.5 (Abu-Issa and Kirby, 2007; Nemer, 2008). Clearly, Nkx2.5 is important in establishing the ventricular gene expression program and septal morphogenesis and it works via combinatorial interactions with other cardiac regulators (Nemer, 2008). These target genes encode structural and transcriptional regulators that confer characteristic cardiomyocyte features (Abu-Issa and Kirby, 2007).

Islet-1 (Isl1) is a basic helix-loop-helix LIM-homeodomain T-box transcription factor that is expressed by the SHF. Cardiogenic progenitors transiently express Isl1 in addition to Nkx2.5. However, Isl1 is not expressed in terminally differentiated cardiomyocytes, unlike Nkx2.5 (Musunuru et al., 2010). $Isl1^+$ progenitors develop into cardiomyocytes, smooth muscle and endothelial cells. *Isl1*-deficient mice lack SHF derivatives, resulting in the absence of the outflow tract, the right ventricle, and some atrial portions (Anton et al., 2007; Kattman et al., 2007; Srivastava, 2006). Zhou *et al.* (2008) identified a $Wt1^+$ precursor cell population that resides in the epicardium. These $Wt1^+$ proepicardial cells arise from progenitors that also express Isl1 and Nkx2.5, indicating that these cells share a developmental origin with these multipotent $Nkx2.5^+$ and $Isl1^+$ progenitors.

GATA-4, -5, and -6 belong to the GATA TF-family (which, in turn, belongs to the zinc finger superfamily) and bind the same DNA sequence, (A/G)GATA(A/T). These three TFs are expressed in the gut epithelium, the precardiac mesoderm, and heart regions overlapping with Nkx2.5 expression (Kattman et al., 2007; Peterkin et al., 2007). In addition, these factors may be involved in the initiation of Nkx2.5 expression (Abu-Issa and Kirby, 2007). GATA-5 is mainly expressed in endocardial cells, and GATA-6 is expressed in myocardial and vascular smooth muscle cells. GATA-4 is expressed in cardiac progenitor cells, regulates the expression of more than 30 cardiac promoters, and interacts with other TFs to regulate cardiac differentiation. The importance of GATA-4 is evident from the presence of congenital heart defects (CHDs) in mice and humans with GATA-4 haploinsufficiency (Nemer, 2008), which include atrial, septal and ventricular defects and tetralogy of Fallot (Musunuru et al., 2010). *Gata-4* null mouse embryos have fewer cardiomyocytes and their bilateral heart primordia fail to fuse, causing a condition known as cardiac bifida. *GATA-4*-negative ESCs, however, are able to form cardiomyocytes (Chen and Fishman, 2000).

The myocyte enhancing factor 2 (MEF2) family of proteins is also involved in cardiomyocyte and vascular cell differentiation (Ieda et al., 2010; Nemer, 2008). These proteins bind an A/T-rich regulatory sequence found on multiple skeletal muscle promoters (Lin et al., 1997). GATA TFs also recruit MEF2 proteins to their

target genes. MEF2 proteins are transcribed from four genes and the different isoforms are produced by alternative splicing (Nemer, 2008).

The T-box (Tbx) family of proteins comprises more than 20 members in mammals. These developmental regulators share a conserved 180 amino acid region responsible for the DNA binding T-domain. Holt-Oram syndrome, characterized by heart and upper limb abnormalities, is caused by a mutation in the *Tbx5* gene; a finding that implicated Tbx proteins as regulators of heart development. Dominant-negative Tbx proteins interfere with heart development in *Xenopus* as well. Tbx5 proteins work in cooperation with the Nkx2.5 transcription factor and mutations in either gene can lead to the same cardiac abnormalities (Nemer, 2008). *Tbx5* mutant mice also harbor defects in the inflow-regions of the heart and develop left ventricular hypoplasia, which leaves the left ventricle underdeveloped. Other T-box TF family members have also been implicated in vertebrate heart development, including Tbx1-4, -18, and -20. Tbx2 and -20 are thought to regulate chamber identity in the developing heart (Kattman et al., 2007). The transduction of mouse fibroblasts with Tbx5 and the aforementioned Gata4 and Mef2c converts these fibroblasts into cardiomyocytes, further illustrating their importance in the adoption of the cardiomyocyte fate in the transdifferentation process (Ieda et al., 2010).

Fetal liver kinase (Flk)-1 is a marker for early cardiac progenitor cells and for smooth muscle, hematopoietic, and endothelial cells (Anton et al., 2007). This protein is expressed in multipotent cardiovascular progenitor cells of the SHF with Isl1 and Nkx2.5 (Musunuru et al., 2010). Flk-1 encodes endothelial growth factor receptor-2 and is expressed in different mesodermal subpopulations (Kattman et al., 2007).

Notch signaling regulates the differentiation of cardiac muscle and conduction cells in ventricles (Chau et al., 2006). Humans have four Notch receptors: Notch-1 to -4. These receptors have five ligands: delta-like-1, -3, -4 and Jagged-1, and -2. Notch signaling suppresses cardiac differentiation, and the activation of Notch signaling in *Xenopus* decreases myocardial gene expression in early heart field crescent cells. Notch signaling also inhibits cardiac differentiation in the chick embryo. Conversely, the inhibition of Notch signaling promotes myogenic cell fate in *Drosophila* (Pedrazzini, 2007). Notch-1 mutations in humans are related to valvular abnormalities and tetralogy of Fallot (Musunuru et al., 2010). Notch1 activation in mice leads to abnormal cardiogenesis characterized by atrioventricular canal and ventricular deformities. Mutations in genes related to Notch signaling pathways can also cause cardiac abnormalities like pericardial edema, cardiac cushion and valve defects, as well as atrial and ventricular septal defects. These

genes include *Jagged-1*, *Hesr1/Hey1*, *Hesr2/Hey2*, and *mind bomb* (Chau et al., 2006).

With regard to these studies, it must be noted that the most common model organism used in research to understand the genetic regulation of heart formation is the mouse. Interpreting the results must, therefore, be performed with great care to avoid erroneous extrapolations to human conditions. For instance, one study found myosin light chain (MLC)-2a, -1v, and atrial natriuretic factor (ANF) expression to be essentially chamber-restricted in mice by mid-gestation; however, in humans, there was a broader distribution, and in addition, MLC-2v was more restricted to the ventricles in humans than in mice (Chuva de Sousa Lopes et al., 2006). This study highlights the importance of careful interpretation of results obtained from different species.

2.2.2 Cardiomyocyte differentiation of human pluripotent stem cells

Human PSCs (hPSCs) provide a renewable cell supply and can be differentiated into cardiomyocytes quite rapidly, usually in approximately 20 days or under. There are multiple cardiac differentiation methods, which all share common challenges, namely heterogeneity of the derivative cell population and low differentiation efficiency. The variation in the differentiation efficiency between hESC lines is in part due to their intrinsic cardiomyogenic propensities (Osafune et al., 2008; Pekkanen-Mattila et al., 2009). Figure 3 represents the cardiac diffentiation of hPSCs.

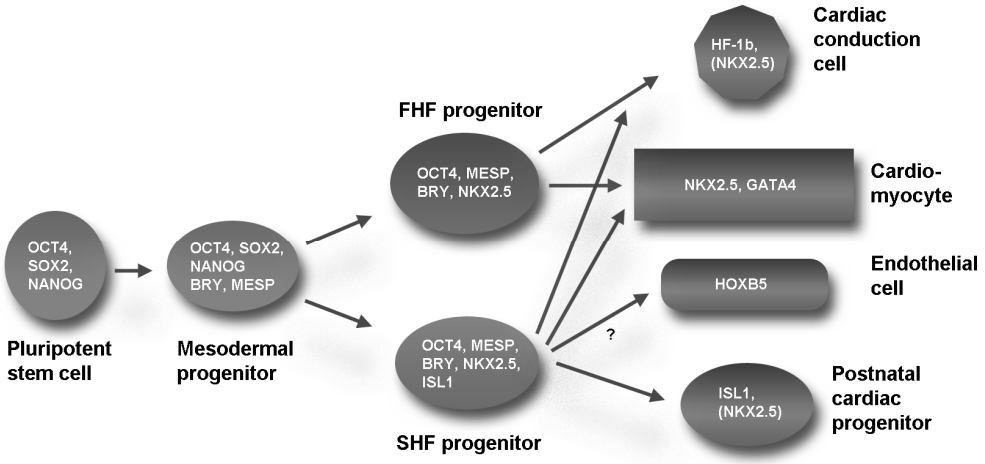

Figure 3. A cartoon of cardiac differentiation of pluripotent stem cells. Pluripotent stem cells express the pluripotency markers OCT3/4, SOX2, and NANOG. Differentiating cardiomyogenic cells express cardiac markers such as ISL1, NKX2.5, and GATA4. FHF: first heart field, SHF: second heart field. NKX2.5 in parentheses indicates that it is not expressed in all the cells. The gene expression data were partially adapted from (Srivastava and Ivey, 2006).

The embryoid body (EB) differentiation method is a conventional way to derive cells from hESCs (Passier and Mummery, 2005). In this method, EBs are allowed to form by dissociating the hESC colonies into smaller pieces and culturing them in suspension to initiate the differentiation process. These differentiating EBs are subsequently plated and allowed to grow in adherent culture. The first hESC-derived cardiomyocytes (hESC-CMs) were described a decade ago, three years after the establishment of the first stable hESC lines (Kehat et al., 2001). This method relied on the EB method to produce cells with phenotypic properties of cardiomyocytes. The authors reported that 8.1% of the EBs generated spontaneously beating areas, which expressed cardiac-specific marker genes and transcription factors, showed myofibrillar organization, stained positively for cardiac proteins, showed distinct electrograms, and showed the type of drug response expected of cardiac cells (Kehat et al., 2001). Other groups have also successfully used this method to derive cardiomyocytes from hESCs (Andersson et al., 2010; Kattman et al., 2011; Kim et al., 2009a; Norstrom et al., 2006; Synnergren et al., 2008) and hiPSCs (Kattman et al., 2011; Yokoo et al., 2009; Zhang et al., 2009; Zwi et al., 2009b). Forced aggregation (FA) is another approach to produce EBs that are more consistent in size. With this method, hESC colonies are dissociated into single cells and plated onto v-shaped bottom 96-well plates to facilitate cell aggregation with centrifugation (Burridge et al., 2007).

Due to the relative inconsistency of the EB method among different hESC lines, other techniques may be more desirable for cardiomyocyte production. The first effort to provide a more robust method of cardiac differentiation was to co-culture

hESCs with mouse visceral endoderm–like (END-2) cells. These END-2 cells guide hESCs towards the endoderm and mesoderm (Beqqali et al., 2006; Mummery et al., 2003; Passier et al., 2005). Cardiomyocytes originate from the mesoderm, but endodermal cues are critical in heart formation (Lough and Sugi, 2000). END-2 cells therefore induce hESCs to adopt a cardiomyocyte fate by providing these endodermal cues for differentiation (Mummery et al., 2003). This method relies on using a 20% fetal calf serum (FCS)-containing medium. However, the cardiomyogenic effectiveness can be increased 24-fold by omitting FCS from the culture medium and by an additional 40% by adding ascorbic acid (commonly known as vitamin C) to the culture medium (Passier et al., 2005). The addition of SB203580, a p38 MAP kinase-specific inhibitor, can also induce greater than 20% of the differentiating cells to adopt a cardiomyocyte fate in the END-2 co-cultures. Furthermore, SB203580 increases the total cell number, resulting in an overall yield of cardiomyocytes 2,5-fold higher than in serum-free END2 co-cultures alone (Graichen et al., 2007). Serum-free culture medium conditioned with the soluble factors secreted by END-2 cells can also be used for hESC-CM production (Braam et al., 2008). One likely mechanism of action for increased cardiomyogenesis with END2-conditioned medium (END2-CM) might be that the conditioning clears insulin, which can inhibit cardiomyogenesis, from the cell culture media (Xu et al., 2008). The same level of cardiac differentiation can be achieved with synthetic insulin-free medium supplemented with prostaglandin I2, which is also an abundant compound in END2-CM (Xu et al., 2008). This synthetic medium represents a step towards a good manufacturing practice (GMP) level of cardiomyocyte production.

Cardiomyocyte differentiation of hPSCs can be enhanced with specific growth factors (GFs). Activin A and bone morphogenetic protein 4 (BMP4) were shown to induce greater than 30% cardiac differentiation of hESCs when activin A was used for the first 24 h to initiate differentiation and BMP4 exposure was then used over the next four days (Laflamme et al., 2007). Further optimization of the activin A and BMP4 conditions can yield highly enriched hESC-CM populations, as was noted in a recent study reporting that the differentiating EBs consisted of 58% $cTNT^{+}$ cells at most (Kattman et al., 2011). Using a more intricate combination of multiple growth factors, including basic fibroblast growth factor (bFGF), vascular endothelial growth factor (VEGF), and dickkopf homolog 1 (DKK1), as well as activin A and BMP4, an approximately 50% cardiomyocyte differentiation efficiency can be achieved. In this case, growth factors were used for two weeks in a more complex sequence that more accurately mimicked embryonic heart development (Yang et al., 2008).

2.2.3 Properties of pluripotent stem cell-derived cardiomyocytes

One of the first signs of *in vitro* cardiomyocyte development is the appearance of spontaneously beating foci (Kehat et al., 2002; Mummery et al., 2003). The beating frequencies of the hESC-CMs differ among the foci (Asp et al., 2010). Beqqali and co-workers investigated the transcriptional regulation of developing hESC-CMs and found several genes that were upregulated during the first 12 days of development in END2 co-cultures. In this study, the group used DNA microarray analysis, quantitative polymerase chain reaction (qPCR), and *in situ* hybridization (ISH) to study gene expression in undifferentiated hESCs, hESC-CMs and the human fetal heart (HFH). During hESC-CM differentiation, several genes were up-regulated at the mRNA level, including many non-cardiac genes. The gene expression pattern reflected early embryonic events; the first genes to be up-regulated were primary mesodermal, followed by cardiac progenitor-associated genes and those expressed in fetal cardiomyocytes. The cardiomyocyte-enriched genes included troponin C (slow), actinin (α2), myosin light chain 2, and cardiac troponin T2 (Beqqali et al., 2006).

Synnergren and colleagues also investigated gene expression during the cardiomyocyte development of hESCs. In this study, microarray technology was used to investigate the global mRNA expression profile of hESC-CM clusters, and these profiles were compared with undifferentiated hESCs. The comparison revealed 520 up-regulated and 40 down-regulated genes in hESC-CMs. Up-regulated genes in cardiomyocytes were classified according to their Gene Ontology annotation. Several of the genes belonged to a “biological process” category. These genes were involved in mesoderm development, muscle development, striated muscle contraction, and the regulation of muscle contraction. Several genes also encoded cellular components, such as the troponin complex, striated muscle thin filament, the myosin complex, actin filament, and contractile fiber. The annotations for the up-regulated genes in the differentiated cardiomyocytes were associated with cardiomyocytes and cardiac development (Synnergren et al., 2008).

hESC-CM differentiation is characterized by the expression of specific genes and proteins. The expression of the mesodermal marker Brachyury T is upregulated during early phases of cardiogenesis and its expression peaks on the third day in END-2 co-cultures (Beqqali et al., 2006; Pekkanen-Mattila et al., 2009) and on the fourth day in differentiating EBs (Bettiol et al., 2007; Pekkanen-Mattila et al., 2010b). Cardiomyocyte differentiation is also characterized by the upregulated expression of cardiac TFs, including the mesoderm posterior 1 homolog (MESP1), ISL-1, GATA-4, and NKX2.5 (Graichen et al., 2008; Yang et al., 2008). The mRNA expression of *NKX2.5* and cardiac muscle actin is higher in hESC-CMs than in

human heart samples, according to one study (Asp et al., 2010). Over time, however, *NKX2.5* expression in developing hESC-CMs drops close to that of human heart samples. Cardiac troponin T (cTNT) is expressed at higher levels in hESC-CMs and ventricular heart samples compard to the atria. In hESC-CMs, cTNT mRNA expression ultimately declines as well (Asp et al., 2010). Phospholamban (a calcium [Ca^{2+}] ion pump) is expressed at lower levels in hESC-CMs and human atrial samples than in the ventricle. The cardiac structural protein α-myosin heavy chain (α-MHC) is more highly expressed in fast-beating hESC-CMs that have a beating rate of more than 50 beats per minute and atrial samples. The expression of this protein also increases in hESC-CMs as they age. In contrast, a related cardiac structural component, β-MHC, is expressed at higher levels in human ventricular samples. The mRNA expression of the potassium (K^+) ion channel coding human ether-a-go-go-related gene (*hERG*) in hESC-CMs resembles that of neonatal and adult atrial samples. According to that study, it seems the difference between hESC-CMs with slow or fast beating frequencies parallels the difference between human atrial and ventricular tissues, respectively (Asp et al., 2010).

With regard to structural features, developing hESC-CMs have an isotropic myobibrillar organization at early stages. Clear sarcomeric A, I, and Z bands develop later (Kehat et al., 2001; Pekkanen-Mattila et al., 2009; Snir et al., 2003), along with the development of structural proteins such as troponin I, T or C, myosins, and α-actinin (Kehat et al., 2001; Mummery et al., 2003). hESC-CMs also express desmosomes and gap junctions that facilitate coupling to neighboring cells (Kehat et al., 2001; Pekkanen-Mattila et al., 2009; Snir et al., 2003).

2.2.4 Ways to improve cardiomyogenesis of pluripotent stem cells

Proper cardiomyocyte differentiation and maturation may need more coaxing than just using END-2 co-culturing or GFs. Indeed, the oxygen concentration and mechanical stimulation have important roles in coaxing hESC-CMs. The oxygen tension of the cell cultures can guide hESC-CM differentiation. Under hypoxic conditions (i.e., 4% oxygen tension), the cardiomyocyte yield has been reported to be higher than in normoxic conditions (21% oxygen tension). Under hypoxia, the cell-fold expansion at day 16 was also reported to be significantly higher compared to under normoxia. These experiments were performed in dynamic hESC cultures with different kinds of bioreactors. Such conditions yielded at most 30% contracting EBs (Niebruegge et al., 2008). An essential point of these studies was that the cardiomyocyte yield and cell-fold expansion was greater under these conditions than

in traditional static cultures. Physical strain can also positively influence the generation of cardiomyocytes, at least from mouse ES cells (Gwak et al., 2008), cardiac progenitor cells harvested from mice and bone marrow stromal cells (Forte et al., 2008). Micrometer-scale surface topography in conjunction with biphasic electrical stimulation can also enhance cardiomyocyte morphology in neonatal rat cardiomyocytes (NRCs) (Heidi Au et al., 2009).

Another way to enrich the proportional number of cardiomyocytes in culture is through selection with fluorescence-activated cell sorting (FACS) after heterogenous differentiation. After sorting, the purified hESC-CM populations can be subcultured as a more homogenous population. Murine ESC-CMs have been successfully subcultured after CXCR4/FLK-1 double-positive selection with FACS. The cardiomyocyte properties of the differentiated ES cells were determined by immunocytochemical staining against cardiac nuclear TFs, cardiac alpha actinin and the presence of beating foci in approximately 40% of the double positive cells clusters (Nelson et al., 2008). Knocking in a reporter gene such as enhanced green fluorescent protein (eGFP) under a cardiac-specific promoter sequence is another way to select cardiomyocytes from hESC derivates. Huber and colleagues created a transgenic hESC line by knocking in eGFP under the myosin light chain-2V promoter sequence. This method allowed eGFP-expressing cardiomyocytes to be selected and subcultured using positive selection with FACS. The sorted cardiac subpopulations retained greater than 95% purity and 85% viability. The cells also expressed cardiac-specific proteins in immunostaining studies, had electrophysiological properties characteristic of cardiomyocytes as detected by microelectrode array and patch clamp studies, and integrated into host rat myocardium (Huber et al., 2007). Lentiviral vector-based drug resistance selection of cardiomyocytes has also been successfully used to purify these cells from other hESC derivatives (Kita-Matsuo et al., 2009).

2.3 Electrophysiology of cardiomyocytes

2.3.1 Electrophysiological aspects of human cardiomyocyte differentiation

The electrical properties of cardiomyocytes have been investigated using either patch clamp analysis of single cells (Hamill et al., 1981; Sakmann and Neher, 1984; Zilberter et al., 1982) or a microelectrode array (MEA) platform with beating cellular aggregates (Kehat et al., 2002; Reppel et al., 2004; Reppel et al., 2005). The

MEA platform is discussed in greater detail later in this thesis. Using the patch clamp method, ion channels in excitable membranes can be studied by attaching a recording electrode pipette to the cell membrane. A so-called gigaohm seal is formed between the cell membrane and the recording electrode. The membrane located within the electrode tip is subsequently removed by suction or perforation, thereby establishing an electrical circuit allowing for the measurement of current and voltage changes across the cell membrane.

The main ions involved in the cardiac action potential are sodium (Na^+), Ca^{2+}, and K^+ cations. Some key cardiac ion channel types involved in the human ventricular action potential (AP) have been identified with patch clamp. These channels include (respective currents in brackets) $Na_{V1.5}$ (I_{Na}), $K_{V4.3}$ (I_{to}), $Ca_{V1.2}$ ($I_{Ca,L}$) $K_{V11.1}$ (I_{Kr}), $K_{V7.1}$ (I_{Ks}), and $K_{ir2.X}$ (I_{K1}) (Pollard et al., 2010). Ion channels mediate the complex interaction between the currents, resulting in a characteristic AP shape. The cardiac AP can be divided into five distinct phases (0-4) shown in figure 4. Phase 0 is a membrane potential depolarization from negative to positive, called the upstroke. Phase 1 is a short transient repolarization, which ends in phase 2, the plateau. The AP plateaus at a slightly less positive membrane potential than the peak of the upstroke and is more pronounced in ventricular cardiomyocytes. Phase 3 is the repolarization back to the resting membrane potential. The resting phase is phase 4 (Nerbonne and Kass, 2005). Na^+, Ca^{2+}, and K^+ cations work in different phases of this cycle. Na^+ affects phase 0 depolarization. Ca^{2+} works in phase 2 and 3 to mediate cardiac contractions by binding to troponin C. K^+ mediates repolarization in phase 3.

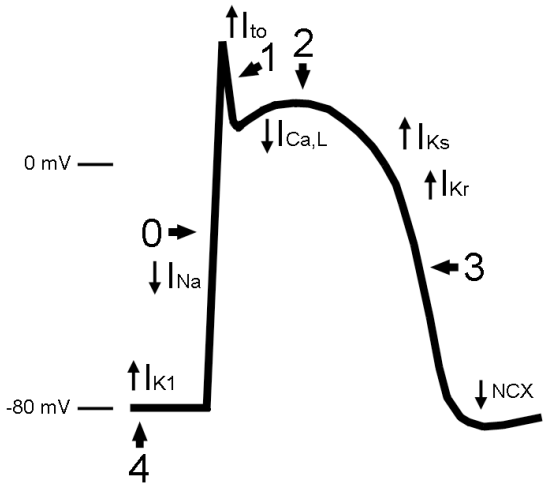

Figure 4. A schematic of a ventricular cardiac action potential. Some key currents (small arrows) during each phase (0-4) of the action potential are represented. Downward arrow: inward current, upward arrow: outward current. The different phases are indicated by the larger arrows: 0) upstroke, 1) transient repolarization, 2) plateau, 3) final repolarization, and 4) resting phase.

The cardiac action potentials in humans and rodents differ in the way they express ion currents and hence in their electrophysiological properties. To study the development of currents in human cardiomyocytes, Sartiani and colleagues investigated multiple ion channels and their respective current expression in hESCs and their early- (15 to 40 days old) and late-stage (50 to 110 days old) cardiomyocyte derivatives during their differentiation using the patch clamp technique (Sartiani et al., 2007). I_{Kr}, I_f, $I_{ca,L}$ currents could be readily recorded from hESCs. During cardiomyocyte development, new currents (I_{to} and I_{K1}) were also detectable, indicating cardiac maturation (Sartiani et al., 2007).

mRNA levels of the two isoforms $K_{v1.4}$ and $K_{v4.3}$, mediating transient outward K^+-current (I_{to}), were differentially expressed in developing cardiomyocytes. The longer splice variant ($K_{v1.4}$) was expressed in the early (25-day-old) cardiomyocytes, and the shorter variant ($K_{v4.3}$) was expressed in cardiomyocytes more than 57 days old. $K_{v4.3}$ mRNA was also expressed in hESCs, but no I_{to} current could be recorded. I_{to} current was detected on day 12 of differentiation in developing hESC-CMs, and the current density grew higher in later-stage cardiomyocytes (Sartiani et al., 2007).

An important repolarizing current in cardiomyocytes is the rapid component of the delayed rectifying K^+ current (I_{Kr}) mediated by the *hERG* channel. I_{Kr} is expressed in hESCs and developing cardiomyocytes, according to Sartiani and colleagues. The presence of I_{Kr} in undifferentiated hESCs was deduced from the fact that an outward K^+-current sensitive to a compound called E-4031, which selectively blocks I_{Kr} current, could be recorded from the cells. The shorter splice variant mRNA (*HERG1b*), however, was expressed only in the hESC-CMs (Sartiani et al., 2007). The hERG current is a dominant factor in determining cardiac AP repolarization and hence its blockade by a multitude of drugs alters the K^+ efflux (Pollard et al., 2010).

Hyperpolarization-activated cyclic nucleotide-gated potassium channel (HCN) isoforms encode the depolarizing funny current (I_f). *HCN1* and *HCN4* are more strongly expressed in hESCs and early stage cardiomyocytes than in late-stage cardiomyocytes (Sartiani et al., 2007). *HCN4* is also expressed at higher levels in hESC-CMs that have fast beating rates (Asp et al., 2010). According to Sartiani and colleagues, the *HCN4* isoform is expressed in the adult heart, but *HCN1* is not. *HCN2* is expressed in all of these relevant systems: hESCs, early- and late-stage hESC-CMs, and the adult heart. I_f current was detected using the voltage clamp mode in hESCs and early- and late-stage developing cardiomyocytes. However, during maturation there is a reduction in the I_f current activation rate (Sartiani et al., 2007).

Inward rectifying K^+-current (I_{K1}) is mediated by the $K_{ir2.1}$ channel. However, $K_{ir2.1}$ mRNA was already present in hESCs, while no current was present. The I_{K1} current could only be detected in developing cardiomyocytes (Sartiani et al., 2007).

Voltage-dependent Ca^{2+}-current ($I_{Ca,L}$) is mediated by the α1C subunit of the Ca^{2+}-channel in many tissues and is encoded by the *CACNA1C* gene. *CACNA1C* mRNA is expressed in hESCs and hESC-CMs, and $I_{Ca,L}$ current is also present in both of these cells (Sartiani et al., 2007).

In terms of AP properties during hESC-CM development, the upstroke velocity (dV/dt) and AP duration (APD) increase markedly upon cardiac maturation. In contrast, the beating rate decreases during maturation and the diastolic depolarization rate flattens in late-stage cardiomyocytes. Pharmacological tests have demonstrated intact ion channel function: expected responses were achieved using E-4031, $BaCl_2$ (I_{K1} blocker), zatebradine (I_f blocker), and lacidipine ($I_{Ca,L}$ blocker). Challenging hESC-CMs with isoproterenol also demonstrated intact β-adrenergic signaling (Sartiani et al., 2007).

These in-depth results reported by Sartiani and colleagues and other groups indicate that hESC-CMs mature towards the cardiomyocyte phenotype *in vitro* and that the emergence of I_{to} and I_{K1} currents might serve as positive markers of cardiac differentiation (Sartiani et al., 2007). I_{to} current has also been shown to increase in postnatal rat cardiomyocytes (Guo et al., 1996; Shimoni et al., 1997). In contrast, I_{K1} stabilizes the myocytes diastolic potential (Silva and Rudy, 2003).

Compared to the END2 coculture method, the EB method produces cardiomyocytes that have a more consistent beating rate, ventricular type APs, and a significantly more hyperpolarized maximum diastolic potential (MDP) (Pekkanen-Mattila et al., 2010a). Low I_{K1} current seems to be responsible for the low MDP of developing hESC-CMs (Sartiani et al., 2007). The upstroke velocities (dV/dt) of the cardiomyocytes produced with either method, however, do not appear to differ (Pekkanen-Mattila et al., 2010a).

Dolnikov and colleagues studied the mechanical function of hESC-CMs. The authors found hESC-CMs to have a negative force-frequency relationship. In the mature human myocardium, this relationship is positive. Moreover, blockade of the ryanodine receptor (RyR) or the sarcoplasmic-endoplasmic reticulum Ca^{2+}-ATPase (SERCA) did not affect hESC-CM contraction, as it would in mature cardiomyocytes. Further, stimulation with caffeine did not increase the hESC-CMs intracellular Ca^{2+} concentration (Dolnikov et al., 2005). These results are indicative of immature sarcoplasmic reticulum (a critical structure in intracellular Ca^{2+} storage) development in hESC-CMs. Consequent studies have nonetheless documented the

caffeine-induced release of intracellular Ca^{2+} in hESC and hiPSC-derived cardiac cells (Itzhaki et al., 2011; Satin et al., 2008).

Overall, these results indicate that hPSC-derived cardiomyocytes are functional and provide optimism for their potential use in basic and translational cardiac research applications.

2.3.2 Cardiac field potentials and the microelectrode array

Cardiomyocytes can be studied in cell culture conditions using a microelectrode array (MEA) platform (Kehat et al., 2001; Meyer et al., 2004; Reppel et al., 2004). This platform consists of an MEA chip, which has a cell culture well and electrodes for recording electrical activity, an MEA amplifier, a filter amplifier, a heater controller and a data acquisition computer. A portable version of this setup is presented in figure 5.

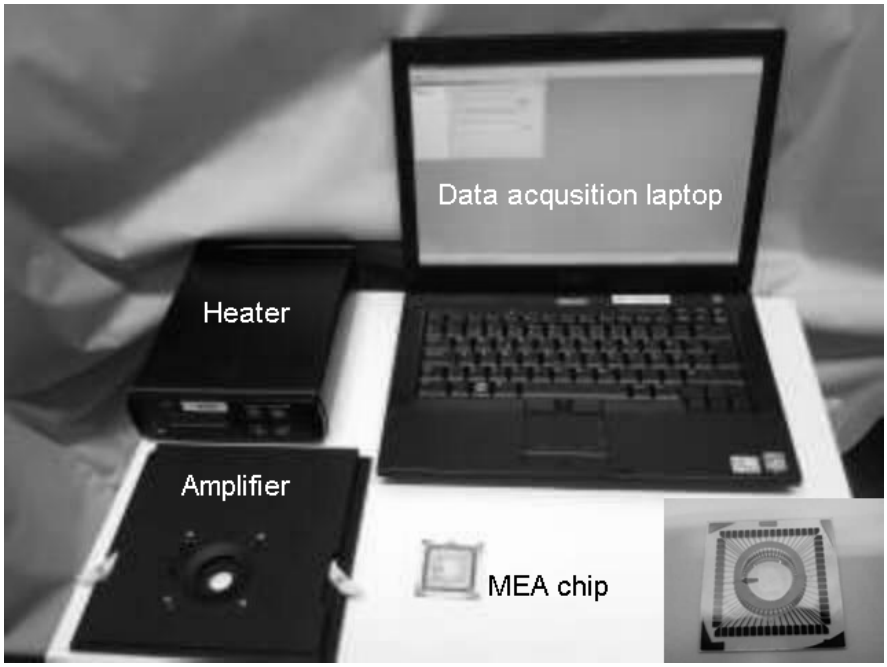

Figure 5. A portable USB-MEA setup depicting the MEA chip (see also inset lower right corner), the amplifier, the heater controller and the data acquisition laptop.

This system allows the changes in the field potential (FP) of cardiomyocytes to be recorded (Reppel et al., 2004). A characteristic field potential recording from hESC-CMs is shown in figure 6. The cardiomyocytes are plated on MEA chips in cell-culture wells. On the bottom of each cell-culture well, there are recording electrodes and, depending on the chip type, an internal reference electrode. Some of the MEA chips are fabricated without internal reference electrodes, in which case an external

reference is needed. MEA chips are manufactured with many electrode configurations, each suitable for a different application. The standard MEA (MEA 200/30iR-Ti-gr) has 59 recording electrodes in an eight-by-eight array (with four electrodes missing, one from each corner). This technique allows for high spatiotemporal resolution FP measurements of electrically active cells, including spontaneously beating cardiomyocytes derived from hPSCs. Temporal resolution is provided by fast sampling frequencies of up to 50 kHz, enough to capture the fast activating components of the cardiac cycle, namely, the depolarizing Na^+ peak. Another MEA chip type is the so-called 6-well MEA (6wellMEA200/30-iR-Ti-mr), in which the cell culture well is divided into six separate areas, each with its own reference electrode and nine individual recording electrodes. The main advantage of this type is that it can accommodate six different cell populations at once.

Figure 6. Field potential trace recorded from human embryonic stem cell–derived cardiomyocytes using a microelectrode array. This trace represents only one recording electrode.

Cardiomyocytes of various origins have been investigated with MEAs. Some of the first recordings were carried out with isolated chick cardiomyocytes (Meyer et al., 2004) and mESC-CMs (Reppel et al., 2007). These cardiomyocytes, however, are not a very relevant model for studying human heart development. Mouse models are more frequently used in the preclinical testing phase of drug development, but with respect to human cardiac electrophysiology, they still make for a suboptimal model. Neonatal rat cardiomyocytes (NRCs) have been used for MEA experiments as well (Berdondini et al., 2005). None of these cardiomyocyte types fully capture the intricacy of the human cardiomyocyte physiology. Human primary cardiomyocytes are difficult to obtain and culture; thus, to study human electrophysiology, researchers have relied on hESC-CMs. These cells provide the appropriate electrophysiological network to study human conditions. The identical genome of hESC-CMs affords a more reliable comparison of results to NRCs. In addition,

hiPSCs have been used to derive cardiomyocytes, which have been studied using MEA (Itzhaki et al., 2011; Mehta et al., 2011).

2.3.2.1 Cardiac field potential parameters

Cardiac FPs have a definitive morphology if the cardiomyocytes are plated as monolayers on the MEA. For example, isolated neonatal rat cardiomyocytes (NRCs) and chick cardiomyocytes can have defined interexperimental FP properties, and in some cases, hESC-CMs do as well, as shown in figure 7. In addition to the peak-to-peak interval (PPI, which is measured as the time between two individual FP peaks), from which the beating rate can also be calculated (see equation 1), the two most important FP parameters are the amplitude and the FP duration (FPD). *In vitro* FPD measurements can be used as a surrogate for the clinical QT interval and are usually measured as the time between the initial deflection and the return to baseline (i.e., the isoelectric point, see figure 7) (Caspi et al., 2009).

$$BR = \frac{60}{PPI} \tag{1}$$

where BR is the beating rate in beats per minute and PPI is the peak-to-peak interval in seconds.

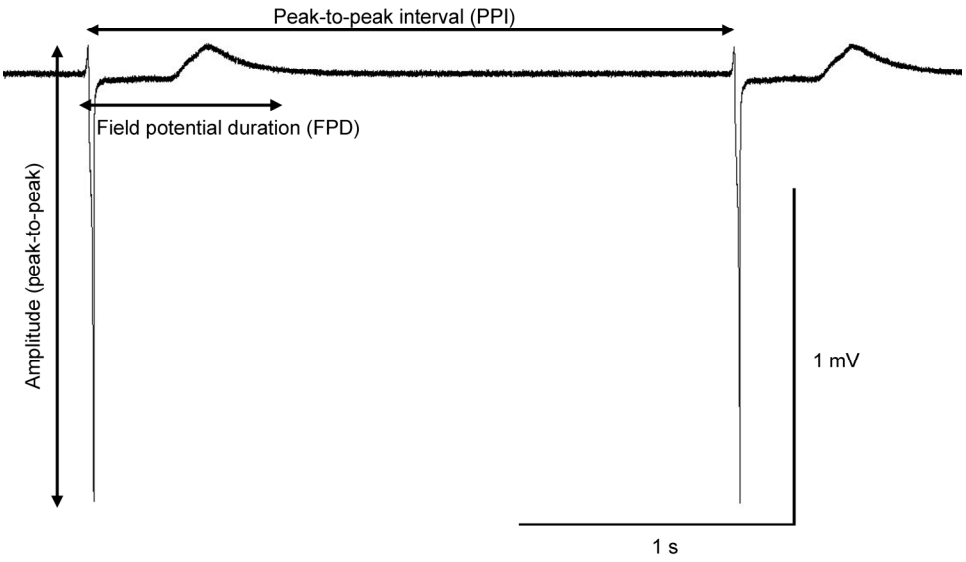

Figure 7. The cardiac field potential (FP) of human embryonic stem cell-derived cardiomyocytes and the nomenclature of FP components. The nomenclature data (with modifications) is from (Reppel et al., 2004).

2.3.2.2 Signal analysis

MEA FP recordings from the three-dimensional cardiomyocyte aggregates exhibit more variation in signal shape between recordings and also between different electrodes. This phenomenon is due to the three-dimensional structure of the cardiomyocyte aggregates. The orientation of these aggregates on the MEAs cannot be controlled, which presents a challenge for generating robust software algorithms for the analysis of cardiac FP properties.

High-quality FP recordings can also be difficult to acquire at times, particularly with hPSC-derived cardiomyocytes, as the signal quality can be limited by the low amount of differentiated cardiomyocytes in the beating hESC-CM foci. Irregular beating rhythms can present a challenge in analyzing the signals as well (Pekkanen-Mattila et al., 2010a). Acquiring clear high-quality signals is important in determining the cardiac FP components, particularly the return to baseline. A higher signal-to-noise ratio (SNR) indicates a higher signal quality.

Programs like MEA-tools have been developed for signal analysis. This program was developed by Ulrich Egert and colleagues for multielectrode data analysis but is a MATLAB (Mathworks, Inc.) toolbox that requires the software to run (Egert et al., 2002). Custom-made MATLAB toolboxes are also widely used for MEA analysis (Bussek et al., 2009; Halbach et al., 2006; Hannes et al., 2008; Liang et al., 2010; Reppel et al., 2005). FPD measurements have also been performed by an independent operator (Caspi et al., 2009).

2.4 Pluripotent stem cell–derived cardiomyocytes and drug testing

Over the years, many cardiac and non-cardiac drugs have been withdrawn from the market due to their adverse cardiac side effects. Although every new chemical entity (NCE) is tested according to set requirements, during the course of drug development, unexpected effects such as syncope (fainting), arrhythmia, a specific polymorphic ventricular tachycardia known as Torsade de pointes (TdP), and even sudden death are sometimes observed when a drug is already approved and on the market (Lexchin, 2005; Redfern et al., 2003a; Roden, 2004). Pharmaceutical regulatory authorities, namely the International Conference on Harmonisation (ICH), have specified and expanded the requirements for drug safety testing. This now includes tests to be performed using two different mammalian (a rodent and a

non-rodent) species. Required tests include electrocardiogram (ECG) recordings and histological examination of cardiac tissue (EMEA, 2008; ICH, 2005a; ICH, 2005b).

The QT interval (figure 8), as seen on the ECG recordings, is the cornerstone for assessing the proarrhythmic potential of NCEs (ICH, 2005a; ICH, 2005b). The QT interval marks the length of the ventricular repolarization time in the heart. Prolongation of the QT interval can lead to life-threatening arrhythmias such as TdP (Redfern et al., 2003b). Many drugs can prolong the QT interval (Fenichel et al., 2004; Roden, 2004), making this the leading cause for drug use restrictions and withdrawal from the marketplace (Roden, 2004). ICH has a defined evaluation of this risk as a standard preclinical process for all NCEs (Bode and Olejniczak, 2002; Cavero and Crumb, 2005).

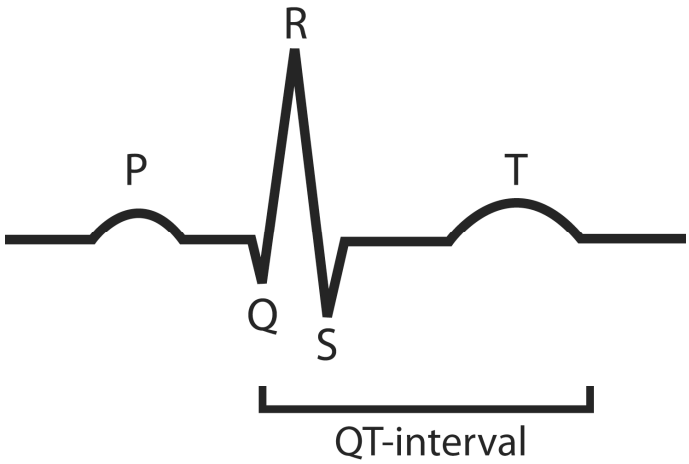

Figure 8. A cartoon of an elecrocardiogram trace. The different peaks and the QT interval are depicted.

The inhibition of the hERG channel ($K_{V11.1}$) is the predominant basis for drug-induced QT-interval prolongation and TdP (Carlsson, 2006; Pollard et al., 2008). Pharmaceutical companies utilize many different preclinical assays and models to assess the risks of NCEs (Miyazaki et al., 2005). These assays include *in vivo* studies such as ECG telemetry with conscious dogs (Finlayson et al., 2004; Martin et al., 2004), *in vitro* assays such as a repolarization assay that detects APD changes in isolated animal Purkinje fibers, papillary muscles or cardiomyocytes, the hERG assay in which I_{Kr} current is expressed in heterologous expression systems like CHO or HEK293 cells, or the characterization of the native I_{Kr} current (Lu et al., 2008; Redfern et al., 2003a). These methods, however, are not necessarily sufficient (Braam et al., 2010; Mandenius et al., 2011) and can be very costly; in addition, the large number of required animal tests raises ethical concerns. Consequently, a human cardiomyocyte-based preclinical *in vitro* assay is needed for NCE testing. Cardiomyocytes derived from hPSCs can potentially serve the pharmaceutical industry for compound screening, target validation, and safety testing. These

cardiomyocytes can be produced from an unlimited cell source and could serve as a reproducible human model system. Further, cardiomyocytes can be used in conjunction with MEAs for a medium throughput readout of electrophysiological responses, such as the prolongation of repolarization (Caspi et al., 2009; Liang et al., 2010; Reppel et al., 2005).

Multicellular cardiac syncythia and their repolarization can be studied using MEAs. Thus, drug effects on cardiac repolarization can be investigated using this platform (Reppel et al., 2005). Caspi and colleagues studied drug effects on hESC-CMs using MEAs. The E-4031 compound blocks the I_{Kr} repolarizing current in cardiomyocytes, which was observed as cardiac FP prolongation in an *in vitro* electrocardiogram recorded with MEA. The authors also demonstrated a dose-dependent prolongation of FP duration (FPD) with escalating E-4031 concentrations. Sotalol is a class III antiarrhythmic agent, quinidine and procainamide are both class IA antiarrhythmic agents and cisapride is a gastrointestinal prokinetic drug that was withdrawn from market due to QT-interval prolongation. All of these substances caused FPD prolongation that was detected in MEA recordings (Caspi et al., 2009).

Braam and co-workers also investigated the FPD prolongation potential of multiple drugs using hESC-CMs in conjunction with MEA (Braam et al., 2010), examining 12 different drugs in total. Sodium, calcium and *HERG* potassium channel blockade with lidocaine, nifidipine, and E-4031, respectively, had effects on FPD, as expected. Quinidine and sotalol are both known to prolong cardiac repolarization in patients. These substances increased the FPD at concentrations slightly over the unbound effective therapeutic plasma concentration ($ETCP_{unbound}$) range. FPD prolongation with these drugs occurred at concentrations further from the $ETCP_{unbound}$ range. FPD could be reliably measured despite the variable FP shapes produced by hESC-CMs. (Braam et al., 2010). This study provided FPD data on many drugs over a high range of concentrations using hESC-CMs as a human cardiac model system.

2.5 Long QT syndrome

2.5.1 Acquired and congenital long QT syndrome

Long QT syndrome (LQTS) is mainly characterized by prolonged ventricular repolarization in individuals. The condition is observed as an abnormally long QT

interval on ECG, as discussed above, and is associated with an increased risk of the life-threatening arrhythmia known as TdP (see above). LQTS can be congenital or acquired. So far, 12 different congenital LQTS subtypes (LQT1-12) have been identified, and each one is caused by a mutation in a specific gene (Hedley et al., 2009). Acquired LQTS usually results from drug therapy, hypokalemia, or hypomagnesemia.

Some drugs have the undesired side effect of prolonging the QT interval as discussed above, thus resulting in acquired LQTS. This is caused by the ability of some drugs to block the hERG K^+-channel trans-membrane pore. The hERG channel's S6 trans-membrane domain, which forms the K^+ permeable pore in the tetrameric form, is pharmacologically vulnerable due to its atypical amino acid sequence in comparison to other ion channels. Although QT prolongation, caused by hERG pore blockade, might not be harmful, it is nonetheless associated with TdP. Naturally, this has an effect on the safety of drugs. Because of their tendency to prolong the QT interval, several drugs have been withdrawn from the market or their use has been restricted with warning labels, resulting in the loss of commercial value. The early drug discovery process aims to optimize compound efficacy, pharmacokinetics, and safety to patients (Pollard et al., 2010). In this context, hPSC-derived cardiomyocytes could be used in early preclinical compound safety assays to minimize this risk of QT prolongation.

The overall prevalence of the genetic form of LQTS in the general population is estimated to be as high as 1:2,000 (Hedley et al., 2009; van Noord et al., 2010). Of the different subtypes, LQT1 is caused by a mutation in the *KCNQ1* gene (Hedley et al., 2009) and LQT2 is caused by a mutation in the *hERG* gene (also known as *KCNH2*) (Curran et al., 1995; Hedley et al., 2009). Symptoms in LQT1 patients are triggered mainly by stress or exercise and in LQT2 patients by emotional stress or auditory stimuli accompanied by a reduced heart rate (van Noord et al., 2010). Specific types of mutations are enriched in both of these genes in Finland and these are known as founder mutations, causing approximately 73% of all LQTS cases in Finland. These founder mutations are named KCNQ1-FinA, KCNQ1-FinB, HERG-FinA, and HERG-FinB; all of these mutations impair the outward K^+ efflux in cardiomyocytes during the cardiac repolarization phase (Fodstad et al., 2006; Zareba, 2007). LQT1 impairs the slow component of the delayed rectifying K^+ current (I_{Ks}), whereas LQT2 impairs the I_{Kr} current (Fodstad et al., 2004). The KCNQ1-FinA founder mutation (studied in this thesis) is caused by a G589D missense mutation near the C-terminus of the *KCNQ1* gene, after the S6 domain. All the mutation carriers have mean QTc times of 457 ms and the KCNQ1-FinA carriers have corresponding mean times of 492 ms. On the other hand hERG-FinB (the other

founder mutation studied in this thesis) is caused by a R176W missense mutation in the proteins' N-terminus, close to the Per-Arnt-Sim (PAS) domain. Mutations in the PAS domain result in altered hERG channel-gating kinetics, which, in this case, is seen as an accelerated deactivation of the ion channel. This accelerated deactivation results in reduced K^+ efflux during repolarizations and hence prolongs the QT interval. hERG-FinB mutation carrier patients have QTc times with a mean of 448 ms (Fodstad et al., 2006). In the Finnish population, this mutation is estimated to be present in every one out of 400 individuals (Marjamaa et al., 2009b). The mean QTc of the se mutation carriers' unaffected relatives is 417 ms (Fodstad et al., 2004).

Having two recessive disease-causing alleles (also known as compound heterozygote) can cause severe cases of LQTS, where the patient has very long QTc times and is more likely to suffer cardiac events and cardiac arrest (Westenskow et al., 2004).

2.5.2 Modeling long QT syndrome with patient-specific induced pluripotent stem cell–derived cardiomyocytes

The potential to reprogram somatic cells into hiPSCs and subsequently differentiate them into cardiomyocytes creates a splendid *in vitro* opportunity for studying molecular interactions in LQTS. Modeling congenital LQTS is a pressing task for the biomedical field, and in addition to results presented in this dissertation, only three studies have reported LQTS modeling using hiPSC technology. The first report focused on LQT1 (Moretti et al., 2010b) and the second two on LQT2 (Itzhaki et al., 2011; Matsa et al., 2011).

Moretti and colleagues reprogrammed *KCNQ1* (R190Q) mutant pluripotent stem cells from fibroblasts of two family members with LQT1. The group subsequently differentiated cardiomyocytes from hiPSCs. These cardiomyocytes possessed the LQT1 genotype and had prolonged APD as seen in single-cell patch-clamp recordings. The AP prolongation was determined to be caused by an ion-channel trafficking defect resulting in a 70-80% I_{Ks} current density reduction. The group also noted altered activation and deactivation kinetics of the ion channel and demonstrated increased arrhythmogenicity with isoproterenol (a β-adrenergic agonist), which was rescued by β-blockade (Moretti et al., 2010b).

Itzhaki and colleagues had similar findings with LQT2, using *hERG* (A614V) missense-mutated hiPSC-CMs derived from a patient with severe LQT2. The patient had previously presented with episodes of TdP. The LQT2-cardiomyocytes derived from the patient's hiPSCs demonstrated increased arrhythmogenicity that was associated with early after depolarizations (EADs). These cells also had significant

APD prolongation due to a reduced I_{Kr} current density (Itzhaki et al., 2011). Matsa and colleagues also produced LQT2-cardiomyocytes from patient-specific hiPSCs with a *hERG* (G1681A) mutation. Exposing these LQT2-cardiomyocytes to E-4031 caused EADs and arrhythmia. In another study, isoproterenol treatment led to EADs that were reversed by β-blockade (Matsa et al., 2011).

Other cardiac-related diseases have been also modeled using hiPSC-CMs, including Timothy syndrome. Timothy syndrome is caused by a mutation in *CACNA1C*. This gene encodes the $Ca_V1.2$ Ca^{2+} channel; therefore, cardiomyocytes carrying a mutation in this gene have excessive Ca^{2+} influx and hence abnormal calcium transients and irregular contractions, and they exhibit AP prolongation (Yazawa et al., 2011).

These reports support the idea that disease modeling *in vitro* in the cardiac context is feasible. These human cell models allow thorough analysis of the cellular signaling pathways and molecular interactions that occur in the pathological state. Because these cells are also patient-specific, they provide the necessary human genome in which to study the diseased state.

3. Aims of the study

The aim of the first study (I) was to investigate the growth and propensity of cardiomyocyte differentiation among eight different hESC lines. More importantly, the aim was to study spatiotemporal germ layer marker expression in developing embryoid bodies at the protein level using novel tissue microarray technology, as most studies have relied on marker profiles at the mRNA level.

In the second study (II), our aim was to develop analysis software based on averaging the cardiac field potential signals that were recorded from neonatal rat cardiomyocytes and human embryonic stem cell-derived cardiomyocytes with microelectrode arrays. Using this new software, our aim was to investigate the effects and feasibility of averaging the recorded field potential signals for downstream analysis of cardiac FP parameters, such as field potential duration and peak-to-peak interval.

In the third study (III), we sought to develop a patient-specific cell model based on long QT syndrome type 2 (LQT2), using induced pluripotent stem cell technology. Using this cell model, our aim was to recapitulate the electrophysiological phenotype of LQT2 *in vitro* and to validate this method for further studies.

In the fourth (IV) study, we used the induced pluripotent stem cell technology developed in the third study (III) to expand the investigations to also include LQTS type 1. Using these patient-specific cardiomyocytes that have mutations for LQT1 and -2, we performed a series of drug tests to determine whether the responses of these LQTS cardiomyocytes differed from those of control cardiomyocytes.

4. Materials and methods

4.1 Ethical approval (I-IV)

The Institute of Biomedical Technology has permission (1426/32/300/05) to conduct research on hESCs from the National Authority for Medicolegal Affairs. The ethical committee of Pirkanmaa Hospital District has granted the Institute of Biomedical Technology permission for the derivation, culturing, characterization, and differentiation of hESC lines (R05116) and iPS cell lines (Aalto-Setälä R08070). Regarding the HS hESCs, the Karolinska Institute has approval for the derivation, characterization and differentiation of hESCs from the ethics committee of the Karolinska Institute. All of the embryos used were surplus embryos that were donated by couples after both partners provided informed consent. The couples received no monetary compensation.

4.2 Culture of primary and other cell types (III, IV)

Culture medium for the primary fibroblasts obtained from skin biopsies for hiPSC induction was composed of Dulbecco's Modified Eagle Medium (DMEM, Lonza, Switzerland) supplemented with 10 % fetal bovine serum (FBS, Lonza), 2 mM L-glutamine, and 50 U/mL penicillin/streptomycin. The medium for commercial 293FT cells (Invitrogen, Carlsbad, CA, USA) was additionally supplemented with 1% non-essential amino acids (NEAA, Cambrex, NJ, USA). Mouse embryonic fibroblasts (MEF, Millipore, MA, USA) and Plat-E cells were cultured without penicillin/streptomycin.

4.3 Establishment of induced pluripotent stem cell lines (III, IV)

The primary fibroblasts for hiPSC induction were obtained from skin biopsies donated by healthy volunteers and patients diagnosed with either LQT1 or LQT2.

Control (from healthy subjects) and patient-specific (from patients with a confirmed mutation predisposing them to LQTS) hiPSC lines were induced from primary fibroblasts using lentiviral and subsequent retroviral infections. This was achieved using 293FT and Plat-E cells as packaging cells along with the following plasmids and reagents: pLenti6/UbC/mSlc7a1-vector (Addgene, Cambridge, MA, USA), ViraPower packaging mix (Invitrogen), Lipofectamine 2000 (Invitrogen), pMX retroviral vector (with hOCT3/4/3, hSOX2, hKLF4, or hc-MYC, Addgene), and Fugene (Roche Diagnostics, Mannheim, Germany). The hiPSC lines were induced as described previously (Takahashi et al., 2007).

H7 hESCs and hiPSC lines UTA.01006.WT (hereafter called WTa), UTA.00112.hFF (WTb), and FiPS 6-14 (derived at University of Helsinki, kindly provided by Prof. Timo Otonkoski) were used as controls. UTA.00208.LQT1 (LQT1a) and UTA.00313.LQT1 (LQT1b) were used as patient-specific hiPSCs with a KCNQ1-FinA (G589D) mutation. UTA.00514.LQT2 (LQT2a) and UTA.00525.LQT2 (LQT2b) were used as patient-specific cells lines, which had a hERG-FinB (R176W) mutation. Both mutations were detected by PCR.

4.3.1 Karyotype and teratoma formation analysis (III, IV)

Karyotypes of the cell lines were defined using standard G-banding chromosome analysis by a commercial company (Medix laboratories, Espoo, Finland), according to standard procedures. For teratoma formation, hiPS cells were injected into nude mice testis capsules. Tumor samples were collected 8 weeks after injection and fixed with 4 % paraformaldehyde (PFA). The sections were stained with haematoxylin and eosin.

4.4 Stem cell culture (I-IV)

The human embryonic stem cell (hESC) lines Regea 06/015 and Regea 06/040 derived at the Regea Institute for Regenerative Medicine (University of Tampere, Finland) and HS181, HS293, HS346, HS360, HS362 and HS401 derived at Karolinska University Hospital, Huddinge (Karolinska Institute, Stockholm, Sweden) were cultured as follows: commercially available human foreskin fibroblast cells (CRL-2429, ATCC, Manassas, VA, USA) were used as feeder cells for hESCs. The hESCs were passaged mechanically. The hESC culture medium consisted of knockout DMEM (Invitrogen, Carlsbad, CA, USA), 20% serum

replacement (SR) (Invitrogen), 2 mM GlutaMax (Invitrogen), 1% NEAA (Cambrex Bio Science Inc., Walkersville, MD, USA), 50 U/mL penicillin/streptomycin (Cambrex Bio Science Inc.), 0.1 mM 2-mercaptoethanol (Invitrogen), and 8 ng/mL basic fibroblast growth factor (bFGF) (R&D Systems, Minneapolis, MN, USA). Colonies were passaged mechanically on a weekly basis. The undifferentiated state of the colonies was confirmed daily by morphologic analysis, and periodic testing for the expression of the stem cell markers NANOG, POU5F1, SSEA4, and TRA-1-60 was carried out. The differentiation ability of the lines has been tested in vivo and in vitro.

H7 hESCs (WiCell) and established control and patient-specific hiPSCs were cultured on mitomycin C-inactivated mouse embryonic fibroblasts (MEF) in hES medium, which consisted of DMEM/F-12 (Invitrogen) supplemented with 20% knockout serum replacement (KO-SR) (Invitrogen), 1% nonessential amino acids (Lonza), 2 mM L-glutamine (Glutamax, Invitrogen), 50 U/ml penicillin/streptomycin (Lonza), 0.1 mM beta mercaptoethanol (Invitrogen), and 7.8 or 4 ng/ml basic fibroblast growth factor (R&D Systems). The medium was refreshed daily, and the hESC colonies were passaged onto a new MEF layer once a week using 1 mg/ml collagenase IV (Invitrogen).

4.5 Cardiomycoyte differentiation (I-IV)

4.5.1 Embryoid body formation and cardiac differentiation (I)

EB formation was performed by mechanically excising undifferentiated hESC colonies into small pieces and placing them on a U-shaped low attachment 96-well plate (Nunc, Roskilde, Denmark) (one piece per well) in EB-medium consisting of Knockout DMEM (KO DMEM) (Gibco Invitrogen, USA) supplemented with 20% fetal bovine serum (FBS) (Gibco Invitrogen, USA), 1% non-essential amino acids (Cambrex BioSciences, Verviers, Belgium), 1% L-glutamine (Invitrogen, USA), and 50 U/ml penicillin/streptomycin (Cambrex BioSciences, Verviers, Belgium). The hESC colonies were cut and detached in the same way as with the normal passaging of hESCs; however, the pieces were cut larger (one cell colony into 2-4 pieces). For each hESC line, three individual 96-well plates were prepared: one for immunocytological analysis (2-12 days) and two for determining growth and differentiation. EBs were cultured on the 96-well plates for 7 days and were subsequently plated onto 0.1% gelatin type A-coated (Sigma-Aldrich, Germany)

Nunclon™ D surface 12-well plates (Nunc) in EB medium. A total of eight EBs were transferred from the 96-well plate to each 12-well plate well. The EBs were allowed to adhere. Medium was refreshed three times per week. Cultures were checked daily for formation of beating foci under a phase contrast microscope (Olympus, Tokyo, Japan). Cells were grown on 12-well plates for up to six weeks before they were further analyzed or discarded. Additional EBs were collected from the Regea 06/015 and Regea 06/040 lines for western blotting and qRT-PCR. Thirty-day-old beating foci were collected from some of the lines for immunocytochemistry. The cardiomyocyte differentiation efficiency was calculated as a percentage of beating areas per plated EB on each plate. Efficiency was calculated for each plate and the mean value was calculated from two individual plates for each cell line. The standard deviation for the differentiation efficiency of each cell line was calculated between the differentiation efficiency percentages of each plate. EB formation was also performed using forced aggregation (FA) (Burridge et al., 2007). In this method, undifferentiated hESC colonies were dissociated into single cells enzymatically with tryple and collagenase IV (Gibco) or by Accutase (Millipore), and 3,000–15,000 cells/well were plated in EB medium on untreated V-shaped 96-well plates (Nunc) and centrifuged for 5 min at 950 *g*. EBs formed on the bottom of the wells were transferred to a 0.1% gelatin type A-coated (Sigma-Aldrich) Nunclon™ D surface 12-well plate (Nunc) in EB-medium after 4–7 days of culturing.

The hiPSC EBs were cultured in EB-medium (KO-DMEM with 20 % FBS, NEAA, L-glutamine and penicillin/streptomycin) without bFGF for 5 weeks. The expressions of the ectodermal, endodermal, and mesodermal markers were determined using RT-PCR.

4.5.2 Co-culture with mouse visceral endoderm–like cells (II-IV)

Cardiomyocyte differentiation was carried out by co-culturing hESCs and hiPSCs with mouse visceral endodermal-like (END-2) cells, which were a kind gift from Professor Mummery (Humbrecht Institute, Utrecht, The Netherlands). END-2 cells were cultured as described previously (Mummery et al., 1991). Briefly, to initiate cardiomyocyte differentiation, undifferentiated hESC colonies were dissected mechanically into small aggregates and plated on mitomycin C-treated END-2 cells in hESC medium without serum, serum replacement, or bFGF (Mummery et al., 2003). Differentiating cell colonies were monitored with phase-contrast microscopy, and medium was changed on days 5, 8, and 12 onto the co-cultures. After two weeks, 10% SR was added to the medium.

4.6 EB morphology and size analysis (I)

The growth and morphology of plated hESCs were examined daily with phase contrast microscopy. Pictures were taken from ten plated EBs, and the sizes were determined from the pictures during the suspension phase (7 days from the start of the differentiation protocol). EBs diameters and cross-sectional areas were measured from the pictures with Cell^D imaging software (Olympus Soft Imaging Solutions GmbH, Japan). The overall EB size for each cell line and each day was determined from the mean value of ten EBs.

4.7 Immunocytochemical analysis (I, III, IV)

For immunocytochemical (ICC) staining, undifferentiated hESC colonies from the Regea 06/015 and Regea 06/040 lines were fixed with 4% paraformaldehyde for 20 min and stained as previously described (Pekkanen-Mattila et al., 2009). Antibodies included anti-OCT3/4 (1:300, R&D Systems, Minneapolis, MN, USA), anti-Brachyury T (1:100, Abcam, Cambridge, UK), anti-alphafetoprotein (AFP) and anti-SOX1 (both 1:100 and both from Santa Cruz Biotech, Santa Cruz, CA, USA). The time series of developing EBs for immunocytochemical staining was 2, 4, 6, 8, 10 and 12 days (n=8), and these cells were fixed with 4% PFA for 2 h. Older EBs with and without beating foci were prepared for immunocytochemistry as well. Samples were cryoprotected with 20% sucrose in phosphate-buffered saline (PBS) for several days. A tissue 10% agarose gel (Biowhittaker Molecular Applications, Rockland, ME, USA) multiarray was prepared with 1-mm holes as originally developed by Pelto-Huikko (Parvinen et al. 1992). 400 EBs were individually transferred into the wells filled with OCT compound. The multiarray was frozen on dry ice, and 6-lm frozen sections were cut throughout the chuck and thaw mounted on Polysine glass slides (Menzel, Braunschweig, Germany). Sections were stored at -70°C until use. Immunocytochemistry was performed using the N-Histofine simple stain MAX PO staining method (Nichirei Biosciences Inc., Tokyo, Japan). Antibodies used were mouse anti-OCT3/4 (1:200), goat anti-SOX-1 (1:500), goat anti-AFP (1:500, all from Santa Cruz Biotech) and rabbit anti-Brachyury T (1:300, Abcam), NKX2.5 (1:200, R&D Systems), caspase-3 (1:500, Cell Signaling Tech., Danvers, MA, USA), anti-PAX6 (1:300, Developmental Studies Hybridoma Bank, The University of Iowa, Iowa City, IA, USA) and anti-cardiac troponin T (1:50, Abcam). Several sections (n=5-6) cut from different levels of the tissue multiarrays were labeled with each antibody. Sections were incubated overnight at +4°C with

primary antibodies followed with appropriate N-Histofine staining reagent for 30 min. ImmPACTTM (Vector Laboratories, Burlingame, CA, USA) diaminobenzidine solution was used as the chromogen. All antibodies were diluted in PBS containing 1% bovine serum albumin (BSA) and 0.3% Triton X-100. The sections were briefly counterstained with haematoxylin, dehydrated and then embedded in Entellan. Controls included omitting the primary antibodies or replacing them with non-immune sera. No staining was observed in these controls.

hiPSCs were fixed with 4 % PFA (Sigma-Aldrich) at passage 8 and stained with anti-Oct3/4 (1:400, R&D Systems), anti-TRA1-60 (1:200, Millipore), and anti-Sox2, anti-Nanog, anti-SSEA4, and anti-TRA1-81 (all 1:200, from Santa Cruz Biotechnology, Santa Cruz, CA, USA). Secondary antibodies (Invitrogen) included Alexa-Fluor-568-donkey-anti-goat-IgG, Alexa-Fluor-568-goat-anti-mouse-IgM and Alexa-Fluor-568-donkey-anti-mouse-IgG.

4.8 Protein expression studies by Western blot (I)

Regea 06/015 and Regea 06/040 EBs were collected at days 0, 3, 7, 10 and 20 for protein isolation. Proteins were isolated using the M-PER reagent (Pierce, Rockford, IL, USA), and protein concentrations were determined by the BCA method (Pierce). Proteins were separated on a 12% SDS-PAGE gel and transferred to a PVDF membrane (Hybond-P, GE-Healthcare). The membrane was blocked with 2% BSA (Sigma-Aldrich, St. Louis, USA) overnight at 4°C. Primary antibodies used were anti-OCT3/4 (1:100, Santa Cruz Biotech.), anti-Brachyury T (1:400, Abcam), anti-AFP (1:200, Santa Cruz Biotech) and anti-SOX1 (1:400, Abcam) and were diluted with TBS-Tween. Beta-actin (1:1,000, Santa Cruz) was used as an endogenous control. Primary antibodies were incubated overnight at +4°C. Peroxidase-conjugated antibodies (1:4,000, Zymed, Invitrogen) were used for 1 h at room temperature (RT), and the ECLplus kit (GE Healthcare) was used as the detection reagent. Exposure was performed using a CCD camera and Quantity One software (Biorad, Hercules, CA, USA).

4.9 Gene expression studies (I, III, IV)

Quantitative reverse-transcriptase polymerase chain reaction (qRT-PCR) was performed according to the standard protocols using Abi Prism 7300 (Applied Biosystems, Foster City, CA, USA). Total RNA was isolated from Regea 06/015

and 06/040 EBs on days 0, 3, 7, 10, 20, 32 and 41 using the RNAeasy Plus Mini Kit (Qiagen, Valencia, CA, USA). The concentration and the quality of RNA were monitored spectroscopically with a nanodrop (Wilmington, DE, USA). 0.2 µg of total RNA was transcribed to cDNA in a total volume of 20 µl. Each PCR reaction consisted of 0.25 µl of cDNA, 7.5 µl of 2x SYBR green PCR master mix (Applied Biosystems, Foster City, CA, USA) and 200 nM of each primer. Brachyury T, AFP, and SOX1 mRNA expression was examined using previously described primer sequences (Pekkanen-Mattila et al., 2009), and peptidyl-prolyl isomerise G (PPIG) was used as a housekeeping control. OCT3/4 was also determined using the same cDNA, but detection was made with Taqman chemistry and using the primer-probe sets Hs99999905_m1 for GAPDH and Hs00999632_g1 for OCT3/4 (Applied Biosystems). Cs values were determined for every reaction, and the relative quantification was defined using the ΔΔCt method (Livak and Schmittgen, 2001). Data were normalized to the expression of the housekeeping genes PPIG or GAPDH, and the 0-day sample (or 3-day sample for AFP) of the hESC line Regea 06/040 was used as the calibrator.

For markers of pluripotency, hiPSC total RNA was collected at passages 3, 6, and 11 and after cardiac differentiation. H7 hESC RNA was used as a positive control and EB RNA was used as a negative control. RNA was purified using the NucleoSpin RNA II kit (Macherey-Nagel, Düren, Germany), and cDNA conversion was performed using a high-capacity cDNA reverse transcriptase kit (Applied Biosystems, Carlsbad, CA, USA). PCR was performed with Dynazyme II (Finnzymes Oy, Espoo, Finland), using 1 µl of cDNA as the template and 2 µM of the primers. As positive controls for the exogenous primers, PCR was also performed using the transfected plasmids (hOCT3/4, hSOX2, hKLF4, and hc-MYC) as templates. PCR primers for hiPSC characterization and detailed reaction conditions have been described previously (Takahashi et al., 2007). Housekeeping controls were *β-actin* and *GAPDH*.

4.10 Electrophysiological characterization of cardiomyocytes (II-IV)

4.10.1 Patch clamp analysis (III)

APs were recorded from spontaneously beating dissociated cells using amphotericin for the perforated patch configuration of the patch clamp technique. Data were

acquired with an Axopatch 200B amplifier (Molecular Devices, Sunnyvale, CA, USA). A coverslip with adherent cardiomyocytes was placed in a recording chamber and perfused with an extracellular solution consisting of 143 mmol/L NaCl, 4 mmol/L KCl, 1.8 mmol/L $CaCl_2$, 1.2 mmol/L $MgCl_2$, 5 mmol/L glucose, and 10 mmol/L HEPES (pH 7.4 with NaOH; osmolarity of 301 ± 3 mOsm). Patch pipettes were pulled from borosilicate glass capillaries (Harvard Apparatus, Kent, UK) and had resistances of 1.5-3.5 MΩ when filled with a solution consisting of 122 mmol/L K-gluconate, 30 mmol/L KCl, 1 mmol/L $MgCl_2$, and 5 mmol/L HEPES (pH 7.2 with KOH; osmolarity adjusted to 290 ± 3 mOsm). The final concentration of amphotericin B (solubilized in dimethylsulfoxide) in the pipette was 0.24 mg/ml.

Data were filtered at 2 kHz and digitized (Digidata 1322A, Molecular Devices) at 10 kHz; data acquisition and analysis was performed with pClamp 9.2 software (Molecular Devices). Voltage-clamp experiments were also performed using some cardiomyocytes to record I_{Kr}. Experiments were conducted at 36 ± 1 °C.

4.10.2 Cardiac field potential recordings (II-IV)

Spontaneously beating hESC- and hiPSC-cardiomyocyte aggregates were mechanically excised from the cell cultures and plated onto FBS (30 minutes, Invitrogen) and 0.1% gelatin-coated (1 hour, Sigma-Aldrich) MEAs (Multi Channel Systems MCS GmbH) in EB medium. Medium was refreshed three times per week.

NRC were extracted from the hearts of newborn Sprague-Dawley rats as described elsewhere (Tokola et al., 1994). Neonatal rats were quickly decapitated, and their hearts were then harvested. Cardiomyocytes were extracted with multiple rounds of collagenase treatment, preplated for 1 hour at +37 °C, 5% CO_2 and plated on coated MEAs. 800,000 NRCs per MEA were plated, and culture medium was refreshed daily.

The FP recordings took place in room air with an MEA1060-Inv-BC or USB-MEA amplifier at a 20-kHz sampling rate (Multi Channel Systems MCS GmbH). MC_rack software (Multi Channel Systems MCS GmbH) was used for data acquisition. Standard 200/30iR-Ti-gr or 6-well-MEA200/30iR-Ti-mr MEAs were covered with a gas-permeable membrane (ALA Scientific) during recording to keep the cultures sterile. The temperature was kept at +37 °C using the heating element of the MEA amplifier during the recordings.

4.11 Pharmacological tests (II-IV)

Baseline conditions as well as drug effects were recorded for two minutes after a two-minute stabilization period. In study II, E-4031 (Alomone labs) was diluted in the cell culture medium to a final concentration of 600 nM. The FP signals were recorded from MEAs with NRCs (n=9) and from MEAs with hESC-CMs (n=4). In study III, baseline FPDs were measured from 43 control cardiomyocyte aggregates and 30 LQT2-cardiomyocyte aggregates. In study IV data were recorded from 11 hESC-CM, 6 WTa-CM, 11 WTb-CM, 9 LQT1a-CM, 5 LQT1b-CM, 6 LQT2a-CM, and 7 LQT2b-CM aggregates.

Cisapride monohydrate, quinidine, and D,L-sotalol (all from Sigma-Aldrich) were solubilized in dimethyl sulphoxide (DMSO, Sigma-Aldrich) at 10 mM. E-4031 (Alomone labs) and erythromycin (Abboticin i.v., Amdipharm, Abbott, IL, USA) were solubilized in sterile H_2O at 1 mg/mL and 50 mg/mL, respectively. Isoprenaline (Isuprel, Hospira, Lake Forest, Illinois, USA) was supplied in ready-ampoules. The drug stock solutions were diluted in 5 % FBS-containing EB medium for drug tests. The tested concentrations of cisapride monohydrate, quinidine, (±)-sotalol hydrochloride and erythromycin were chosen accordingly: half the concentration of the lower limit for therapeutic blood serum concentration, the lower limit of therapeutic blood serum concentration range, the average therapeutic serum concentration, the upper limit of therapeutic range and twice the upper limit of therapeutic concentration (Schulz and Schmoldt, 2003). Isoprenaline concentrations were chosen according to previously published values and multiples thereof (Pekkanen-Mattila et al., 2009). Serial dilutions of the drugs were made in EB medium with 5% fetal bovine serum (FBS, see below).

4.12 Cardiac field potential analysis

4.12.1 Field potential averaging (II)

A MATLAB-based (Mathworks, Inc.) analysis program was programmed to obtain average FP complexes to calculate specific cardiac parameters from this average. Files were imported into the MATLAB-based, in-house programmed analysis program. The program had two peak detection algorithms from which the appropriate one can be selected to align individual FPs correctly for the calculation of the average FP. The files were analyzed with the algorithm that detected the

peaks correctly. Both algorithms have a tenth-order FIR low-pass filter with a cutoff frequency of 1 kHz.

The first peak detection algorithm is based on the QRS peak detection originally presented by Pan and Tompkins (Pan and Tompkins, 1985). The algorithm squares the signals after which the edges of the squared signal are detected. The peak is identified as the maximum of the original signal between the samples under these squares. The second peak detection algorithm applies first- and second-order derivatives of the signal to obtain the signals local maxima. The signals are divided into 0.05-second sections, and the local maxima within these sections are identified with the Matlab implementation, provided by Vargas Aguilera (http://www.mathworks.com/matlabcentral/fileexchange/12275-extrema-mextrema2-m). To be identified as a peak, the detected maxima must register above a threshold. This threshold is adaptive and is set to 90% of the maximum of the previous group.

A detection dead time option was provided to avoid detecting double peaks related to the same FP complex. Any peaks during the dead time were ignored. Detected peaks were later used to calculate an average complex as one activation cycle produced from the continuous FP signals. This was achieved by aligning the cardiac cycles by the detected peaks and normalizing them for averaging. This representative average was used to calculate the FPD. BR was calculated from the detected peaks of the original imported signal. To validate the algorithms for detecting the correct peaks in the imported recordings, we performed manual, user-operated peak detection and generated an FP average based on the detected points. We then compared the averages generated by the automatic peak detection algorithms to the averages based on manual user-operated peak detection. The mean square error (MSE, equation 2) was used to calculate the errors between the results found manually and those found automatically.

$$MSE = \sqrt{\frac{\sum_{i=0}^{n} (x'i - x''i)^2}{n}} \tag{2}$$

where *x'* is the automatically generated complex, *x''* is the average complex based on the manual peak detection, and *n* is length of the complex. Analysis results from the program are saved automatically, and the options also permit creating a session for analyzing multiple files.

4.12.2 Noise attenuation (II)

Equation 3 presents the calculation of noise attenuation in decibels (dB), which served as the signal quality criterion.

$$A[dB] = 20\log\left(\frac{V_{average}}{V_{signal}}\right) \quad (3)$$

Where $V_{average}$ is the root mean square (RMS) voltage of the averaged signal, and V_{signal} is the RMS voltage of the unaveraged signal. Noise attenuation (3) was calculated from periods of the averaged and unaveraged signals resulting from noise (i.e., without cardiac FP activation).

4.12.3 Mean field potential duration (II-IV)

In study II, the FPD was measured from three individual cardiac cycles of the original unaveraged recordings and the mean FPD and the standard deviation were calculated based on these values. In study III, cardiomyocytes from the two LQT2-hiPSC lines were performed similarly, so the data were combined. Data from cardiomyocytes from the three control hiPSC lines was combined for the same reason. In study IV we calculated the beating rate-corrected FPD (cFPD) using the Bazett formula (equation 4). The drug-induced prolongation of the cFPD for individual signals were calculated as relative changes from the baseline among the cell lines.

$$cFPD = \frac{FPD}{\sqrt{PPI}} \quad (4)$$

Where cFPD is the beating rate corrected FPD, FPD is the uncorreted field potential duration measured in milliseconds, and PPI is the peak-to-peak interval measured in seconds.

4.13 Statistical analyses (I-IV)

In study I, the statistical significance of the EB growth data was determined by paired samples t-test and the standard deviation (SD) for the differentiation

efficiency of each cell line was calculated between the differentiation efficiency percentages of each plate. In study II, data are presented as the mean ±SD. In study III, data are given as the mean ±SEM or SD. A comparison of patch clamp data between LQT2 cardiomyocytes and control cardiomyocytes was performed using Student's t-test for independent data. One-way analysis of variance followed by Tukey's test was used for comparison of multiple groups. The I_{Kr} data were assessed using Student's t-test for independent data. The difference in FPDs between different populations of spontaneously beating cardiomyocyte aggregates was determined by nonlinear regression analysis using R software. In study IV, data are given as the mean ±SD and the differences in basal beating rate and rate-corrected FPD (cFPD) were determined using the t-test.

5. Results

5.1 Stem cell characteristics and pluripotency and cardiac marker expression (I, II, IV)

5.1.1 Human embryonic stem cells (I)

The hESC colonies had defined edges and the hESCs themselves had a round shape and a high nuclear-to-cytoplasm ratio. When investigating the pluripotency markers, we detected robust expression of the OCT3/4 pluripotency marker in undifferentiated hESCs. We also observed some sporadic Brachyury T^+ cells in the hESC colonies (figure 9).

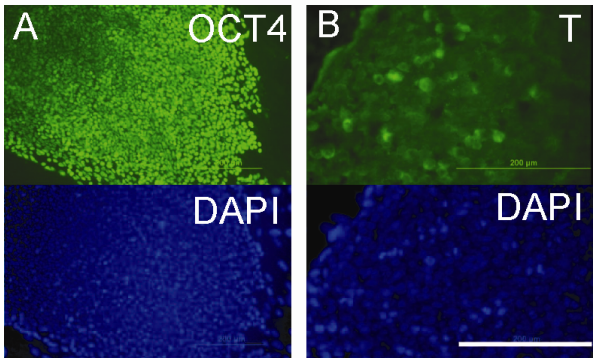

Figure 9. A) All of the human embryonic stem cell colonies had robust OCT3/4 protein expression (green). B) Infrequent brachury T positive cells (green) were present in the human embryonic stem cell colonies. DAPI (blue) stained the DNA. Figure modified from study I (Pekkanen-Mattila et al., 2010b) supplementary figure 3. Scale bar: 200 µm.

5.1.2 Human induced pluripotent stem cells (III, IV)

The characteristics of our reprogrammed WT and LQT hiPSCs resembled those of normal hESC features. The hiPSCs had clear colony edges, a round shape and a high nuclear-to-cytoplasm ratio, as expected of *bona fide* pluripotent cells. A typical hiPSC colony is seen in figure 10A. The hiPSCs also expressed endogenous pluripotency marker mRNAs (studies III & IV), and their cardiac derivatives expressed the cardiac transcription factor NKX2.5 and the structural protein cTNT, as seen in figure 10B, as well as alpha-actinin and connexin 43 (Study III), as

normally expressed by differentiated cardiomyocytes. The retrovirally introduced transgenes were silenced in the hiPSCs by the sixth passage of the cell lines and these transgenes were not reactivated following cardiomyocyte differentiation (study III). All the pluripotency markers were also expressed at the protein level (studies III & IV). The karyotypes were normal in the hiPSCs as well, after the primary fibroblasts had been reprogrammed into the pluripotent state (study III).

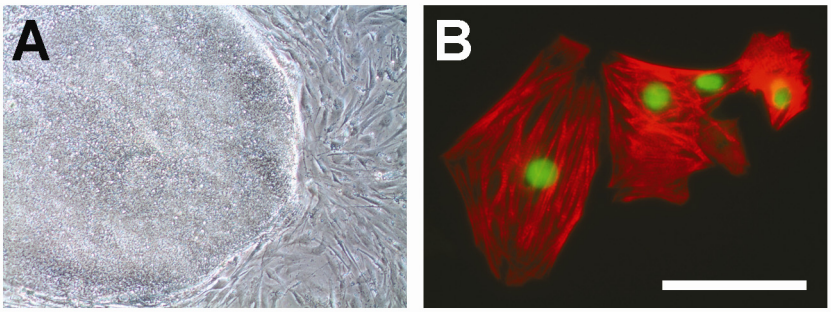

Figure 10. A) Phase contrast image of a colony of human induced pluripotent stem cells (hiPSCs) surrounded by mouse embryonic feeder cells. B) Dissociated single cardiomyocytes differentiated from hiPSCs expressed the NKX2.5 transcription factor (green in nuclei) and the structural cardiac troponin T protein (red), as detected by immunofluorescence. Scale bar: 100 µm for panel B.

With regard to their differentiation potential, the EBs from WT and LQT hiPSCs expressed the endodermal, ectodermal, and mesodermal germ layer markers that are expected of pluripotent cells (study III). The teratoma formation assay confirmed the pluripotency of the LQT2b-, WTa-, and WTb-hiPSC lines, as they resulted in the tissue formation of all germ layers (study III).

5.2 Embryoid body growth (I)

For differentiation of the hESCs, the FA method (Burridge et al., 2007) formed no viable EBs. Therefore, using the hESC Regea 06/015, Regea 06/040, HS181, HS293, HS346, HS360, HS362 and HS401 lines, we decided to initiate EB formation manually by cutting the hESC colonies with a scalpel. These manually cut EBs were allowed to form and differentiate on U-shaped, low attachment, 96-well plate wells for 7 days. In most cases, during this time, a thin layer of cellular outgrowth was observed in the cell culture wells. The initial EBs had a mean diameter of 444 µm (210 µm min., 847 µm max.) on day 1. One week later, the mean diameter had increased to 563 µm (139 µm min., 1,288 µm max.). Approximately one month after the EBs were transferred onto the 12-well plates, we noticed that the outgrowth from the EBs covered the bottom of the wells. The

expansion of the differentiating cells differed among the hESC lines. We also noticed differences in the densities of the outgrowths, and in some cases, cystic structures were evident in them as well. With regard to cardiomyocyte differentation, only viable and well-growing EBs gave rise to spontaneously beating foci containing the differentiated cardiomyocytes.

5.3 Marker expression in developing embryoid bodies and their progeny (I)

To analyze how the different germ layer and cardiac markers were expressed in the developing EBs, we performed ICC staining to detect the expression of the following proteins: OCT3/4 for pluripotency, Brachyury T for the mesoderm layer, AFP for the endoderm layer, SOX1 for the ectoderm layer, NKX2.5 for cardiac cells, and Caspase-3 for apoptotic cells. We also performed additional western blot protein expression analyses for OCT3/4 and Brachyury T. Corresponding mRNA levels were assessed using qRT-PCR.

The pluripotent OCT3/4$^+$ cells resided in the center of the EBs or on the edges, and their amounts reduced during differentiation. However, persistent OCT3/4$^+$ cells were detected sporadically up to day 10 or 12. In general, all the hESC lines had similar expression patterns of the OCT3/4 protein. Our western blot experiments verified that OCT3/4 protein expression persisted up to day 20. However, on day 20, *OCT3/4* mRNA was not detectible.

Overall, we detected few Brachyury T positive cells in the EBs on days 4 to 12. Multiple positive cells were observed in only a few cases. Surprisingly, scarce Brachyury T$^+$ mesodermal cells were detectable in the HS346 hESC line, which produced the most beating foci out the eight stem cell lines. The western blot experiments also verified the low expression of the Brachyury T protein. Brachyury T mRNA expression peaked in day 7 EBs and decreased steadily thereafter.

We detected AFP$^+$ endodermal cells in 4-day-old and older EBs. These cells resided in the centers as well as the edges of the EBs. While the AFP proteins were irregularly expressed in some of the samples and more copiously in others, they were not systematically expressed in any of the hESC lines nor were they affected by the age of the EBs. AFP expression was non-overlapping with the endodermal SOX1 and mesodermal Brachyury T proteins. However, AFP and OCT3/4, which mark the pluripotent cells, overlapped in multiple EBs. In terms of mRNA expression, *AFP* was detectable on day 3 and peaked on day 20. In our own hESC

lines, the amount of *AFP* mRNA was higher in Regea 06/015 hESCs than in Regea 06/040 hESCs.

The earliest $SOX1^+$ cells first appeared on day 4 in the center and on the edges of the EBs and most of the positive cells were detected from day 8 onward. The expression varied to some extent, however, depending on the hESC line. The strongest SOX1 expression was detected in HS362 and HS181 EBs. HS181 EBs had a few positive cells already on day 4. HS346 demonstrated a high cardiogenic potential, and $SOX1^+$ cells were few in these EBs. $SOX1^+$ expression did not overlap with any other germ layer markers or OCT3/4. The mRNA expression peaked at around day 20.

NKX2.5 transcription factor proteins, marking the developing cardiac cells, were detectable on day 4 in a few of the cells. The expression usually persisted until day 12, and all the hESC lines expressed NKX2.5 in a similar manner. NKX2.5 mRNA increased during the initial 7-day EB formation and peaked at around day 11.

Many cells in the developing EBs had fragmented nuclei, and we observed caspase-3 immunoreactivity throughout the experiment. In the beginning, the caspase-3^+ apoptotic cells were located in the middle of the EBs, and in the later stages of EB development, caspase-3 reactivity diminished upon random cavity formation.

We also stained the excised beating foci with antibodies for the OCT3/4, Brachyury T, SOX1, AFP, cTNT, PAX6 and NKX2.5 proteins. We detected no OCT3/4 or SOX1 reactivity and only few Brachyury T^+ cells in these older clusters. We observed discrete positive areas of AFP, cTNT and PAX6 in the beating foci and only spontaneously beating cells expressed the cardiac structural protein cTNT. AFP expression co-localized with cTNT in some of the EBs, and we observed AFP^+ areas where cTNT was absent. $PAX6^+$ ectodermal areas were non-overlapping with respect to AFP and cTNT. The cardiac $NKX2.5^+$ areas were irregularly expressed and partly co-expressed cTNT. The number of the cells and the size of the excised beating foci differed considerably between the samples from tens to hundreds of cells. These spontaneously beating cells expressed striated patterns of the cardiac structural protein cTNT.

5.4 Efficiency of cardiac differentiation (I)

We initiated spontaneous EB differentation by manually cutting the hESC colonies. To investigate approximately how well the hESC lines produced cardiac cells, we determined the efficiency of cardiac differentiation as the amount of formed beating

foci per plated EBs. These cardiac differentiation efficiencies varied from 0% to 12.5% across the hESC lines, with most lines having an efficiency of approximately 1 or 7%. The earliest spontaneously beating foci appeared on day 7. In most cases, we first detected the appearance of these foci at around day 14. The size and shape of the foci differed from 100 μm diameter circular areas to larger millimeter-scale areas in length with complex shapes and structures.

5.5 Cardiac field potential analysis (II)

5.5.1 Validity of the peak detection algorithms (II)

To analyze the electrophysiological cardiac MEA data, we developed automatic peak-detection algorithms that worked well in analyzing the cardiac FP traces. The averaged signals produced using the automatic peak detection were highly identical to those averaged signals that we obtained by manually selecting the correct peaks in the cardiac FP signals, and the root mean square (RMS) errors between the averages generated using the two methods were small. With regard to FPD, the errors were 0.13 ms using NRCs and 0.95 ms using hESC-CMs and with regard to amplitude they were 49 μV using NRCs and 79 μV using hEC-CMs. In addition to the small RMS error values, the proper functioning of the peak detection and averaging algorithms was demonstrated by the E-4031 drug tests, in which the alteration of the FP signal shape and FPD prolongation from the baseline was clearly detectable.

5.5.2 Noise attenuation in averaging (II)

Using our averaging method, we achieved approximately $-10^{1.2}$ dB noise attenuation in the cardiac FP signals when we applied 50 complexes for the average. This level of attenuation reduced the noise in the FP recordings to one-sixth of the initial level, reducing the noise sufficiently for the accurate analysis of the cardiac FP parameters.

5.5.3 Variation of cardiac field potential parameters (II)

5.5.3.1 Field potential duration and beating rate (II)

Overall, we noted greater FPD and BR parameter fluctuations with NRCs than with hESC-CMs, as seen in table II.

Table II. Relative fluctuations of field potential duration (FPD) and beating rate (BR) in neonatal rat cardiomyocytes (NRC) and human embryonic stem cell-derived cardiomyocytes (hESC-CMs, H7) during different parts of the microelectrode array recordings. σ: standard deviation.

Population and parameter	*Beginning (%)*	*σ (%)*	*Middle (%)*	*σ (%)*	*End (%)*	*σ (%)*
NRC FPD	0.6	16.2	-8.4	6.4	1.1	20.1
NRC BR	15.9	33.2	13.5	28.8	7.8	18.5
hESC-CM FPD	-3.9	8.3	-2.7	9.9	-7.1	10.1
hESC-CM BR	-6.5	0.6	-3.4	1.1	0.9	0.9

The BRs of different cardiomyocyte clusters differentiated from hESCs and hiPSCs had high deviations within some of the cell lines. The rate-corrected cFPDs also varied across and within all the CMs from the seven hPSC lines, but they did not differ significantly from each other between the different lines.

Table III. Beating rates (BR in beats per minute [bpm]) of cardiomyocytes differentiated from hESCs (H7) or from control or long QT syndrome (LQTS) type 1– or 2–specific human induced pluripotent stem cells (UTA lines) and their minimum and maximum values as measured from different cardiomyocyte clusters. σ: standard deviation.

Stem cell line	*BR (bpm)*	*σ (bpm)*	*Minimum (bpm)*	*Maximum (bpm)*
hESC-CM	74	20	48	101
WTa	95	81	13	199
WTb	91	33	59	153
LQT1a	61	47	29	177
LQT1b	86	67	23	160
LQT2a	57	20	28	78
LQT2b	79	38	47	155

5.5.3.2 Amplitude and peak-to-peak interval (II)

To further validate the averaging method used by our analysis program, we also investigated the relationship of the FP amplitude variation and PPI using scatter plots. Recordings with stable beating rhythms (i.e., consistent PPI) and consistent systolic amplitudes naturally had tightly grouped data points on the scatter plots, whereas those with a higher variability due to arrhythmic behavior had scattered

data points. Interestingly, even though the amplitude varied with PPI in the less stable recordings, the FPDs were still rather stable, allowing us to use, in some cases, the less stable FP recording for analysis.

5.5.4 Cardiac field potential durations (II-IV)

To test the reliability of the measured cardiac FPD values using our analysis program, we compared the mean NRC and hESC-CM FPD values measured from three individual cardiac FP cycles by hand to FPDs measured with the program. The FPDs measured using the program fell mostly within one SD and all within two SDs of the manually measured FPD values (study II).

To investigate the relationship between FPD and BR (as *in vitro* surrogates of QT interval and heart rate) in the control and LQTS2-specific cardiomyocytes (LQT2-CMs), we plotted these values on a scatter plot. We found that these two variables had an exponential negative correlation (study III) within the control CM and LQT2-CM populations. For the LQT2-CMs, however, this relationship was significantly more pronounced, particularly when the BR was low ($p=0.014$).

The mean cFPDs in study IV were 389 ms in hESC-CMs, 310 ms in WTa-CMs, 376 ms in WTb-CMs, 355 ms in LQT1a-CMs, 335 ms in LQT1b-CMs, 365 ms in LQT2a-CMs, and 374 ms in LQT2b-CMs.

5.6 Pharmacological responses of pluripotent stem cell-derived cardiomyocytes (II-IV)

To test the pharmacological responses of the hESC-CMs and control and LQTS patient-specific CMs we challenged them with multiple drugs while recording their electrophysiological responses with MEAs. From the recordings we calculated the cFPDs (i.e. beating rate corrected FPDs) as well as counted any incidences of adverse effects (EADs and pauses). The changes in cFPD prolongation were plotted in relation to the baseline values as ΔcFPD.

To investigate the β-adrenergic responses of the cardiomyocytes we exposed them to isoprenaline, which is a β-adrenergic agonist. All cardiomyocytes demonstrated increased chronotrophy upon an isorprenaline challenge which was seen as increased BR in FP recordings (studies III, IV). Isoprenaline increased the BR at 80 nM concentrations in all of the lines, but higher than 80 nM concentrations had no further BR increasing effect (study IV).

Erythromycin, a macrolide antibiotic, is known to prolong the QT interval in patients (Shaffer et al., 2002). Erythromycin prolonged the ΔcFPD in all of the cardiomyocytes. The magnitude of prolongation varied between ~10-40% among the lines. Controls had ΔcFPD prolongations of ~10-35% at maximal concentration. The highest prolongation (~40%) was seen with LQT2a-CMs at the lower therapeutic level. Between the LQT1-lines erythromycin prolonged ΔcFPD slightly more in the LQT1a-CMs, from the symptomatic patient, than in the LQT1b-CMs which were from the symptomatic patient. We did not observe any adverse effects in control or in LQT–CMs with erythromycin.

Cisapride is a serotonin 5-HT4 receptor agonist that was used a gastrointestinal stimulant and an anti-emetic (Salvi et al., 2010). It was drawn from the market due to its tendency to induce TdP in patients (Darpö, 2001). We detected no adverse effects but among the lines cisapride caused ΔcFPD prolongations of 6-19% at the maximal test concentration. The controls had approximately 10% prolongation. The lowest ΔcFPD prolongation was seen with LQT2b-CMs and the highest with LQT1b-CMs.

Sotalol is both a Vaughan-Williams class III antiarrhythmic due to its tendency to block K^+ channels and a β-adrenergic antagonist (Edvardsson et al., 1980). Sotalol caused ΔcFPD prolongation in all of the cardiomyocytes. Controls exhibited a 25-35% prolongation at the maximal concentration. The most pronounced effect was seen in LQT1b-CMs, which exhibited a 57% prolongation, whereas in the other lines the prolongations were more moderate. We also noted sotalol-induced EADs in some of the cardiomyocytes. These EADs were more numerous in the LQT2-CMs than in the LQT1-CMs. Notably, the LQT1b-CMs from the asymptomatic sibling did not present with any EADs even though they exhibited the highest ΔcFPD prolongation among the lines. In the controls we noted only transient EADs once in the WTb-CMs.

Quinidine, a class IA antiarrhytmic and multiple ion channel blocker that is known to trigger TdP (Bauman et al., 1984), caused ΔcFPD prolongation in all lines. Among controls the prolongation was approximately 25-40% at maximal concentration. The LQT-CM responses varied, but at maximal concentration the LQT2- and LQT1a-CMs had more prolonged ΔcFPD than the LQT1b-CMs from the asymptomatic patient. Quinidine also induced EADs and pauses in the cardiomyocytes. Figure 11 depicts a case of quinidine-induced EADs on LQT2-CMs. Pauses occurred in cardiomyocytes differentiated from all lines. The controls were more resistant to pauses than the LQT lines in that they exhibited pauses at higher concentrations. Quinidine-induced adverse effects were most prominent in the LQT1a-CMs from the symptomatic patient. These cardiomyocytes exhibited

EADs already at low concentrations (3 uM) and the number of EADs increased with escalating drug doses.

E-4031, the HERG K^+ channel blocker, prolonged the ΔcFPD in all cardiomyocytes. Especially in some hESC-CMs we saw massive prolongations. The WT-CM controls behaved similarly and had at most ~40% prolongation. The prolongation among LQT-CMs varied between ~30-50%. Overall, the LQT1-CMs were more consistent between the two lines and had less prolonged ΔcFPD than the LQT2-CMs and the controls. E-4031 also caused adverse effects in LQT-CMs at lower concentrations than in control cardiomyocytes. Overall, the LQT2-CMs were more susceptible to adverse effects than the LQT1-CMs. Importantly, LQT1a-CMs from the symptomatic patient exhibited adverse effects at lower E-4031 concentrations than the LQT1b-CMs from the asymptomatic patient. E-4031-induced pauses and EADs were evident already at 10 nM and 300 nM concentrations, respectively, with the LQT1a-CMs, whereas in LQT1b-CMs these effects were recorded only at the highest (700 nM) concentration.

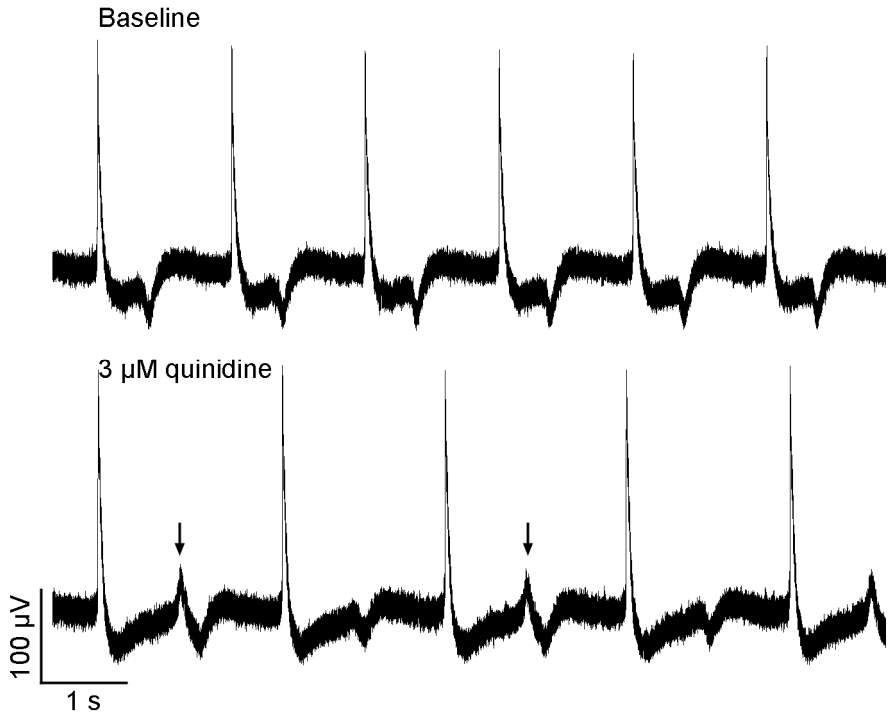

Figure 11. Quindine-induced early after depolarizations (EADs) on long QT syndrome type 2 –specific cardiomyocytes. The upper field potential trace recorded with a microelectrode array shows the baseline condition and the lower trace shows the effects of added 3 µM quinidine. The arrows mark the EADs.

5.7 Action potential and potassium current properties of long QT syndrome 2–specific cardiomyocytes (III)

To investigate the electrophysiological properties of single dissociated cardiomyocytes from the control and LQT2-specific hiPSC lines, we subjected them to patch clamp analysis. The differentiated and subsequently dissociated cardiomyocytes had either ventricular- or atrial-like cardiac AP properties according to their AP morphology. The ventricular-like APs had a clear phase 2 plateau, whereas the atrial-like APs were more triangular in shape. The majority of the investigated AP parameters had non-significant differences between control and LQT2 CMs ($p>0.05$). Importantly, however, in a subset of beating rate-matched cardiomyocytes, we noted a significantly prolonged AP duration (APD) at 50% and 90% repolarization (APD_{50} and APD_{90}, respectively) in the ventricular-like APs of LQT2-CMs versus control cardiomyocytes, as shown in figure 12 ($p<0.001$). These values were non-significant between the atrial-like cardiomyocytes. APD_{90} had a mean value of 516 ms in LQT2-CMs, 310 ms in control hiPSC-CMs, and 338 ms in hESC-CMs, and these values were non-significant between the different LQT2-CM groups as well as between all the control cardiomyocyte groups. Spontaneous EADs were observed in just one out of the 20 patch-clamped LQT-CMs and in none of the control cardiomyocytes.

To study the current properties of cardiomyocytes with ventricular-like APs using the voltage clamp mode of patch clamp, we isolated the I_{Kr} current, mediated by the hERG channels, by blocking it with E-4031. The isolation of the I_{Kr} current revealed that it was noticeably reduced in the LQT2-CMs compared to the control cardiomyocytes. We noted a significant decrease of 40-46% in the tail I_{Kr} density upon depolarization of the cells from 0 to +40 mV ($p<0.01$) during I_{Kr} blockade by E-4031 as well as by isotonic cesium conditions (Zhang, 2006). A patch clamp ramp protocol also illustrated the role of reduced I_{Kr} in the LQT2-CMs.

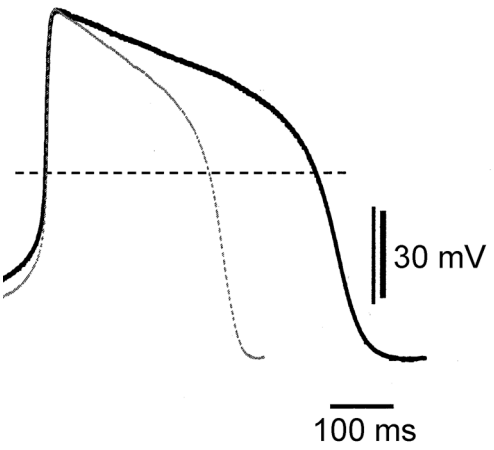

Figure 12. Action potential properties of a ventricular-like control cardiomyocyte (shorter dashed line) and a long QT syndrome type 2 (LQT2)-specific cardiomyocyte (longer solid line). The control cardiomyocytes were differentiated from induced pluripotent stem cells (hiPSCs) derived from fibroblasts obtained from a healthy donor and the long QT type 2 cardiomyocytes were derived from hiPSCs obtained from a LQT2 patient with a defined ion channel mutation.

6. Discussion

6.1 Embryoid body development (I)

We aimed to see if there were any differences between the eight hESC lines in germ layer marker organization or in the temporal sequence of expression during EB development and whether such patterns might help in predicting the cardiomyogenic potential of the hESC lines we studied.

6.1.1 Forced aggregation and embryoid body size (I)

The FA method has been reported to increase cardiac differentiation in the HUES-7 stem cell line by 13-fold when activin A and bFGF were also added (Burridge et al., 2007). Since in our study the FA method failed to produce any viable EBs, we focused our analysis to include only the mechanically excised EBs. The initial size of the EB is known to affect cardiomyocyte differentiation potential (Bauwens et al., 2008; Mohr et al., 2010), and hESCs are a rare cell type that undergo dissociation-induced apoptosis as single cells (Amit et al., 2000) (a phenomenon known as anoikis). This can be counteracted to some extent using Rho-associated, coiled-coil containing protein kinase (ROCK) inhibitor during dissociation (Watanabe et al., 2007), which protects the cells against dissociation-induced apoptosis. Other factors that may have affected the relative inefficiency of the FA method might have included the possible detrimental effects of the centrifugal forces on the cells during the hESC plating phase and the fact that these hESCs were not adapted to handle dissociation, as they were passaged mechanically as a cell line.

In the EB initiation phase, the size of the cut hESC colony pieces by mechanical excision was kept as constant as possible. The success of this strategy was corroborated by the fact that in the initial stage (i.e., on day 1), differences between EB sizes were non-significant. A week after the spontaneous EB differentiation was initiated, the average areas of the EBs from all of the hESC lines were significantly larger than on day one. The size and shape of the differentiating EBs varied widely, and no clear protein expression patterns occurred in early stage EBs. This might be, in part, due to differences in the diffusive transport of biochemicals between the

EBs, which was previously observed (Sachlos and Auguste, 2008). Nonetheless, we observed expression of every germ layer marker in the 12-day period.

6.1.2 Marker expression (I)

Compared to the first 12 days of differentiation, the month-old EB progeny had a more defined arrangement, with clear and separate $PAX6^+$, AFP^+, and $cTNT^+$ areas. Interestingly, the mRNA levels of the pluripotency marker *OCT3/4* declined faster than the protein expression levels, which persisted up to 20 days. The *OCT3/4* gene expression results were consistent with previous observations (Adewumi et al., 2007), and our results suggest lower turnover rates for OCT3/4 protein than mRNA.

AFP mRNA expression in the EBs was also in agreement with earlier reports (Bettiol et al., 2007). The protein was expressed rather abundantly in the inner and outer parts of the EBs in the first 12 days. AFP^+ areas have previously been reported in the peripheral sections of early EBs or in the inner EB elements in later stages (Conley et al., 2004; Itskovitz-Eldor et al., 2000; Kim et al., 2007). The co-localization of AFP and OCT3/4 suggested that some of the differentiated endodermal cells expressed OCT3/4 TF. Indeed, mouse primitive endodermal cells have been previously shown to express OCT4 protein (Palmieri et al., 1994). After a month of spontaneous EB differentiation, we detected co-localization of the endodermal AFP with the cardiac structural protein cTNT. Because endodermal cells are capable of inducing cardiac differentiation in hESCs (Mummery et al., 2003), this raises the possibility that endodermal areas might coax the formation of cardiomyocytes in the developing EBs as well.

Ectodermal SOX1 was differentially expressed in the developing EBs among different hESC lines. SOX1 was more abundantly expressed in lines that had poor cardiac differentiation. Interestingly, the hESC lines with higher SOX1 expression have previously been shown to have a good neurogenic capacity (Lappalainen et al., 2010).

Brachyury T is an early mesodermal marker. *Brachyury T* mRNA expression peaked on day 7 in our EBs but earlier reports have placed this peak around the third day of differentiation (Bettiol et al., 2007; Graichen et al., 2008; Pekkanen-Mattila et al., 2009). The protein expression was scant in all EBs, and there was no clear link with the hESC lines' cardiomyogenic potential and Brachyury T expression. The hESC line that produced the most cardiomyocytes (HS346) did not have many Brachyury T^+ areas. This observation contrasts with some previous studies (Kim et al., 2007; Zhang et al., 2009). However, the spontaneous formation of beating foci was relatively low among all the hESC lines we studied (12% maximum),

suggesting that they have a naturally low occurrence of mesodermal derivatives. This possibility was further reinforced by a previous observation that prolonged *Brachyury T* expression in combination with *OCT3/4* might be indicative of an absence of endo- and mesodermal derivatives (Bettiol et al., 2007).

The expression profile of the early cardiac marker NKX2.5 in the EBs was in harmony with previous reports (Graichen et al., 2008; Hsiao et al., 2008), but previous observations on the cardiomyogenic propensity and *NKX2.5* mRNA expression (Osafune et al., 2008; Pekkanen-Mattila et al., 2009) did not translate to the protein level in our study. In early-phase (days 4-12) EBs, NKX2.5 protein expression was random and in month-old structures it overlapped with cTNT only partially. Previously it was shown that Nkx2.5 is expressed in mESC-derived non-cardiac cells as well (Hsiao et al., 2008), supporting the observation that not all cells expressing NKX2.5 are necessarily cardiomyocytes.

Caspase-3 is involved in apoptosis and is critical for normal development (Jacobson et al., 1997). In mESCs, this protein has also been shown to turn off Nanog expression (Fujita et al., 2008). We performed staining for this protein after noticing many fragmented nuclei in the histological sections of EBs. Overall, caspase-3-positive cells were observed from the second day onward, which was in accordance with previous observations with mESC EBs (Joza et al., 2001). Cavity formation was detectable on the fourth day and previous reports have also noted cavity formation in early-stage hESC EBs (Conley et al., 2004). Thus, our results recapitulated the previous observations on caspase-3 in developing EBs.

Overall we could not detect any major differences among the lines in their marker expression pattern. The EB development and the spatiotemporal expression of different markers were comparable across the eight hESC lines. All of the markers were detectable but had no conclusive expression trajectories. Older (month-old) structures had specialized regions and a distinct localization of the germ layers. However, predicting any cardiogenic potential of the hESC lines based on early phase marker localization during the first 12 days of development was inconclusive, most likely due to the time frame involved in the formation of distinct regions in the spontaneously differentiating EBs.

6.2 Cardiac field potential averaging (II)

Alongside the well-established patch clamp technique (Hamill et al., 1981; Sakmann and Neher, 1984), the MEA platform is gaining ground as a means to investigate cardiac electrophysiology *in vitro*. While patch clamp is an excellent method to

study specific ion current properties of single cardiomyocytes, for example, it requires a lot of training and is tedious to perform. Further, some experimental settings may require cardiomyocyte coupling via gap junction proteins such as connexin 43 to tease out a proper phenotype. MEAs may assist in determining cardiac parameters such as the duration of repolarization in three-dimensional cardiac syncytia. Therefore, one application could be to study drug effects with hPSC-CMs for possible adverse effects (Braam et al., 2010; Caspi et al., 2009).

For accurate analysis of the cardiac FP parameters recorded with MEAs, high-quality signals are needed because low SNR leads to reduced signal quality. Especially with hESC-CMs, the low SNR may be a consequence of the potentially low amount of cardiomyocytes in a given spontaneously beating cluster. Low cardiomyocyte amounts lead to weaker FP signals in MEA recordings. The quality of these lower quality signals can be improved by averaging multiple individual cardiac FP cycles from a single recording to provide a representative higher quality cardiac FP cycle. These averaged signals provide a more accurate basis for analysis of FP parameters.

Our averaging program, which was based on Matlab software, was able to detect the correct cardiac FP peaks, align these peaks on top of each other, and generate a representative average cardiac FP complex from a single MEA recording. We were able to accomplish this using both of the two algorithms that were available for peak detection in the program. Correct peak detection by the program was validated by comparing the averages generated using the algorithms to averages generated based on manual peak selection. Due to the diverse nature of the cardiac FP traces, different approaches had to be implemented for peak detection. Therefore, for each recording, the algorithm that detected the peaks correctly was selected.

Two NRC signals demonstrated arrhythmic behavior, which was seen as a variation in the PPI (or BR). The irregular beating rhythm obstructed accurate PPI calculations, but surprisingly the FPD remained quite stable and could subsequently be determined from the averaged signal.

Noise attenuation in the cardiac FP signals presents an interesting conundrum. On one hand, the more cardiac FP cycles that are included in the average, the less there is noise. On the other hand, when more of these cycles are used for the average, there is a greater potential for a misalignment of the peaks, thus resulting in a distorted average. In our experiments, we found that including approximately 50 cardiac FP cycles generates a high-quality average without compromising the integrity. Fewer cycles might suffice as well, however, because the noise reduction varies case by case. On the same note, we found that the NRCs showed greater a variation of FPD and BR in different parts of the recording than hESC-CMs. The

greater the variation of these parameters, the higher the chance of introducing alignment errors in the average, based on the whole recording period. Interestingly, we noted that the individual cardiac FP cycles retained rather stable duration (FPD), making it feasible to produce the averages. Overall, the FPD and BR values of the averages from the different parts of the recordings were sufficiently close to those of the averages from whole recordings.

When the amplitude of the signals was compared to the PPI values, we noticed that most of the signals had quite stable dynamics. There was some variation in a few of the signals, and when the PPI increased, the amplitude decreased. Comparing the cardiac FP cycles and their FPD in arrhythmic recordings showed little variation compared to the average FP complex. The first cardiac FP cycles in the arrhythmic "bursts" had a slightly prolonged FPD, but these first cycles are automatically in the minority and thus skew the average complex negligibly.

When the FPDs of averaged signals were compared to averages measured from three individual cycles by hand from the same MEA recording, we noticed that the values were close to each other (mostly within one SD, all within two SDs). Additionally, the sensitivity of averaging algorithms was proven by the clear detection of an altered FP signal shape upon exposure to a pharmacological agent, thus validating the peak detection and averaging algorithms of the program as a basis for proper cardiac FP analysis.

In summary, the averaging method can be reliably used in certain conditions to analyze cardiac FP properties of otherwise hard-to-interpret, low-SNR MEA signals. In particular, the comparison of different conditions (e.g., in drug tests) by signal averaging might present a useful opportunity. Creating algorithms for the automatic online detection and recording of FPD based on this technology might be beneficial, as the MEA platform has been previously been used in hESC-CM drug tests (Braam et al., 2010; Liang et al., 2010). However, automatic FPD algorithms are harder to implement than amplitude or PPI measurements, as the signal shape with hESC-CMs varies and the FPD end-point therefore often depends on interpretation.

6.3 Long QT syndrome modeling (III, IV)

6.3.1 Long QT syndrome type 1 (IV)

The KCNQ1-FinA founder mutation lies in the C-terminal end of the K^+ channel and likely renders its assembly domain, which is needed to form the $K_{v7.1}$ channel,

dysfunctional (Piippo et al., 2001). This effect leads to LQTS by obstructing the K^+ flux in cardiomyocytes. Hence, this mutation may obstruct the K^+ channels' ability to form functional tetramers and thus mediate the I_{Ks} current. Patients with the KCNQ1-FinA mutation have a mean QTc of 462 ms (Marjamaa et al., 2009a). Our symptomatic patient had a QTc time of 456 ms and the asymptomatic patient had a QTc time of 426 ms. The mean basal cFPD times in the MEA recordings were 335 ms and 365 ms (for the symptomatic and asymptomatic, respectively). In the first LQT1 paper by Moretti and colleagues, the AP_{90} was increased by half in R190Q *KCNQ1*-mutated cardiomyocytes, whereas the ECG only revealed up to 15% QT prolongation (Moretti et al., 2010b). In our MEA drug tests with the KCNQ1-FinA mutant LQT1-CMs, we noted more adverse effects in the LQT1a-CMs derived from the only symptomatic patient in these studies. The LQT1b-CMs derived from the asymptomatic sibling had less EADs and pauses and at higher drug concentrations than the LQT1a-CMs.

6.3.2 Long QT syndrome type 2 (III, IV)

hERG-FinB is another Finnish LQTS founder mutation (Fodstad et al., 2004) that predisposes individual to LQT2. Most of these mutation carriers in the Finnish population are asymptomatic, but mutations in hERG have also been associated with sudden cardiac death (Tester and Ackerman, 2007; Tu et al., 2011). The LQT2-patients carrying hERG-FinB have QTc times of 448 ms on average, which have been documented to be as high as 596 ms. Non-carriers typically have average QTc times of 416 ms (Fodstad et al., 2006).

The patient from whom we obtained the skin biopsy had a latent LQT2 mutation. Immediate relatives carrying the same mutation had, however, suffered from palpitations, syncope, and even sudden cardiac death triggered by auditory stimuli during sleep, all of which are typical symptoms of LQT2 (Roden, 2008; Schwartz, 2001).

We aimed to recapitulate the LQTS2 phenotype *in vitro* for disease modeling purposes. Indeed, the cardiomyocytes differentiated from hiPSCs reprogrammed from fibroblasts of a LQTS2 patient exhibited prolonged cardiac repolarization. This was observed in both the patch clamp experiment and the MEA recordings. The MEA recordings also revealed that the prolongation was more pronounced at slow beating rates, which corresponds to the clinical observations of LQT2 where QT-interval prolongation is observed at slower heart rates (Swan et al., 1999). This prolongation effect was likely due to decreased I_{Kr} current caused by the R176W (hERG-FinB) missense mutation in *hERG*, as observed in voltage clamp recordings.

6.3.2.1 Rapid delayed rectifier current properties (III)

In heterologous expression systems, hERG-FinB reduces the tail current density by approximately 75%, and wild-type (WT) hERG co-expression blocks this effect (Fodstad et al., 2006). The I_{Kr} current density in hERG-FinB cardiomyocytes may be modified by an interaction with misshapen-like kinase (MINK)-related peptide (MiRP) subunits (Abbott et al., 1999) and the co-expression of endogenous hERG1a and hERG1b isoforms. We noted a 43% reduction in the hERG current in our LQTS2-CMs.

hERG-FinB does not have a dominant-negative effect like the *hERG* A614V missense mutation (Nakajima et al., 1998), which another reported case of patient-specific hiPSC-derived LQT2-CMs possessed (Itzhaki et al., 2011). The A614V LQTS2 hiPSCs reported in this study were reprogrammed from fibroblasts obtained from a highly symptomatic patient who had documented episodes of TdP. *In vitro* the A614V mutation caused a more severe decrease in I_{Kr} current density (-72% at 0 mV membrane potential and -64% at +20 mV) in the LQT2-CMs. The corresponding values in our study were -43% and -40%. These A614V cardiomyocytes also had more prolonged APD_{90} (+200% compared to control cardiomyocytes) than our hERG-FinB cardiomyocytes (+166%) at a 1Hz (60 pbm) beating frequency. The patch clamp recordings also revealed the A614V cardiomyocytes to have EADs in 66% of cases as opposed to 5% (only one cell) in our study. These results, and the fact that the A614V *hERG* mutation has a dominant-negative effect, imply that the severity of the mutation is well represented by the *in vitro* LQT2 model. Matsa and colleagues have also recapitulated the LQT2 phenotype with G1681A-mutated cardiomyocytes using patient-specific hiPSCs. The patient in this study had a prolonged QTc interval of up to 571 ms and also suffered from arrhythmic episodes. Interestingly, the G1681A LQT2-CMs did not demonstrate any spontaneous arrhythmias. Such episodes were nonetheless triggered by β-adrenergic stimulation with isoproterenol. With the exception of APD, other AP properties were comparable to those reported for WT cardiomyocytes in other studies (Gai et al., 2009; Yokoo et al., 2009; Zwi et al., 2009a).

6.3.2.2 Genotype-phenotype relationship (III)

The concept of repolarization reserve (Roden, 1998) states that, in cardiomyocytes, there are redundant mechanisms that can bring about normal repolarization at times of stress, such as during a pharmacological challenge (Couderc et al., 2009;

Kannankeril et al., 2005). A full-scale LQT2 phenotype might, therefore, require compromising multiple ion channel targets. Interestingly, we were able to show that the LQT2-CMs generated more adverse effects in terms of EADs than controls when these cells were exposed to certain drugs. Sotalol caused arrhythmias only in LQT2-CMs at a therapeutic ($ETCP_{unbound}$) range. Sotalol has indeed been known to trigger TdP in *hERG* mutation carriers (Couderc et al., 2009; Lehtonen et al., 2007), most likely by intensifying the K^+ efflux deficiency because it blocks the hERG WT and variant hERG channel alike (Männikkö et al., 2010). Blocking the I_{Kr} current with E-4031 caused EADs in both LQT2-CMs and controls.

6.3.2.3 Potential mitigating effects of cardiomyocyte coupling (III)

Interestingly, comparing the relationship between single-cell patch-clamp recordings, MEA recordings and clinical ECG recordings revealed some interesting discordances. The single-cell recordings indicated prolongative differences of up to 66% in APD_{90} of LQT2-CMs versus the control cardiomyocytes. However, the FPDs in the MEA recordings differed by a maximum of only 20% between the groups and thus resembled more of the differences in clinical ECG data from LQT2 patients and healthy individuals (Fodstad et al., 2006). The two previous LQT2-CM studies also reported an agreement between ECG and MEA data (Itzhaki et al., 2011; Matsa et al., 2011) as well as more prolonged (up to 2.5 fold) repolarization in single cells. This led us to postulate that there may be a compensatory mechanism in the cardiac syncytia.

6.3.3 Drug testing with long QT syndrome cardiomyocytes (IV)

The hiPSC-CMs had more deviation in the BR than the hESC-CMs. Within all of the lines, however, isoprenaline increased the BR and showed a saturating effect after 80 nM. This observation was in accordance with previous studies from our group, as this concentration has previously been shown to increase the BR in hESC-CMs (Pekkanen-Mattila et al., 2009).

The LQT1-CMs had a more prolonged repolarization than controls when exposed to higher than clinically relevant concentrations of cisapride. This might suggest that LQT1-CMs are more vulnerable to hERG block than control CMs. Previous studies have reported approximately 20% relative cFPD prolongation in hESC-CMs at 100 nM, which is in the therapeutic range, (Caspi et al., 2009) and up to 200% at higher than therapeutic concentrations (Braam et al., 2010). The effects

of erythromycin on the prolongation of ΔcFPD varied among the cell lines in our study, but nonetheless caused prolongation in all of them, which was expected as it has led to QT prolongation (Shaffer et al., 2002). The 19-24% ΔcFPD prolongation in hESC-CMs at 6-10 μM sotalol concentrations was in accordance with previous reports of 20% prolongation in hESC-CMs at 1.8-14 μM (Braam et al., 2010) and up to 60% prolongations with concentrations up to 200-400 μM (Caspi et al., 2009). Exposing the cardiomyocytes to quinidine resulted in bigger prolongations in all lines even at the therapeutically relevant concentrations. Previously published prolongation values for hESC-CMs vary between 20 and 50% (Braam et al., 2010; Caspi et al., 2009), which corresponds to the values observed in our study. Caspi and colleagues have previously reported ΔcFPD prolongation of approximately 30% for hESC-CMs with 8 μM quinidine exposure, which is similar to our results. The hERG channel blocker E-4031 prolonged repolarization in all lines and also caused adverse effects. Braam and colleagues have also previously reported EADs at micromolar E-4031 concentrations (Braam et al., 2010), which is in line with our results from hESC-CMs, although we noted EADs and pauses at concentrations as low as 10 nM and 100 nM in LQT-CMs.

The difference in the beating rates of hPSC-CMs may reflect the differences related to atrial and ventricular CMs, with the fast-beating CMs being more atrial-like (Asp et al., 2010). We noted a high variability in the BR of the spontaneously beating control and LQT1 and -2-CMs. Taking into consideration that these CM subtypes have different ion channel compositions, the drug responses in our studies might reflect the atrial versus ventricular compositions in the beating foci and the responses of different cardiomyocyte subtypes to the same drug. The hESC-CMs had a more consistent and physiological beating rate and therefore were in agreement with previously published reports. These subtype- and mutation-dependent drug responses might be affected by the differences in their repolarization reserve (Roden, 1998), which might, along with the cardiomyocyte subtype variation, explain these different drug responses. The challenge in this system is to differentiate enough CMs from the patient-specific hiPSC lines to choose the beating foci with an appropriate BR.

6.3.4 Outlook for patient-specific long QT syndrome cardiomyocytes in research (III, IV)

As stated previously, most of the LQTS mutation carriers are unaware of their mutation (i.e., they have latent LQT2). The two previous LQT2 *in vitro* models were generated from highly symptomatic patients whereas in our study the patient had a

mild LQT2. While the studies by Itzhaki and colleagues and Matsa and colleagues highlight the successful creation of an *in vitro* model, it might be more practical to study *in vitro* models of mild or even latent LQT2; this might represent the general LQT2 patient population more accurately and, according to our results, this phenotype can also be teased out *in vitro*. Finland is in advantageous position in the sense that we can potentially collect a large amount of data on the effects of one mutation type in multiple patients because of the founder mutation effect. This should help in determining the putative modifiers of the LQTS phenotype. It will also be interesting to study drug effects on latent LQTS to see if particular drugs might have more deleterious effects in combination with the mutation.

In conclusion, hiPSC-derived cardiomyocytes from an LQT2 patient displayed the disease cardiac phenotype in cell culture conditions even though the patient was relatively asymptomatic. This model provides an additional platform to study the basic pathology of LQTS and to individualize drug treatment in a patient-specific manner. It also provides the means to explore the differences between clinical patients and mutation carriers and to scan the cardiac effects of different drugs on both.

Taken together, the results from our studies indicate that patient-specific LQT-CMs derived from LQT1 and -2 patients recapitulate the phenotype *in vitro*, namely, delayed cardiac repolarization, and that these patient-specific CMs can likely, upon refinement, be used to generate robust cellular human *in vitro* models for drug testing. Drug testing with LQTS-CMs generated from donors with mild or latent LQTS could be beneficial, especially in the Finnish population, as many mutation carriers are unaware that they are carriers for these mutations with a subclinical phenotype. Consequently, the patients may experience a severe adverse reaction only after being prescribed a drug that is potentially life-threatening for LQTS patients.

However, there are still challenges related to this hiPSC strategy. One challenge is that while we can generate patient-specific hiPSC lines rather easily, the validation of these lines and the pluripotency assays are still very time-consuming, thus limiting the time frame for downstream applications such as drug testing. Another challenge is providing proper controls. Ideally, the best control would have the same genetic background as the patient-specific hiPSc line. To this end, the genetic mutation in the patient-specific hiPSC line could be corrected using gene technology, or specific mutations could be introduced to WT hiPSC or hESC lines. This is however also very time-consuming and requires expertise and validation of the cells lines and their genetics.

6.4 Future perspectives

The ultimate goals for hPSC applications are in regenerative medicine, disease modeling and preclinical drug testing. All of these goals present crucial steps in bringing these fields to the next level for more accurate treatments and for safer, efficacious drugs. While academia can often provide the basic proof-of-concept studies for these applications, the full-scale realization of these goals often requires investing a large amount of capital. Close-knit, multidisciplinary academia-industry collaborations are likely to be important for success. These goals require plenty of hard work and large financial investments but promise to produce immense medical advancements and possibly relative economical savings.

While hiPSCs can be a reliable source of material for disease modeling and pharmacotoxicological applications, the currently widely used and successful reprogramming strategy developed by Dr. Yamanaka's research group (Takahashi et al., 2007) curb their use in applications requiring transplantation into a host due to retroviral integration into the recipient genome. This is of concern because, at least in mouse iPSC (miPSC), the differentiated secondary neurospheres (SNS) were found to cause teratomas upon transplantation into mice. The teratoma-forming propensity of SNS varied depending on the origin of tissue from which the miPSCs were derived, and the highest propensity was with miPSCs reprogrammed from mouse tail-tip fibroblasts (Miura et al., 2009). In addition, the time frame of deriving hiPSCs and their subsequent differentiation into functional, specialized cells might be too long for some acute conditions like myocardial infarction (MI). To this end, direct reprogramming of dermal fibroblasts into specialized subtypes, for example, might overcome this issue. Direct reprogramming of mouse fibroblasts into induced cardiomyocytes (iCMs) using *Gata4*, *Mef2c*, and *Tbx5* transgenes has already been reported (Ieda et al., 2010), and this work might lay the foundation for future work aimed for regenerative medicine applications in MI. Currently, however, in the MI treatment context, this strategy suffers from the same retroviral integration issues as the hiPSC approach.

All of these aforementioned examples of current hPSC research fall under the concepts of human spare parts or novel disease models and preclinical pharmaceutical testing. This early progress provides cautious optimism for new treatment options and improved discovery of novel drugs for patients suffering from currently difficult-to-treat diseases. Certainly there is great anticipation of progress in regenerative medicine taking place perhaps even within the next decade. Only time will tell whether the regenerative medicine applications become a reality, but,

at the least, important initial advances have been made in disease modeling and drug testing.

7. Conclusions

The aim of this thesis was to study the EB differentiation of hESCs and their cardiomyocyte derivatives and to study the electrophysiological properties and pharmacological responses of the hPSC-derived cardiomyocytes. Based on the four studies presented here the following conclusions can be made:

- hESCs were able to differentiate into functional, spontaneously beating cardiomyocytes, but did so with different propensities depending on the hESC line. During the cardiac differentiation they expressed endo-, meso-, and ectodermal as well as cardiac protein markers in specific regions of the embryoid bodies.
- Spontaneously beating hESC-CM aggregates had field potential properties that differed from those of NRC monolayers due to their three-dimensional nature. Using our custom-made analysis program, the hESC-CM and NRC field potentials could be averaged for more accurate analysis of their properties, such as field potential duration and peak-to-peak interval, by generating higher quality cardiac FP signals.
- Using hiPSC technology, we established LQT1- and LQT2-specific stem cell lines, and the cardiomyocytes derived from them harbored the genetic mutations affecting their electrophysiological properties. The LQT2-cardiomyocytes recapitulated the disease phenotype *in vitro*, and this was observed as prolonged cardiac repolarization.
- The cardioactive effects of different drugs could be investigated using the hiPSC-derived control and LQTS cardiomyocytes. The LQT1- and LQT2-cardiomyocytes had more of adverse drug effects than controls. Thus, these cells can be used as *in vitro* models of LQTS and they can perhaps be used to tailor medication for individual use.

Acknowledgements

These studies were funded by the Finnish Cultural Foundation, the Academy of Finland, the Finnish Funding Agency for Technology and Innovation (TEKES), the Finnish Cardiovascular Research Foundation, Biocenter Finland and the Competitive Research Funding of Pirkanmaa Hospital District. The MEA system was funded by BioneXt, Tampere, Finland.

I would like to thank all the personnel at former Regea – Institute for Regenerative Medicine, now a part of the Institute of Biomedical Technology and BioMediTech, and especially its hESC maintenance laboratory members. I particularly thank the whole heart team and its past and present members for providing such a nice work environment. Special thanks to Erja Kerkelä, PhD and Mari Pekkanen-Mattila, PhD for all their guidance – especially in the beginning when I started at Regea. Thanks to Bachelor of Laboratory Services Henna Venäläinen for all her technical help and Anna Lahti, MSc in the LQT projects. Naturally, I'd like to extend a very warm thank you to our group leader and my supervisor Docent Katriina Aalto-Setälä, MD, PhD for all her guidance in my work, her advice on science and of course for providing interesting projects to work on.

Thanks to professor Outi Hovatta for kindly providing the HS hESC lines and to professor Christine Mummery for kindly providing the END-2 cells. Thanks to professor Markku Pelto-Huikko and lab. tech. Ulla Jukarainen for all their work on the tissue microarray to stain and study the embryoid body development. I'd also like to thank Zaida C. Jimenez for all the programming she did to study the cardiomyocyte field potential recordings. Thanks to Heini Huhtala for help with statistical analyses. Also I'd like to thank Juho Väisänen D.Tech; Jarno M.A. Tanskanen, D.Tech and professor Jari Hyttinen for their help in analyzing the microelectrode array cardiomyocyte recordings.

Thanks to Hugh Chapman, Ari-Pekka Koivisto, Kimmo Kontula, Heikki Swan, Bruce R. Conclin, Shinya Yamanaka, and Olli Silvennoinen for their help in the hiPS cell project so that we could generate and study the long QT syndrome - specific cardiomyocytes.

I'd also like to thank my thesis committee: Professor Jari Hyttinen and Docent Heli Skottman, PhD and my thesis reviewers: Docent Mika Laine and Dr. Robert Passier.

Big thanks to my family for all their support and especially my dear mother who is ever so positive and of course to my brother Antti. Thanks to my in-laws: Tuula and Linda Sundberg, Mika and Heidi Selin, and of course little Henrik. I'd also like to express my sincere gratitude to Seppo Sundberg, whom it was a great privilege to know and who will always be someone to look up to.

Finally, with all my heart and love I'd like to thank my beautiful and brilliant wife Maria Sundberg. You truly are my inspiration. In personal life I love you for all the joy you've brought to my life and in science I'm always inspired by our discussions. Thank you, my love!

"Nothing in biology makes sense except in the light of evolution."
-Theodosius Dobzhansky

References

Abbott GW, Sesti F, Splawski I, Buck ME, Lehmann MH, Timothy KW, Keating MT, Goldstein SAN (1999): MiRP1 Forms IKr Potassium Channels with HERG and Is Associated with Cardiac Arrhythmia. Cell 97: 175-187.

Abu-Issa R, Kirby ML (2007): Heart field: from mesoderm to heart tube. Annu Rev Cell Dev Biol 23: 45-68.

Adewumi O, Aflatoonian B, Ahrlund-Richter L, Amit M, Andrews PW, Beighton G, Bello PA, Benvenisty N, Berry LS, Bevan S, Blum B, Brooking J, Chen KG, Choo AB, Churchill GA, Corbel M, Damjanov I, Draper JS, Dvorak P, Emanuelsson K, Fleck RA, Ford A, Gertow K, Gertsenstein M, Gokhale PJ, Hamilton RS, Hampl A, Healy LE, Hovatta O, Hyllner J, Imreh MP, Itskovitz-Eldor J, Jackson J, Johnson JL, Jones M, Kee K, King BL, Knowles BB, Lako M, Lebrin F, Mallon BS, Manning D, Mayshar Y, McKay RD, Michalska AE, Mikkola M, Mileikovsky M, Minger SL, Moore HD, Mummery CL, Nagy A, Nakatsuji N, O'Brien CM, Oh SK, Olsson C, Otonkoski T, Park KY, Passier R, Patel H, Patel M, Pedersen R, Pera MF, Piekarczyk MS, Pera RA, Reubinoff BE, Robins AJ, Rossant J, Rugg-Gunn P, Schulz TC, Semb H, Sherrer ES, Siemen H, Stacey GN, Stojkovic M, Suemori H, Szatkiewicz J, Turetsky T, Tuuri T, van den Brink S, Vintersten K, Vuoristo S, Ward D, Weaver TA, Young LA, Zhang W (2007): Characterization of human embryonic stem cell lines by the International Stem Cell Initiative. Nat Biotechnol 25: 803-816.

Amit M, Carpenter MK, Inokuma MS, Chiu CP, Harris CP, Waknitz MA, Itskovitz-Eldor J, Thomson JA (2000): Clonally derived human embryonic stem cell lines maintain pluripotency and proliferative potential for prolonged periods of culture. Dev Biol 227: 271-278.

Andersson H, Steel D, Asp J, Dahlenborg K, Jonsson M, Jeppsson A, Lindahl A, Kagedal B, Sartipy P, Mandenius CF (2010): Assaying cardiac biomarkers for toxicity testing using biosensing and cardiomyocytes derived from human embryonic stem cells. J Biotechnol 150: 175-181.

Anton R, Kuhl M, Pandur P (2007): A molecular signature for the "master" heart cell. Bioessays 29: 422-426.

Aoi T, Yae K, Nakagawa M, Ichisaka T, Okita K, Takahashi K, Chiba T, Yamanaka S (2008): Generation of Pluripotent Stem Cells from Adult Mouse Liver and Stomach Cells. Science: 1154884.

Asp J, Steel D, Jonsson M, Ameen C, Dahlenborg K, Jeppsson A, Lindahl A, Sartipy P (2010): Cardiomyocyte clusters derived from human embryonic stem cells share similarities with human heart tissue. Journal of Molecular Cell Biology 2: 276-283.

Bauman JL, Bauernfeind RA, Hoff JV, Strasberg B, Swiryn S, Rosen KM (1984): Torsade de pointes due to quinidine: Observations in 31 patients. American Heart Journal 107: 425-430.

Bauwens CL, Peerani R, Niebruegge S, Woodhouse KA, Kumacheva E, Husain M, Zandstra PW (2008): Control of human embryonic stem cell colony and aggregate size heterogeneity influences differentiation trajectories. Stem Cells 26: 2300-2310.

Beqqali A, Kloots J, Ward-van Oostwaard D, Mummery C, Passier R (2006): Genome-wide transcriptional profiling of human embryonic stem cells differentiating to cardiomyocytes. Stem Cells 24: 1956-1967.

Berdondini L, van der Wal PD, Guenat O, de Rooij NF, Koudelka-Hep M, Seitz P, Kaufmann R, Metzler P, Blanc N, Rohr S (2005): High-density electrode array for

imaging in vitro electrophysiological activity. Biosensors and Bioelectronics 21: 167-174.
Bettiol E, Sartiani L, Chicha L, Krause KH, Cerbai E, Jaconi ME (2007): Fetal bovine serum enables cardiac differentiation of human embryonic stem cells. Differentiation 75: 669-681.
Bode G, Olejniczak K (2002): ICH Topic: The draft ICH S7B step 2: Note for guidance on safety pharmacology studies for human pharmaceuticals. Fundamental & Clinical Pharmacology 16: 105-118.
Bongso A, Fong C-Y, Ng S-C, Ratnam S (1994): Fertilization and early embryology: Isolation and culture of inner cell mass cells from human blastocysts. Human Reproduction 9: 2110-2117.
Braam SR, Denning C, Matsa E, Young LE, Passier R, Mummery CL (2008): Feeder-free culture of human embryonic stem cells in conditioned medium for efficient genetic modification. Nat Protoc 3: 1435-1443.
Braam SR, Tertoolen L, van de Stolpe A, Meyer T, Passier R, Mummery CL (2010): Prediction of drug-induced cardiotoxicity using human embryonic stem cell-derived cardiomyocytes. Stem Cell Research 4: 107-116.
Briggs R, King TJ (1952): Transplantation of Living Nuclei From Blastula Cells into Enucleated Frogs' Eggs. Proc Natl Acad Sci U S A 38: 455-463.
Bruneau BG, Nemer G, Schmitt JP, Charron F, Robitaille L, Caron S, Conner DA, Gessler M, Nemer M, Seidman CE, Seidman JG (2001): A Murine Model of Holt-Oram Syndrome Defines Roles of the T-Box Transcription Factor Tbx5 in Cardiogenesis and Disease. Cell 106: 709-721.
Bu L, Jiang X, Martin-Puig S, Caron L, Zhu S, Shao Y, Roberts DJ, Huang PL, Domian IJ, Chien KR (2009): Human ISL1 heart progenitors generate diverse multipotent cardiovascular cell lineages. Nature 460: 113-117.
Buckingham M, Meilhac S, Zaffran S (2005): Building the mammalian heart from two sources of myocardial cells. Nat Rev Genet 6: 826-835.
Burridge PW, Anderson D, Priddle H, Barbadillo Munoz MD, Chamberlain S, Allegrucci C, Young LE, Denning C (2007): Improved human embryonic stem cell embryoid body homogeneity and cardiomyocyte differentiation from a novel V-96 plate aggregation system highlights interline variability. Stem Cells 25: 929-938.
Bussek A, Wettwer E, Christ T, Lohmann H, Camelliti P, Ravens U (2009): Tissue slices from adult mammalian hearts as a model for pharmacological drug testing. Cell Physiol Biochem 24: 527-536.
Carlsson L (2006): In vitro and in vivo models for testing arrhythmogenesis in drugs. J Intern Med 259: 70-80.
Caspi O, Itzhaki I, Kehat I, Gepstein A, Arbel G, Huber I, Satin J, Gepstein L (2009): In vitro electrophysiological drug testing using human embryonic stem cell derived cardiomyocytes. Stem Cells and Development 18: 161-172.
Cavero I, Crumb W (2005): ICH S7B draft guideline on the non-clinical strategy for testing delayed cardiac repolarisation risk of drugs: a critical analysis. Expert Opinion on Drug Safety 4: 509-530.
Chang CW, Lai YS, Pawlik KM, Liu K, Sun CW, Li C, Schoeb TR, Townes TM (2009): Polycistronic lentiviral vector for "hit and run" reprogramming of adult skin fibroblasts to induced pluripotent stem cells. Stem Cells 27: 1042-1049.
Chau MD, Tuft R, Fogarty K, Bao ZZ (2006): Notch signaling plays a key role in cardiac cell differentiation. Mech Dev 123: 626-640.
Chen JN, Fishman MC (2000): Genetics of heart development. Trends Genet 16: 383-388.
Chien KR, Domian IJ, Parker KK (2008): Cardiogenesis and the complex biology of regenerative cardiovascular medicine. Science 322: 1494-1497.
Chuva de Sousa Lopes SM, Hassink RJ, Feijen A, van Rooijen MA, Doevendans PA, Tertoolen L, Brutel de la Riviere A, Mummery CL (2006): Patterning the heart, a template for human cardiomyocyte development. Dev Dyn 235: 1994-2002.

Conley BJ, Trounson AO, Mollard R (2004): Human embryonic stem cells form embryoid bodies containing visceral endoderm-like derivatives. Fetal Diagn Ther 19: 218-223.
Couderc J-P, Kaab S, Hinterseer M, McNitt S, Xia X, Fossa A, Beckmann BM, Polonsky S, Zareba W (2009): Baseline Values and Sotalol-Induced Changes of Ventricular Repolarization Duration, Heterogeneity, and Instability in Patients With a History of Drug-Induced Torsades de Pointes. The Journal of Clinical Pharmacology 49: 6-16.
Curran ME, Splawski I, Timothy KW, Vincen GM, Green ED, Keating MT (1995): A molecular basis for cardiac arrhythmia: HERG mutations cause long QT syndrome. Cell 80: 795-803.
Darpö B (2001): Spectrum of drugs prolonging QT interval and the incidence of torsades de pointes. European Heart Journal Supplements 3: K70-K80.
Davis RL, Weintraub H, Lassar AB (1987): Expression of a single transfected cDNA converts fibroblasts to myoblasts. Cell 51: 987-1000.
Dolnikov K, Shilkrut M, Zeevi-Levin N, Danon A, Gerecht-Nir S, Itskovitz-Eldor J, Binah O (2005): Functional properties of human embryonic stem cell-derived cardiomyocytes. Annals of the New York Academy of Sciences 1047: 66-75.
Domian IJ, Chiravuri M, van der Meer P, Feinberg AW, Shi X, Shao Y, Wu SM, Parker KK, Chien KR (2009): Generation of functional ventricular heart muscle from mouse ventricular progenitor cells. Science 326: 426-429.
Edvardsson N, Hirsch I, Emanuelsson H, Pontén J, Olsson SB (1980): Sotalol-induced delayed ventricular repolarization in man. European Heart Journal 1: 335-343.
Egert U, Knott T, Schwarz C, Nawrot M, Brandt A, Rotter S, Diesmann M (2002): MEA-Tools: an open source toolbox for the analysis of multi-electrode data with MATLAB. J Neurosci Methods 117: 33-42.
EMEA (2008). Guideline on repeated dose toxicity. In: European Medicines Agency editor.
Evans MJ, Kaufman MH (1981): Establishment in culture of pluripotential cells from mouse embryos. Nature 292: 154-156.
Fenichel RR, Malik M, Antzelevitch C, Sanguinetti M, Roden DM, Priori SG, Ruskin JN, Lipicky RJ, Cantilena LR, Independent Academic Task F (2004): Drug-Induced Torsades de Pointes and Implications for Drug Development. Journal of Cardiovascular Electrophysiology 15: 475-495.
Finlayson K, Witchel HJ, McCulloch J, Sharkey J (2004): Acquired QT interval prolongation and HERG: implications for drug discovery and development. Eur J Pharmacol 500: 129-142.
Fodstad H, Swan H, Laitinen P, Piippo K, Paavonen K, Viitasalo M, Toivonen L, Kontula K (2004): Four potassium channel mutations account for 73% of the genetic spectrum underlying long-QT syndrome (LQTS) and provide evidence for a strong founder effect in Finland. Ann Med 36 Suppl 1: 53-63.
Fodstad H, Bendahhou S, Rougier JS, Laitinen-Forsblom PJ, Barhanin J, Abriel H, Schild L, Kontula K, Swan H (2006): Molecular characterization of two founder mutations causing long QT syndrome and identification of compound heterozygous patients. Ann Med 38: 294-304.
Forte G, Carotenuto F, Pagliari F, Pagliari S, Cossa P, Fiaccavento R, Ahluwalia A, Vozzi G, Vinci B, Serafino A, Rinaldi A, Traversa E, Carosella L, Minieri M, Di Nardo P (2008): Criticality of the Biological and Physical Stimuli Array Inducing Resident Cardiac Stem Cell Determination. Stem Cells: 2008-0061.
Fujita J, Crane AM, Souza MK, Dejosez M, Kyba M, Flavell RA, Thomson JA, Zwaka TP (2008): Caspase activity mediates the differentiation of embryonic stem cells. Cell Stem Cell 2: 595-601.
Gai H, Leung EL-H, Costantino PD, Aguila JR, Nguyen DM, Fink LM, Ward DC, Ma Y (2009): Generation and characterization of functional cardiomyocytes using induced pluripotent stem cells derived from human fibroblasts. Cell Biology International 33: 1184-1193.
Graichen R, Xu X, Braam SR, Balakrishnan T, Norfiza S, Sieh S, Soo SY, Tham SC, Mummery C, Colman A, Zweigerdt R, Davidson BP (2007): Enhanced

cardiomyogenesis of human embryonic stem cells by a small molecular inhibitor of p38 MAPK. Differentiation.
Graichen R, Xu X, Braam SR, Balakrishnan T, Norfiza S, Sieh S, Soo SY, Tham SC, Mummery C, Colman A, Zweigerdt R, Davidson BP (2008): Enhanced cardiomyogenesis of human embryonic stem cells by a small molecular inhibitor of p38 MAPK. Differentiation 76: 357-370.
Guenther MG, Frampton GM, Soldner F, Hockemeyer D, Mitalipova M, Jaenisch R, Young RA (2010): Chromatin structure and gene expression programs of human embryonic and induced pluripotent stem cells. Cell Stem Cell 7: 249-257.
Guo W, Kamiya K, Toyama J (1996): Modulated expression of transient outward current in cultured neonatal rat ventricular myocytes: comparison with development in situ. Cardiovascular Research 32: 524-533.
Gupta MK, Illich DJ, Gaarz A, Matzkies M, Nguemo F, Pfannkuche K, Liang H, Classen S, Reppel M, Schultze JL, Hescheler J, Saric T (2010): Global transcriptional profiles of beating clusters derived from human induced pluripotent stem cells and embryonic stem cells are highly similar. BMC Developmental Biology 10: 98.
Gwak S-J, Bhang SH, Kim I-K, Kim S-S, Cho S-W, Jeon O, Yoo KJ, Putnam AJ, Kim B-S (2008): The effect of cyclic strain on embryonic stem cell-derived cardiomyocytes. Biomaterials 29: 844-856.
Halbach M, Pillekamp F, Brockmeier K, Hescheler J, Muller-Ehmsen J, Reppel M (2006): Ventricular slices of adult mouse hearts--a new multicellular in vitro model for electrophysiological studies. Cell Physiol Biochem 18: 1-8.
Hamill OP, Marty A, Neher E, Sakmann B, Sigworth FJ (1981): Improved patch-clamp techniques for high-resolution current recording from cells and cell-free membrane patches. European Journal of Physiology 391: 85-100.
Hannes T, Halbach M, Nazzal R, Frenzel L, Saric T, Khalil M, Hescheler J, Brockmeier K, Pillekamp F (2008): Biological pacemakers: characterization in an in vitro coculture model. J Electrocardiol 41: 562-566.
Hedley PL, Jorgensen P, Schlamowitz S, Wangari R, Moolman-Smook J, Brink PA, Kanters JK, Corfield VA, Christiansen M (2009): The genetic basis of long QT and short QT syndromes: a mutation update. Hum Mutat 30: 1486-1511.
Heidi Au HT, Cui B, Chu ZE, Veres T, Radisic M (2009): Cell culture chips for simultaneous application of topographical and electrical cues enhance phenotype of cardiomyocytes. Lab on a Chip 9: 564-575.
Hsiao EC, Yoshinaga Y, Nguyen TD, Musone SL, Kim JE, Swinton P, Espineda I, Manalac C, deJong PJ, Conklin BR (2008): Marking embryonic stem cells with a 2A self-cleaving peptide: a NKX2-5 emerald GFP BAC reporter. PLoS One 3: e2532.
Huber I, Itzhaki I, Caspi O, Arbel G, Tzukerman M, Gepstein A, Habib M, Yankelson L, Kehat I, Gepstein L (2007): Identification and selection of cardiomyocytes during human embryonic stem cell differentiation. Faseb J 21: 2551-2563.
ICH (2005a). E14: The Clinical Evaluation of QT/QTc Interval Prolongation and Proarrhythmic Potential for Non-Antiarrhythmic Drugs In: International Conference on Harmonisation editor.
ICH (2005b). S7B: The nonclinical evalution of the potential for delayed ventricular repolarization (qt interval prolongation) by human pharmaceuticals. In: International Conference on Harmonisation editor.
Ieda M, Fu J-D, Delgado-Olguin P, Vedantham V, Hayashi Y, Bruneau BG, Srivastava D (2010): Direct Reprogramming of Fibroblasts into Functional Cardiomyocytes by Defined Factors. 142: 375-386.
Itskovitz-Eldor J, Schuldiner M, Karsenti D, Eden A, Yanuka O, Amit M, Soreq H, Benvenisty N (2000): Differentiation of human embryonic stem cells into embryoid bodies compromising the three embryonic germ layers. Mol Med 6: 88-95.
Itzhaki I, Maizels L, Huber I, Zwi-Dantsis L, Caspi O, Winterstern A, Feldman O, Gepstein A, Arbel G, Hammerman H, Boulos M, Gepstein L (2011): Modelling the long QT syndrome with induced pluripotent stem cells. Nature 471: 225-259.

Jacobson MD, Weil M, Raff MC (1997): Programmed cell death in animal development. Cell 88: 347-354.

Joza N, Susin SA, Daugas E, Stanford WL, Cho SK, Li CY, Sasaki T, Elia AJ, Cheng HY, Ravagnan L, Ferri KF, Zamzami N, Wakeham A, Hakem R, Yoshida H, Kong YY, Mak TW, Zuniga-Pflucker JC, Kroemer G, Penninger JM (2001): Essential role of the mitochondrial apoptosis-inducing factor in programmed cell death. Nature 410: 549-554.

Kaji K, Norrby K, Paca A, Mileikovsky M, Mohseni P, Woltjen K (2009): Virus-free induction of pluripotency and subsequent excision of reprogramming factors. Nature 458: 771-775.

Kannankeril PJ, Roden DM, Norris KJ, Whalen SP, George JAL, Murray KT (2005): Genetic susceptibility to acquired long QT syndrome: Pharmacologic challenge in first-degree relatives. Heart Rhythm 2: 134-140.

Kattman SJ, Adler ED, Keller GM (2007): Specification of Multipotential Cardiovascular Progenitor Cells During Embryonic Stem Cell Differentiation and Embryonic Development. Trends in Cardiovascular Medicine 17: 240-246.

Kattman SJ, Witty AD, Gagliardi M, Dubois NC, Niapour M, Hotta A, Ellis J, Keller G (2011): Stage-Specific Optimization of Activin/Nodal and BMP Signaling Promotes Cardiac Differentiation of Mouse and Human Pluripotent Stem Cell Lines. Cell Stem Cell 8: 228-240.

Kehat I, Kenyagin-Karsenti D, Snir M, Segev H, Amit M, Gepstein A, Livne E, Binah O, Itskovitz-Eldor J, Gepstein L (2001): Human embryonic stem cells can differentiate into myocytes with structural and functional properties of cardiomyocytes. The Journal of Clinical Investigation 108: 407-414.

Kehat I, Gepstein A, Spira A, Itskovitz-Eldor J, Gepstein L (2002): High-Resolution Electrophysiological Assessment of Human Embryonic Stem Cell-Derived Cardiomyocytes: A Novel In Vitro Model for the Study of Conduction. Circ Res 91: 659-661.

Kim C, Majdi M, Xia P, Wei KA, Talantova M, Spiering S, Nelson B, Mercola M, Chen H-sV (2009a): Non-Cardiomyocytes Influence the Electrophysiological Maturation of Human Embryonic Stem Cell-Derived Cardiomyocytes During Differentiation. Stem Cells and Development 19: 783-795.

Kim D, Kim CH, Moon JI, Chung YG, Chang MY, Han BS, Ko S, Yang E, Cha KY, Lanza R, Kim KS (2009b): Generation of human induced pluripotent stem cells by direct delivery of reprogramming proteins. Cell Stem Cell 4: 472-476.

Kim JB, Zaehres H, Wu G, Gentile L, Ko K, Sebastiano V, Arauzo-Bravo MJ, Ruau D, Han DW, Zenke M, Scholer HR (2008): Pluripotent stem cells induced from adult neural stem cells by reprogramming with two factors. Nature 454: 646-650.

Kim SE, Kim BK, Gil JE, Kim SK, Kim JH (2007): Comparative analysis of the developmental competence of three human embryonic stem cell lines in vitro. Mol Cells 23: 49-56.

Kita-Matsuo H, Barcova M, Prigozhina N, Salomonis N, Wei K, Jacot JG, Nelson B, Spiering S, Haverslag R, Kim C, Talantova M, Bajpai R, Calzolari D, Terskikh A, McCulloch AD, Price JH, Conklin BR, Chen HS, Mercola M (2009): Lentiviral vectors and protocols for creation of stable hESC lines for fluorescent tracking and drug resistance selection of cardiomyocytes. PLoS One 4: e5046.

Klimanskaya I, Rosenthal N, Lanza R (2008): Derive and conquer: sourcing and differentiating stem cells for therapeutic applications. Nat Rev Drug Discov 7: 131-142.

Laflamme MA, Chen KY, Naumova AV, Muskheli V, Fugate JA, Dupras SK, Reinecke H, Xu C, Hassanipour M, Police S, O'Sullivan C, Collins L, Chen Y, Minami E, Gill EA, Ueno S, Yuan C, Gold J, Murry CE (2007): Cardiomyocytes derived from human embryonic stem cells in pro-survival factors enhance function of infarcted rat hearts. Nature Biotechnology 25: 1015-1024.

Lappalainen RS, Salomäki M, Ylä-Outinen L, Heikkilä TJ, Hyttinen JAK, Pihlajamäki H, Suuronen R, Skottman H, Narkilahti S (2010): Similarly derived and cultured hESC

lines show variation in their developmental potential towards neuronal cells in long-term culture. Regenerative Medicine 5: 749-762.
Lehtonen A, Fodstad H, Laitinen-Forsblom P, Toivonen L, Kontula K, Swan H (2007): Further evidence of inherited long QT syndrome gene mutations in antiarrhythmic drug-associated torsades de pointes. Heart Rhythm 4: 603-607.
Lexchin J (2005): Drug withdrawals from the Canadian market for safety reasons, 1963-2004. Cmaj 172: 765-767.
Liang H, Matzkies M, Schunkert H, Tang M, Bonnemeier H, Hescheler J, Reppel M (2010): Human and murine embryonic stem cell-derived cardiomyocytes serve together as a valuable model for drug safety screening. Cell Physiol Biochem 25: 459-466.
Lin Q, Schwarz J, Bucana C, N. Olson E (1997): Control of Mouse Cardiac Morphogenesis and Myogenesis by Transcription Factor MEF2C. Science 276: 1404-1407.
Lister R, Pelizzola M, Kida YS, Hawkins RD, Nery JR, Hon G, Antosiewicz-Bourget J, O'Malley R, Castanon R, Klugman S, Downes M, Yu R, Stewart R, Ren B, Thomson JA, Evans RM, Ecker JR (2011): Hotspots of aberrant epigenomic reprogramming in human induced pluripotent stem cells. Nature 471: 68-73.
Livak KJ, Schmittgen TD (2001): Analysis of relative gene expression data using real-time quantitative PCR and the 2(-Delta Delta C(T)) Method. Methods 25: 402-408.
Lough J, Sugi Y (2000): Endoderm and heart development. Dev Dyn 217: 327-342.
Lu HR, Vlaminckx E, Hermans AN, Rohrbacher J, Van Ammel K, Towart R, Pugsley M, Gallacher DJ (2008): Predicting drug-induced changes in QT interval and arrhythmias: QT-shortening drugs point to gaps in the ICHS7B Guidelines. Br J Pharmacol 154: 1427-1438.
Mandenius CF, Steel D, Noor F, Meyer T, Heinzle E, Asp J, Arain S, Kraushaar U, Bremer S, Class R, Sartipy P (2011): Cardiotoxicity testing using pluripotent stem cell-derived human cardiomyocytes and state-of-the-art bioanalytics: a review. J Appl Toxicol 31: 191-205.
Marjamaa A, Salomaa V, Newton-Cheh C, Porthan K, Reunanen A, Karanko H, Jula A, Lahermo Pi, VÃ¤Ã¤nÃ¤nen H, Toivonen L, Swan H, Viitasalo M, Nieminen MS, Peltonen L, Oikarinen L, Palotie A, Kontula K (2009a): High prevalence of four long QT syndrome founder mutations in the Finnish population. Annals of Medicine 41: 234 - 240.
Marjamaa A, Salomaa V, Newton-Cheh C, Porthan K, Reunanen A, Karanko H, Jula A, Lahermo Pi, VÃ¤Ã¤nÃ¤nen H, Toivonen L, Swan H, Viitasalo M, Nieminen MS, Peltonen L, Oikarinen L, Palotie A, Kontula K (2009b): High prevalence of four long QT syndrome founder mutations in the Finnish population. Annals of Medicine 41: 234-240.
Martin GR (1981): Isolation of a pluripotent cell line from early mouse embryos cultured in medium conditioned by teratocarcinoma stem cells. Proc Natl Acad Sci U S A 78: 7634-7638.
Martin RL, McDermott JS, Salmen HJ, Palmatier J, Cox BF, Gintant GA (2004): The utility of hERG and repolarization assays in evaluating delayed cardiac repolarization: influence of multi-channel block. J Cardiovasc Pharmacol 43: 369-379.
Matsa E, Rajamohan D, Dick E, Young L, Mellor I, Staniforth A, Denning C (2011): Drug evaluation in cardiomyocytes derived from human induced pluripotent stem cells carrying a long QT syndrome type 2 mutation. European Heart Journal 32: 952-962.
Mayshar Y, Ben-David U, Lavon N, Biancotti J-C, Yakir B, Clark AT, Plath K, Lowry WE, Benvenisty N (2010): Identification and Classification of Chromosomal Aberrations in Human Induced Pluripotent Stem Cells. Cell Stem Cell 7: 521-531.
Mehta A, Chung YY, Ng A, Iskandar F, Atan S, Wei H, Dusting G, Sun W, Wong P, Shim W (2011): Pharmacological response of human cardiomyocytes derived from virus-free induced pluripotent stem cells. Cardiovascular Research Epub ahead of print.
Meilhac SnM, Esner M, Kelly RG, Nicolas J-Fo, Buckingham ME (2004): The Clonal Origin of Myocardial Cells in Different Regions of the Embryonic Mouse Heart. Developmental Cell 6: 685-698.

Meyer T, Boven KH, Gunther E, Fejtl M (2004): Micro-electrode arrays in cardiac safety pharmacology: a novel tool to study QT interval prolongation. Drug Safety 27: 763-772.
Miura K, Okada Y, Aoi T, Okada A, Takahashi K, Okita K, Nakagawa M, Koyanagi M, Tanabe K, Ohnuki M, Ogawa D, Ikeda E, Okano H, Yamanaka S (2009): Variation in the safety of induced pluripotent stem cell lines. Nat Biotechnol 27: 743-745.
Miyazaki H, Watanabe H, Kitayama T, Nishida M, Nishi Y, Sekiya K, Suganami H, Yamamoto K (2005): QT PRODACT: sensitivity and specificity of the canine telemetry assay for detecting drug-induced QT interval prolongation. J Pharmacol Sci 99: 523-529.
Mohr JC, Zhang J, Azarin SM, Soerens AG, de Pablo JJ, Thomson JA, Lyons GE, Palecek SP, Kamp TJ (2010): The microwell control of embryoid body size in order to regulate cardiac differentiation of human embryonic stem cells. Biomaterials 31: 1885-1893.
Moretti A, Bellin M, Jung CB, Thies T-M, Takashima Y, Bernshausen A, Schiemann M, Fischer S, Moosmang S, Smith AG, Lam JT, Laugwitz K-L (2010a): Mouse and human induced pluripotent stem cells as a source for multipotent Isl1+ cardiovascular progenitors. The FASEB Journal 24: 700-711.
Moretti A, Bellin M, Welling A, Jung CB, Lam JT, Bott-Flugel L, Dorn T, Goedel A, Hohnke C, Hofmann F, Seyfarth M, Sinnecker D, Schomig A, Laugwitz KL (2010b): Patient-specific induced pluripotent stem-cell models for long-QT syndrome. N Engl J Med 363: 1397-1409.
Mountford JC (2008): Human embryonic stem cells: origins, characteristics and potential for regenerative therapy. Transfusion Medicine 18: 1-12.
Mummery C, Ward-van Oostwaard D, Doevendans P, Spijker R, van den Brink S, Hassink R, van der Heyden M, Opthof T, Pera M, de la Riviere AB, Passier R, Tertoolen L (2003): Differentiation of Human Embryonic Stem Cells to Cardiomyocytes: Role of Coculture With Visceral Endoderm-Like Cells. Circulation 107: 2733-2740.
Mummery CL, van Achterberg TA, van den Eijnden-van Raaij AJ, van Haaster L, Willemse A, de Laat SW, Piersma AH (1991): Visceral-endoderm-like cell lines induce differentiation of murine P19 embryonal carcinoma cells. Differentiation 46: 51-60.
Musunuru K, Domian IJ, Chien KR (2010): Stem Cell Models of Cardiac Development and Disease. Annual Review of Cell and Developmental Biology 26: 667-687.
Männikkö R, Overend G, Perrey C, Gavaghan CL, Valentin JP, Morten J, Armstrong M, Pollard CE (2010): Pharmacological and electrophysiological characterization of nine, single nucleotide polymorphisms of the hERG-encoded potassium channel. British Journal of Pharmacology 159: 102-114.
Nakagawa M, Koyanagi M, Tanabe K, Takahashi K, Ichisaka T, Aoi T, Okita K, Mochiduki Y, Takizawa N, Yamanaka S (2008): Generation of induced pluripotent stem cells without Myc from mouse and human fibroblasts. Nat Biotechnol 26: 101-106.
Nakajima T, Furukawa T, Tanaka T, Katayama Y, Nagai R, Nakamura Y, Hiraoka M (1998): Novel Mechanism of HERG Current Suppression in LQT2 : Shift in Voltage Dependence of HERG Inactivation. Circ Res 83: 415-422.
Nelson TJ, Faustino RS, Chiriac A, Crespo-Diaz R, Behfar A, Terzic A (2008): CXCR4+/FLK-1+ Biomarkers Select a Cardiopoietic Lineage from Embryonic Stem Cells. Stem Cells 26: 1464-1473.
Nemer M (2008): Genetic insights into normal and abnormal heart development. Cardiovascular Pathology 17: 48-54.
Nerbonne JM, Kass RS (2005): Molecular physiology of cardiac repolarization. Physiological Reviews 85: 1205-1253.
Niebruegge S, Bauwens CL, Peerani R, Thavandiran N, Masse S, Sevaptisidis E, Nanthakumar K, Woodhouse K, Husain M, Kumacheva E, Zandstra PW (2008): Generation of human embryonic stem cell-derived mesoderm and cardiac cells using size-specified aggregates in an oxygen-controlled bioreactor. Biotechnol Bioeng.
Norstrom A, Akesson K, Hardarson T, Hamberger L, Bjorquist P, Sartipy P (2006): Molecular and pharmacological properties of human embryonic stem cell-derived cardiomyocytes. Exp Biol Med (Maywood) 231: 1753-1762.

Okita K, Nakagawa M, Hyenjong H, Ichisaka T, Yamanaka S (2008): Generation of mouse induced pluripotent stem cells without viral vectors. Science 322: 949-953.

Osafune K, Caron L, Borowiak M, Martinez RJ, Fitz-Gerald CS, Sato Y, Cowan CA, Chien KR, Melton DA (2008): Marked differences in differentiation propensity among human embryonic stem cell lines. Nat Biotechnol 26: 313-315.

Palmieri SL, Peter W, Hess H, Schöler HR (1994): Oct-4 Transcription Factor Is Differentially Expressed in the Mouse Embryo during Establishment of the First Two Extraembryonic Cell Lineages Involved in Implantation. Developmental Biology 166: 259-267.

Pan J, Tompkins WJ (1985): A Real-Time QRS Detection Algorithm. Biomedical Engineering, IEEE Transactions on BME-32: 230-236.

Passier R, Mummery C (2005): Cardiomyocyte differentiation from embryonic and adult stem cells. Current Opinion in Biotechnology 16: 498-502.

Passier R, Oostwaard DW, Snapper J, Kloots J, Hassink RJ, Kuijk E, Roelen B, de la Riviere AB, Mummery C (2005): Increased cardiomyocyte differentiation from human embryonic stem cells in serum-free cultures. Stem Cells 23: 772-780.

Passier R, van Laake LW, Mummery CL (2008): Stem-cell-based therapy and lessons from the heart. Nature 453: 322-329.

Pedrazzini T (2007): Control of Cardiogenesis by the Notch Pathway. Trends in Cardiovascular Medicine 17: 83-90.

Pekkanen-Mattila M, Kerkelä E, Tanskanen JMA, Pietilä M, Pelto-Huikko M, Hyttinen J, Skottman H, Suuronen R, Aalto-Setälä K (2009): Substantial variation in the cardiac differentiation of human embryonic stem cell lines derived and propagated under the same conditions: a comparison of multiple cell lines. Annals of Medicine 41: 360-370.

Pekkanen-Mattila M, Chapman H, Kerkela E, Suuronen R, Skottman H, Koivisto AP, Aalto-Setala K (2010a): Human embryonic stem cell-derived cardiomyocytes: demonstration of a portion of cardiac cells with fairly mature electrical phenotype. Experimental Biology and Medicine 235: 522-530.

Pekkanen-Mattila M, Pelto-Huikko M, Kujala V, Suuronen R, Skottman H, Aalto-Setala K, Kerkela E (2010b): Spatial and temporal expression pattern of germ layer markers during human embryonic stem cell differentiation in embryoid bodies. Histochem Cell Biol 133: 595-606.

Peterkin T, Gibson A, Patient R (2007): Redundancy and evolution of GATA factor requirements in development of the myocardium. Developmental Biology 311: 623-635.

Piippo K, Swan H, Pasternack M, Chapman H, Paavonen K, Viitasalo M, Toivonen L, Kontula K (2001): A founder mutation of the potassium channel KCNQ1 in long QT syndrome: implications for estimation of disease prevalence and molecular diagnostics. J Am Coll Cardiol 37: 562-568.

Pollard CE, Valentin JP, Hammond TG (2008): Strategies to reduce the risk of drug-induced QT interval prolongation: a pharmaceutical company perspective. Br J Pharmacol 154: 1538-1543.

Pollard CE, Abi Gerges N, Bridgland-Taylor MH, Easter A, Hammond TG, Valentin JP (2010): An introduction to QT interval prolongation and non-clinical approaches to assessing and reducing risk. British Journal of Pharmacology 159: 12-21.

Redfern WS, Carlsson L, Davis AS, Lynch WG, MacKenzie I, Palethorpe S, Siegl PK, Strang I, Sullivan AT, Wallis R, Camm AJ, Hammond TG (2003a): Relationships between preclinical cardiac electrophysiology, clinical QT interval prolongation and torsade de pointes for a broad range of drugs: evidence for a provisional safety margin in drug development. Cardiovasc Res 58: 32-45.

Redfern WS, Carlsson L, Davis AS, Lynch WG, MacKenzie I, Palethorpe S, Siegl PKS, Strang I, Sullivan AT, Wallis R, Camm AJ, Hammond TG (2003b): Relationships between preclinical cardiac electrophysiology, clinical QT interval prolongation and torsade de pointes for a broad range of drugs: evidence for a provisional safety margin in drug development. Cardiovasc Res 58: 32-45.

Reppel M, Pillekamp F, Lu ZJ, Halbach M, Brockmeier K, Fleischmann BK, Hescheler J (2004): Microelectrode arrays: A new tool to measure embryonic heart activity. Journal of Electrocardiology 37: 104-109.
Reppel M, Pillekamp F, Brockmeier K, Matzkies M, Bekcioglu A, Lipke T, Nguemo F, Bonnemeier H, Hescheler J (2005): The electrocardiogram of human embryonic stem cell-derived cardiomyocytes. Journal of Electrocardiology 38: 166-170.
Reppel M, Igelmund P, Egert U, Juchelka F, Hescheler J, Drobinskaya I (2007): Effect of cardioactive drugs on action potential generation and propagation in embryonic stem cell-derived cardiomyocytes. Cell Physiol Biochem 19: 213-224.
Roden DM (1998): Taking the "Idio" out of "Idiosyncratic": Predicting Torsades de Pointes. Pacing and Clinical Electrophysiology 21: 1029-1034.
Roden DM (2004): Drug-Induced Prolongation of the QT Interval. New England Journal of Medicine 350: 1013-1022.
Roden DM (2008): Long-QT Syndrome. N Engl J Med 358: 169-176.
Sachlos E, Auguste DT (2008): Embryoid body morphology influences diffusive transport of inductive biochemicals: a strategy for stem cell differentiation. Biomaterials 29: 4471-4480.
Sakmann B, Neher E (1984): Patch clamp techniques for studying ionic channels in excitable membranes. Annual Review of Physiology 46: 455-472.
Salvi V, Karnad DR, Panicker GK, Kothari S (2010): Update on the evaluation of a new drug for effects on cardiac repolarization in humans: issues in early drug development. British Journal of Pharmacology 159: 34-48.
Sartiani L, Bettiol E, Stillitano F, Mugelli A, Cerbai E, Jaconi ME (2007): Developmental changes in cardiomyocytes differentiated from human embryonic stem cells: a molecular and electrophysiological approach. Stem Cells 25: 1136-1144.
Satin J, Itzhaki I, Rapoport S, Schroder EA, Izu L, Arbel G, Beyar R, Balke CW, Schiller J, Gepstein L (2008): Calcium handling in human embryonic stem cell-derived cardiomyocytes. Stem Cells 26: 1961-1972.
Schulz M, Schmoldt A (2003): Therapeutic and toxic blood concentrations of more than 800 drugs and other xenobiotics. Pharmazie 58: 447-474.
Schwartz PJ (2001): Genotype-phenotype correlation in the long-QT syndrome: gene-specific triggers for life-threatening arrhythmias. Circulation 103: 89-95.
Shaffer D, Singer S, Korvick J, Honig P (2002): Concomitant Risk Factors in Reports of Torsades de Pointes Associated with Macrolide Use: Review of the United States Food and Drug Administration Adverse Event Reporting System. Clinical Infectious Diseases 35: 197-200.
Shimoni Y, Fiset C, Clark RB, Dixon JE, McKinnon D, Giles WR (1997): Thyroid hormone regulates postnatal expression of transient K+ channel isoforms in rat ventricle. Journal of Physiology 500: 65-73.
Silva J, Rudy Y (2003): Mechanism of Pacemaking in IK1-Downregulated Myocytes. Circulation Research 92: 261-263.
Snir M, Kehat I, Gepstein A, Coleman R, Itskovitz-Eldor J, Livne E, Gepstein L (2003): Assessment of the ultrastructural and proliferative properties of human embryonic stem cell-derived cardiomyocytes. Am J Physiol Heart Circ Physiol 285: H2355-2363.
Srivastava D (2006): Genetic regulation of cardiogenesis and congenital heart disease. Annu Rev Pathol 1: 199-213.
Srivastava D, Ivey KN (2006): Potential of stem-cell-based therapies for heart disease. Nature 441: 1097-1099.
Stadtfeld M, Nagaya M, Utikal J, Weir G, Hochedlinger K (2008): Induced pluripotent stem cells generated without viral integration. Science 322: 945-949.
Swan H, Viitasalo M, Piippo K, Laitinen P, Kontula K, Toivonen L (1999): Sinus node function and ventricular repolarization during exercise stress test in long QT syndrome patients with KvLQT1 and HERG potassium channel defects. Journal of the American College of Cardiology 34: 823-829.

Synnergren J, Akesson K, Dahlenborg K, Vidarsson H, Ameen C, Steel D, Lindahl A, Olsson B, Sartipy P (2008): Molecular signature of cardiomyocyte clusters derived from human embryonic stem cells. Stem Cells: 2007-1033.

Takahashi K, Yamanaka S (2006): Induction of Pluripotent Stem Cells from Mouse Embryonic and Adult Fibroblast Cultures by Defined Factors. Cell 126: 663-676.

Takahashi K, Tanabe K, Ohnuki M, Narita M, Ichisaka T, Tomoda K, Yamanaka S (2007): Induction of Pluripotent Stem Cells from Adult Human Fibroblasts by Defined Factors. Cell 131: 861-872.

Tanaka T, Tohyama S, Murata M, Nomura F, Kaneko T, Chen H, Hattori F, Egashira T, Seki T, Ohno Y, Koshimizu U, Yuasa S, Ogawa S, Yamanaka S, Yasuda K, Fukuda K (2009): In vitro pharmacologic testing using human induced pluripotent stem cell-derived cardiomyocytes. Biochemical and Biophysical Research Communications 385: 497-502.

Tester DJ, Ackerman MJ (2007): Postmortem Long QT Syndrome Genetic Testing for Sudden Unexplained Death in the Young. Journal of the American College of Cardiology 49: 240-246.

Thomson JA, Itskovitz-Eldor J, Shapiro SS, Waknitz MA, Swiergiel JJ, Marshall VS, Jones JM (1998): Embryonic stem cell lines derived from human blastocysts. Science 282: 1145-1147.

Tokola H, Salo K, Vuolteenaho O, Ruskoaho H (1994): Basal and acidic fibroblast growth factor-induced atrial natriuretic peptide gene expression and secretion is inhibited by staurosporine. Eur J Pharmacol 267: 195-206.

Tu E, Bagnall RD, Duflou J, Semsarian C (2011): Post-Mortem Review and Genetic Analysis of Sudden Unexpected Death in Epilepsy (SUDEP) Cases. Brain Pathology 21: 201-208.

van Noord C, Eijgelsheim M, Stricker BH (2010): Drug- and non-drug-associated QT interval prolongation. Br J Clin Pharmacol 70: 16-23.

Warren L, Manos PD, Ahfeldt T, Loh YH, Li H, Lau F, Ebina W, Mandal PK, Smith ZD, Meissner A, Daley GQ, Brack AS, Collins JJ, Cowan C, Schlaeger TM, Rossi DJ (2010): Highly efficient reprogramming to pluripotency and directed differentiation of human cells with synthetic modified mRNA. Cell Stem Cell 7: 618-630.

Watanabe K, Ueno M, Kamiya D, Nishiyama A, Matsumura M, Wataya T, Takahashi JB, Nishikawa S, Nishikawa S, Muguruma K, Sasai Y (2007): A ROCK inhibitor permits survival of dissociated human embryonic stem cells. Nat Biotechnol 25: 681-686.

Westenskow P, Splawski I, Timothy KW, Keating MT, Sanguinetti MC (2004): Compound mutations: a common cause of severe long-QT syndrome. Circulation 109: 1834-1841.

Woltjen K, Michael IP, Mohseni P, Desai R, Mileikovsky M, Hamalainen R, Cowling R, Wang W, Liu P, Gertsenstein M, Kaji K, Sung HK, Nagy A (2009): piggyBac transposition reprograms fibroblasts to induced pluripotent stem cells. Nature 458: 766-770.

Xu XQ, Graichen R, Soo SY, Balakrishnan T, Bte Rahmat SN, Sieh S, Tham SC, Freund C, Moore J, Mummery C, Colman A, Zweigerdt R, Davidson BP (2008): Chemically defined medium supporting cardiomyocyte differentiation of human embryonic stem cells. Differentiation 76: 958-970.

Yakubov E, Rechavi G, Rozenblatt S, Givol D (2010): Reprogramming of human fibroblasts to pluripotent stem cells using mRNA of four transcription factors. Biochem Biophys Res Commun 394: 189-193.

Yamanaka S, Li J, Kania G, Elliott S, Wersto R, Van Eyk J, Wobus A, Boheler K (2008): Pluripotency of embryonic stem cells. Cell and Tissue Research 331: 5-22.

Yang L, Soonpaa MH, Adler ED, Roepke TK, Kattman SJ, Kennedy M, Henckaerts E, Bonham K, Abbott GW, Linden RM, Field LJ, Keller GM (2008): Human cardiovascular progenitor cells develop from a KDR+ embryonic-stem-cell-derived population. Nature 453: 524-528.

Yazawa M, Hsueh B, Jia X, Pasca AM, Bernstein JA, Hallmayer J, Dolmetsch RE (2011): Using induced pluripotent stem cells to investigate cardiac phenotypes in Timothy syndrome. Nature 471: 230-234.

Yokoo N, Baba S, Kaichi S, Niwa A, Mima T, Doi H, Yamanaka S, Nakahata T, Heike T (2009): The effects of cardioactive drugs on cardiomyocytes derived from human induced pluripotent stem cells. Biochem Biophys Res Commun 387: 482-488.

Yu J, Vodyanik MA, Smuga-Otto K, Antosiewicz-Bourget J, Frane JL, Tian S, Nie J, Jonsdottir GA, Ruotti V, Stewart R, Slukvin II, Thomson JA (2007): Induced Pluripotent Stem Cell Lines Derived from Human Somatic Cells. Science 318: 1917-1920.

Yu J, Hu K, Smuga-Otto K, Tian S, Stewart R, Slukvin, II, Thomson JA (2009): Human induced pluripotent stem cells free of vector and transgene sequences. Science 324: 797-801.

Yuan H, Yamashita YM (2010): Germline stem cells: stems of the next generation. Current Opinion in Cell Biology 22: 730-736.

Zareba W (2007): Drug induced QT prolongation. Cardiol J 14: 523-533.

Zhang J, Wilson GF, Soerens AG, Koonce CH, Yu J, Palecek SP, Thomson JA, Kamp TJ (2009): Functional cardiomyocytes derived from human induced pluripotent stem cells. Circulation Research 104: e30-e41.

Zhou B, Ma Q, Rajagopal S, Wu SM, Domian I, Rivera-Feliciano J, Jiang D, von Gise A, Ikeda S, Chien KR, Pu WT (2008): Epicardial progenitors contribute to the cardiomyocyte lineage in the developing heart. Nature.

Zhou H, Wu S, Joo JY, Zhu S, Han DW, Lin T, Trauger S, Bien G, Yao S, Zhu Y, Siuzdak G, Scholer HR, Duan L, Ding S (2009): Generation of induced pluripotent stem cells using recombinant proteins. Cell Stem Cell 4: 381-384.

Zilberter YI, Timin EN, Bendukidze ZA, Burnashev NA (1982): Patch-voltage-clamp method for measuring fast inward current in single rat heart muscle cells. Pflugers Arch 394: 150-155.

Zwi L, Caspi O, Arbel G, Huber I, Gepstein A, Park I-H, Gepstein L (2009a): Cardiomyocyte Differentiation of Human Induced Pluripotent Stem Cells. Circulation 120: 1513-1523.

Zwi L, Caspi O, Arbel G, Huber I, Gepstein A, Park IH, Gepstein L (2009b): Cardiomyocyte differentiation of human induced pluripotent stem cells. Circulation 120: 1513-1523.

COMPUTER METHODS AND PROGRAMS IN BIOMEDICINE 104 (2011) 199–205

journal homepage: www.intl.elsevierhealth.com/journals/cmpb

Averaging *in vitro* cardiac field potential recordings obtained with microelectrode arrays

Ville J. Kujala[a,1], *Zaida C. Jimenez*[b,1], *Juho Väisänen*[b], *Jarno M.A. Tanskanen*[b], *Erja Kerkelä*[a,2], *Jari Hyttinen*[b], *Katriina Aalto-Setälä*[a,c,*]

[a] *Regea – Institute for Regenerative Medicine, University of Tampere and Tampere University Hospital, Tampere, Finland*
[b] *Department of Biomedical engineering, Tampere University of Technology, Tampere, Finland*
[c] *Heart Center, Tampere University Hospital, Tampere, Finland*

ARTICLE INFO

Article history:
Received 8 November 2010
Received in revised form
13 February 2011
Accepted 9 April 2011

Keywords:
Cardiomyocyte
Field potential
Averaging
Microelectrode array

ABSTRACT

Extracellular field potential (FP) recordings with microelectrode arrays (MEAs) from cardiomyocyte cultures offer a non-invasive way of studying the electrophysiological properties of these cells at the population level. Several studies have examined the FP properties of cardiomyocytes of various origins, including stem cell-derived cardiomyocytes. This focus reflects growing importance and interest in the field of MEA. High-quality cardiac FP signals are often difficult to obtain, especially from stem cell-derived cardiomyocyte cultures, which represent an important new field in cardiac electrophysiology. One way to improve the quality of these recordings is to average the cardiac FP signals. To date, however, no studies have examined the effect of averaging on cardiac FP signals. We report here that cardiac FP averaging can yield higher-quality signals than original individual FPs, and therefore promise more accurate detection of different phases and analysis of the cardiac FP signal. Averaged signals improved the signal-to-noise ratio (SNR), and obtaining reliable averages required approximately 50 cardiac cycles. We therefore propose that routine cardiac FP averaging can serve as a tool to compare the effects of different experimental conditions or stimuli on the properties of cardiac FPs.

1. Introduction

Extracellular field potential (FP) recordings of cardiomyocytes with microelectrode arrays (MEA) enable the study of cardiac electrophysiological properties at the population level [1]. Previous studies have shown cardiac FPD on MEA to correspond with QT interval properties in the electrocardiogram [2]. Thus, FP recordings of beating cardiomyocyte aggregates offer insight into the electrical function of myocardial tissue *in vitro* [3]. The MEA platform has served extensively in the study of cardiomyocytes of various origins, such as the chick heart [4], mouse embryonic stem cell (ESC)-derived cardiomyocytes [5], mouse induced pluripotent stem (iPS) cell-derived cardiomyocytes [6], human ESC-derived cardiomyocytes [7–9] and human induced pluripotent stem (iPS) cell-derived cardiomyocytes [10].

* *Corresponding author at*: University of Tampere, Institute for Biomedical Technology and Tampere University Hospital, Heart Center, Biokatu 12, Finn-Medi 5, FIN-33520 Tampere, Finland. Tel.: +358 40 582 9567; fax: +358 3 3551 8498.
E-mail address: katriina.aalto-setala@uta.fi (K. Aalto-Setälä).
URL: http://www.regea.fi (K. Aalto-Setälä).
[1] These authors contributed equally to this work.
[2] Current address: Finnish Red Cross, Blood Service, Helsinki, Finland.
0169-2607/$ – see front matter © 2011 Elsevier Ireland Ltd. All rights reserved.
doi:10.1016/j.cmpb.2011.04.001

Signals of good quality, especially from pluripotent stem cell-derived cardiomyocytes, are sometimes difficult to obtain. In the case of human embryonic stem cell-derived cardiomyocytes (hESC-CMs), the quality of the signal is often limited by low numbers of cardiomyocytes in the clusters. Irregular beating rhythms can also present a challenge in analysing the signals [11]. Obtaining a clear signal is crucial for determining different parameters, especially the end-point of the field potential duration (FPD), which indicates the end of repolarisation and thus the end of electrical activation in one cardiac cycle. Low signal-to-noise ratio (SNR) recordings can yield higher quality via averaging. To date, however, no studies have investigated the direct effects of averaging on cardiac FP signals.

We hypothesised that averaging several FP cycles from recordings with a stable beating rhythm would yield more accurate and reliable results than would measuring the parameter values from one or a few representative individual FP cycles. This would be especially important when poor quality due to a low signal-to-noise ration obscures identification of the end of the cardiac replolarisation phase in the FP signals. Indeed, our data suggest that averaging can serve to produce reliable results from the cardiac field potential recordings of neonatal rat cardiomyocytes (NRC) and hESC-CMs.

2. Materials and methods

2.1. *Human embryonic stem cell culture*

H7 hESCs (WiCell) were cultured on mitomycin C inactivated mouse embryonic fibroblasts (MEF) in hES medium, which consisted of DMEM/F-12 (Invitrogen) supplemented with 20% KnockOut serum replacement (Invitrogen), 1% non-essential amino acids (Lonza), 2 mM Glutamax (Invitrogen), 50 U/ml penicillin/streptomycin (Lonza), 0.1 mM beta mercaptoethanol (Invitrogen), and 7.8 ng/ml basic fibroblast growth factor (R&D Systems). The medium was refreshed daily, and the hESC colonies were passaged onto a new MEF layer once a week using 1 mg/ml collagenase IV (Invitrogen).

2.2. *Cardiomyocyte sources and field potential recordings*

hESCs were differentiated into cardiomyocytes by co-culturing them with mouse visceral endoderm-like (END-2) cells as described elsewhere [12]. The spontaneously beating cardiomyocyte aggregates were mechanically excised from the cell cultures and plated onto fetal bovine serum (30 min, Invitrogen)-coated and 0.1% gelatine (1 h, Sigma–Aldrich)-coated MEAs (Multi Channel Systems MCS GmbH). The culture medium was refreshed three times a week.

Neonatal rat cardiomyocytes (NRCs) were extracted from the hearts of newborn Sprague-Dawley rats as described elsewhere [13]. The neonatal rats were quickly decapitated, and their hearts were harvested. Cardiomyocytes were extracted with multiple rounds of collagenase treatment, preplated for 1 h at +37 °C, 5% CO_2 and plated on coated MEAs; 800,000 NRCs were plated per MEA well. The culture medium was refreshed daily.

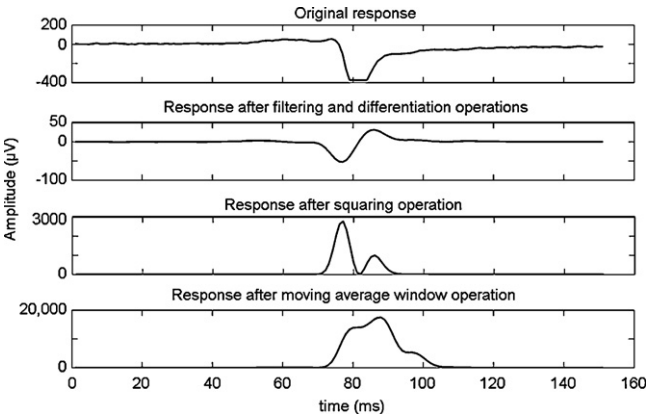

Fig. 1 – The stepwise process of the Pan–Tompkins QRS peak detection algorithm.

The FP recordings took place in room air with an MEA1060-Inv-BC amplifier using a 20-kHz sampling rate and MC_rack software (both from Multi Channel Systems MCS GmbH). Standard 200/30iR-Ti-gr MEAs were covered with a gas-permeable membrane (ALA Scientific) to keep the cultures sterile. During recordings, the temperature was kept at +37 °C using the heating element of the MEA amplifier. In drug test E-4031 (Alomone labs) was diluted in the cell culture medium for a final concentration of 600 nM. The FP signals were recorded from MEAs with NRCs ($n = 9$) and from MEAs with hESC-CMs ($n = 4$).

2.3. *Field potential averaging*

The Matlab-based analysis program was designed to obtain an average FP complex in order to calculate specific parameters from this average. The recorded files were imported into the Matlab (The Mathworks, Inc.)-based in-house programmed analysis program.

The program contains two different peak detection algorithms from which users can select the appropriate one to align the individual FPs correctly for calculation of the average field potential. Because of the variation in the shape of the cardiac FP signals, providing two different peak detection algorithms that correctly detect different forms yielded more accurate results. Both algorithms have a tenth-order FIR low-pass filter with a cut-off frequency of 1 kHz. The files were analysed using the algorithm that detected the peaks correctly.

The first peak detection algorithm is based on the QRS peak detection originally presented by Pan and Tompkins [14]. Fig. 1 illustrates process of the Pan–Tompkins algorithm. Briefly, the algorithm squares the signal after which the edges of the squared signal are detected. The peak is identified as the maximum of the original signal between the samples under these squares.

The second peak detection algorithm applies first- and second-order derivatives of the signal to obtain the signal's local maxima. The signals are divided into sections of 0.05 s, and the local maxima within these sections are identified with the Matlab implementation provided by Vargas Aguilera (http://www.mathworks.com/matlabcentral/fileexchange/

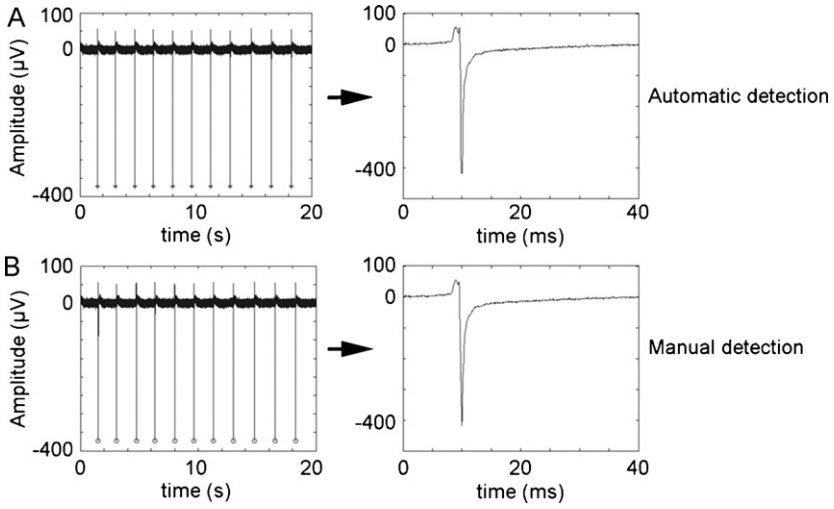

Fig. 2 – Validation of peak detection algorithms. (A) Automatic peak detection by the Matlab program (left panel) and the generated average (right panel). (B) Peaks selected manually by the operator (left panel), and the average (right panel) generated by the Matlab program based on the manually selected peaks. The automatic and manual peak detection methods generated similar averages.

12275-extrema-m-extrema2-m). To be identified as a peak, the detected maxima must register above a threshold. This threshold is adaptive and is set to 90% of the maximum of the previous group.

A detection dead time option was provided to avoid detecting double peaks related to the same FP complex. Any peaks during the dead time were ignored.

The detected peaks were later used to calculate an average complex (i.e. an average cardiac FP cycle) showing one activation cycle produced from the continuous FP signals. This was achieved by aligning the cardiac cycles by the detected peaks and normalizing them for averaging. This representative average was used to calculate the FPD. The beating rate (BR) was calculated from the detected peaks of the original imported signal.

To validate the algorithms for detecting the correct peaks in the imported recordings, we performed manual user-operated peak detection and generated a FP average based on the detected points. We then compared the averages generated by the automatic peak detection algorithms to the averages based on manual user-operated peak detection. The mean square error (MSE, Eq. (1)) was used to calculate the errors between the results found manually and those found automatically.

$$\mathrm{MSE} = \sqrt{\frac{\sum_{i=0}^{n}(x'_i - x''_i)^2}{n}} \quad (1)$$

where x' is the automatically generated complex, x'' is the average complex based on the manual peak detection, and n is the length of the complex.

Analysis results from the program are saved automatically and the options also permit creating a session for analyzing multiple files.

2.4. Noise attenuation

Eq. (2) presents the calculation of noise attenuation in dB, which served as the signal quality criterion.

$$\mathrm{A\ [dB]} = 20 \log\left(\frac{V_{average}}{V_{signal}}\right) \quad (2)$$

where $V_{average}$ is the root mean square (RMS) voltage of the averaged signal, and V_{signal} is the RMS voltage of the unaveraged signal. Noise attenuation (2) was calculated from periods of the averaged and unaveraged signals resulting from the noise (i.e. without cardiac FP activation).

2.5. Mean field potential duration

The FPD was measured from three individual cardiac cycles of the original unaveraged recordings and the mean FPD and standard deviation was calculated based on these values.

3. Results

3.1. Peak detection validation

The automatic peak detection algorithms yielded an average comparable to that generated using manual peak detection. Fig. 2A illustrates the original signal along with automatically selected minimum amplitude values on the left hand panel. The right hand panel in Fig. 2A illustrates the average cardiac FP cycle generated from a 2-min recording of the NRC population utilising automatic peak detection from the Matlab-based program. Fig. 2B illustrates the same situation for the same NRC recording, but using manual peak detection.

Comparing the averages produced with manual and automatic peak detection yielded the following average RMS errors:

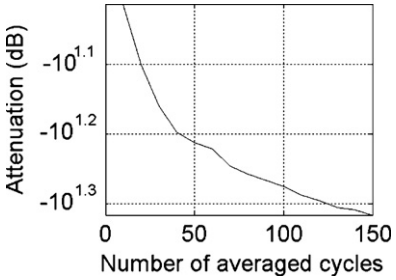

Fig. 3 – Noise attenuation. The noise attenuation in decibels (dB) appears as a function of the increasing number of averaged cardiac FP cycles.

0.13 ms for FPD with NRC population ($n = 6$) and 0.95 ms for hESC-CMs ($n = 3$). Using the same data set, the average RMS error values for the amplitude differences were 49 μV for NRCs and 79 μV for hEC-CMs.

3.2. *Noise attenuation*

Next, we analysed the number of cardiac FP cycles that needed to be included in the average to achieve proper levels of noise attenuation. Fig. 3 presents the effect of averaging on noise attenuation. Noise attenuation is at $-10^{1.2}$ when 50 complexes are applied to the average, thus reducing noise to 1/6 of its original level, which constitutes adequate attenuation.

3.3. *Variation of parameters as a function of time*

3.3.1. *Field potential duration and beating rate*

As two of the most important parameters of cardiac FP analysis are the field potential duration (FPD) and beating rate (BR), we analysed how these important parameters might possibly fluctuate during the recording period.

Twenty individual cardiac FP cycles were taken from the beginning, middle and end of each recording and averaged using our Matlab program. NRC recordings lasted a total of 2 min, and hESC-CM recordings lasted a total of 3 min. These three individual averaged parts of the recording were then compared to the average value of the entire recording so as to reveal how much the parameters changed while recording. The FPD in the beginning of the recordings differed from that of the entire recordings by 0.6 ± 16.2% in the NRC population and by −3.9 ± 8.3% in the hESC-CM population (mean ± SD), whereas the corresponding numbers for the middle part of the recordings were −8.4 ± 6.4% (NRC) and −2.7 ± 9.9% (hESC-CM), and for the end of the recordings, 1.1 ± 20.1% (NRC) and −7.1 ± 10.1% (hESC-CM). FPD fluctuation appears in Fig. 4A.

We then performed similar analysis with regard to the BR of these two cardiomyocyte populations. We found that the average BR for the beginning in the NRC population differed from that of the entire recordings by 15.9 ± 33.2%, and in the hESC-CM population by −6.5 ± 0.6% (mean ± SD). The middle part differed by 13.5 ± 28.8% in the NRC population and by −3.4 ± 1.1% in the hESC-CM population. The end part of the recordings differed by 7.8 ± 18.5% in the NRC population and by 0.9 ± 0.9% in the hESC-CM population. The differences in BR appear in Fig. 4B. The higher variation in BR in the NRCs

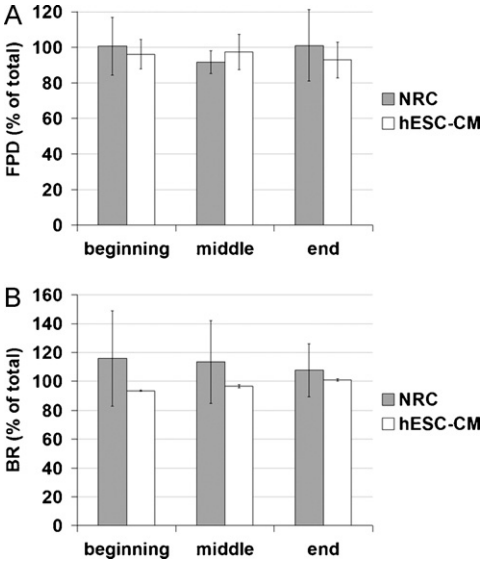

Fig. 4 – Variation of field potential duration and beating rate in different parts of the recording. Using the most suitable detection algorithm for each recording, we averaged 20 individual cardiac FP cycles from the beginning, middle and end of the entire recording. (A) We compared the field potential duration (FPD) of these averages to those generated from entire recording. (B) In the same way, we compared the beating rate (BR) parameters of these beginning, middle and end parts to the average of the entire recordings. The error bars represent ±SD.

was due to more arrhythmic behaviour than in the hESC-CMs, which exhibited more stable beating rhythms.

3.3.2. *Amplitude and beat-to-beat variation*

We investigated the variation in amplitude and beat-to-beat interval by plotting these values from individual recordings onto the same graph. We calculated the amplitude of the MSE of each FP cycle in comparison to the amplitude of the average signal generated from the recording. Fig. 5A represents the variation of these two parameters in a recording with a stable beating rhythm, whereas Fig. 5B demonstrates the variation of these parameters in a recording with arrhythmic behaviour. In recordings with a stable beating rhythm, the variation of parameters was minimal and the data points fell in close proximity to each other. A steadily beating cardiomyocyte population appears in Fig. 5A with an amplitude MSE of around 4 μV and a peak-to-peak interval (PPI) of approximately 1600 ms. In recordings exhibiting arrhythmic behaviour, the data points were more scattered due to the arrhythmic behaviour, thus resulting in larger PPI variation. The systolic peak amplitude of the FP cycle also tended to vary as a function of PPI. Interestingly, the FPD remained quite stable even though the amplitude and PPI varied within the recording (see Fig. 5C).

3.4. *Field potential duration measurements*

The mean FPDs (Table 1) measured from the original recordings corresponded well to the FPDs obtained from the average

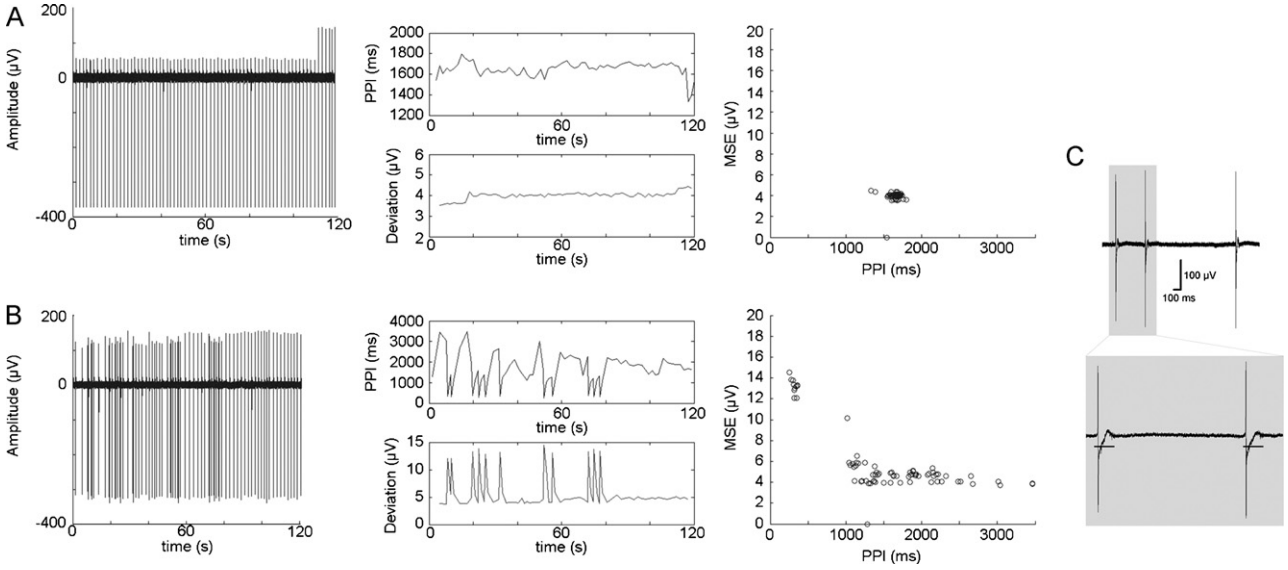

Fig. 5 – Variation of amplitude and peak-to-peak interval (PPI). (A) Original FP recording with a stable beating rhythm appears in the left panel. The middle panel shows the peak-to-peak interval (top-middle panel) and amplitude fluctuation (lower-middle panel) as a function of time. The rightmost panel represents a scatter plot of each FP cycle amplitude in relation to the average FP amplitude as mean square error (MSE) versus PPI. (B) The same parameters also appear for an arrhythmic recording. (C) Representative FP cycles from the file depicted in panel B. The gray area in the top panel of C appears in greater magnification in the panel below. Despite the variation of FP amplitude and PPI, the field potential duration (FPD) is stable. The bars below both FP cycles in the lower panel indicate FDP.

signal produced by the program. Also, the sensitivity of our program in FPD determination was evidenced by challenging the cardiomyocytes with E-4031, which is a hERG potassium channel blocker that causes cardiac FPD prolongation. Exposing the cardiomyocytes to this drug altered their FP signal shape as seen in Fig. 6. The FPD prolongation could clearly be seen in the averages produced under baseline and drug conditions.

4. Discussion

In vitro population-level cardiac electrophysiology will most likely become more significance in the coming years. The electrical properties of single cells have traditionally been studied with the patch clamp technique [15]. This method is time consuming, however, and requires a vast amount of training. Combining MEA technology with human embryonic stem cell-derived cardiomyocytes potentially allows for medium throughput drug screening for adverse cardiac side effects *in vitro* [2,16]. Furthermore, the emergence of induced pluripotent stem cell technology [17,18] and the subsequent ability to generate disease-specific cardiomyocyte populations [19,20] has increased the demand for analysing cardiac cell populations with a simple and reliable method. Furthermore, patch clamp analysis is suitable for single cells, but some cardiac diseases may require cell-to-cell coupling to determine the

Table 1 – Means and standard deviations (σ) of field potential duration (FPD) from three cardiac cycles measured by hand from each recording. The rightmost column presents the corresponding files' FPD measured by averaging the whole signal using our Matlab-based software. The recordings that exhibited arrhythmogenic behaviour are marked with asterisk (*).

Cardiomyocyte type	Mean FPD (3 cycles) (ms)	σ (ms)	FPD measured with program (ms)
NRC #1	275	11	287
NRC #2	278	9	279
NRC #3*	309	19	309
NRC #4	302	10	287
NRC #5*	300	35	256
NRC #6	110	3	120
NRC #7	201	7	201
NRC #8	321	12	331
hESC-CM #1	447	5	450
hESC-CM #2	258	12	260
hESC-CM #3	391	6	392
hESC-CM #4	537	11	555

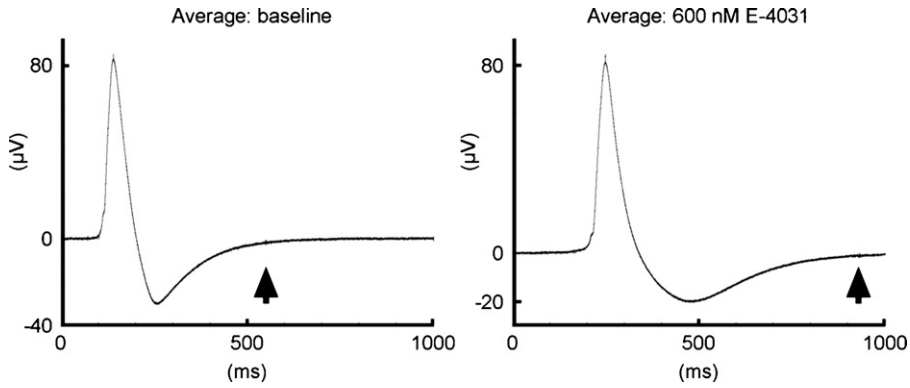

Fig. 6 – Sensitivity of the program. Left panel represents an average signal of baseline conditions for human embryonic stem cell-derived cardiomyocytes. The left panel represents the same signal obtained after the addition of 600 nM E-4031, a hERG channel blocker. The hERG channel contributes to the rapid delayed rectifying potassium current during cardiac repolarization. Note the widening of the negative potassium wave under E-4031 mediated hERG-block. The end of the cardiac cycle is marked by the arrows.

disease phenotype. Consequently, the best way to study the effects of disease on cardiac electrophysiology would be to study beating cardiomyocyte aggregates.

A challenge in studying cardiac FPs is the frequently low quality of signals. Such low quality may confound FPD measurements, which are essential in studying, for example, the effects of drugs. Low SNR may be due to the small number of cardiomyocytes in a given hESC-CM cluster, which leads to weaker MEA signals. One way to improve the FP signals obtained from cardiac recordings, especially in the case of noisy signals, is to average several individual FP cycles and to perform measurements on the averaged signal.

Our Matlab-based program successfully detected appropriate peaks in the imported signals that serve as reference points for aligning the cardiac FP cycles for average calculations. Two different algorithms were implemented, and the user selected the appropriate algorithm for each recording so as to achieve correct peak detection. The quality of the peak detection algorithms was verified by comparing them to manual peak detection results. The FP averages produced with these two methods yielded very similar results. Some recorded signals were arrhythmic, but all the FP cycles were of the same duration. In these cases, the average FP was correct, but the BR could not be calculated properly because the distance between peaks varied due to the arrhythmia. Noise attenuation was investigated in order to determine how the process of averaging affects the noise levels in signals with regard to the increasing number of individual FP cycles used to calculate the average signal. Interestingly, the more signals serve to calculate the average, the more potential exists for misalignment to alter the average signal. Consequently, there exists a trade-off between the noise level and the possibility of error. In our experiments, the best general number of averaged cycles was 50, because beyond this number, noise reduction was hardly noticeable, although noise reduction varies with different setups and cell sources.

We also explored how averaging different parts of the signal affected the results in terms of FPD and BR parameters, because the sections of the signal to be averaged must be sufficiently similar. Otherwise, the average FP cycle deviates from the original signal. In general, the NRC populations showed higher variation in FPD and BR than did hESC-CM aggregates. The overall results from the averages produced from the beginning, middle and end parts of the entire measured signal nevertheless approached the average of the entire recoding regarding these two parameters, thus suggesting that the recorded cardiac FP cycles were indeed stable. In terms of signal amplitude and PPI, the recordings were either very stable or, if arrhythmic behaviour was present, the amplitude decreased with increasing PPI. The arrhythmic behaviour caused the average to deviate little when compared to individual FPs due to burst-like activity. In these bursts, only the first FP cycle had a slightly prolonged duration; the rest were more homogenous. The first peaks in the bursts are in the minority, and therefore skew the results only negligibly (Fig. 5C). The sensitivity of the program was also demonstrated by the detection of drug-induced changes in signal shape. Generally, the program allowed for more accurate FPD measurements compared to measuring mean FPD of several individual cardiac cycles. Accuracy was improved by clearer end-point detection from the average cardiac cycle.

Taken together, our results demonstrate that cardiac field potential averaging can serve as a useful means of analysis, especially in terms of gross measurements, such as the average prolongation of field potential duration by, for example, a pharmacological compound. Averaging can produce signals with which to measure the effects of different cell culture conditions or stimuli on cardiomyocyte populations.

Since hESC-CM drug screenings are routinely performed with MEA [2,16,21], automated cardiac FP analysis based on such an approach would be an attractive application for analysis in the future. While determining amplitude and beating rate is relatively simple, the implementation of automatic FPD determination presents more of a challenge due to user-dependent interpretation and lack of a clear end-point. Another challenge to overcome in determining the end-point in FPD is the varying signal morphology. This must be taken into account, especially when working with stem cell-derived cardiomyocyte aggregates so as to create an FPD detection algorithm unconfounded by this.

Competing interests

The authors declare no competing financial interests.

Acknowledgements

We kindly thank Dr Christine Mummery for the END-2 cells. We also thank Henna Venäläinen for her technical help with the cell culturing. This research was funded by grants from the Academy of Finland (decision numbers: 126888, 122947 and 122959), the Finnish Heart Foundation, competitive funding from Pirkanmaa Hospital District and the Finnish Cultural Foundation. The MEA system was funded by BioneXt, Tampere, Finland.

REFERENCES

[1] M. Reppel, F. Pillekamp, Z.J. Lu, M. Halbach, K. Brockmeier, B.K. Fleischmann, J. Hescheler, Microelectrode arrays: a new tool to measure embryonic heart activity, J. Electrocardiol. 37 (2004) 104–109.

[2] O. Caspi, I. Itzhaki, I. Kehat, A. Gepstein, G. Arbel, I. Huber, J. Satin, L. Gepstein, In vitro electrophysiological drug testing using human embryonic stem cell derived cardiomyocytes, Stem Cells Dev. 18 (2009) 161–172.

[3] M. Reppel, F. Pillekamp, K. Brockmeier, M. Matzkies, A. Bekcioglu, T. Lipke, F. Nguemo, H. Bonnemeier, J. Hescheler, The electrocardiogram of human embryonic stem cell-derived cardiomyocytes, J. Electrocardiol. 38 (2005) 166–170.

[4] T. Meyer, K.H. Boven, E. Gunther, M. Fejtl, Micro-electrode arrays in cardiac safety pharmacology: a novel tool to study qt interval prolongation, Drug Saf. 27 (2004) 763–772.

[5] M. Reppel, P. Igelmund, U. Egert, F. Juchelka, J. Hescheler, I. Drobinskaya, Effect of cardioactive drugs on action potential generation and propagation in embryonic stem cell-derived cardiomyocytes, Cell Physiol. Biochem. 19 (2007) 213–224.

[6] K. Pfannkuche, H. Liang, T. Hannes, J. Xi, A. Fatima, F. Nguemo, M. Matzkies, M. Wernig, R. Jaenisch, F. Pillekamp, M. Halbach, H. Schunkert, T. Saric, J. Hescheler, M. Reppel, Cardiac myocytes derived from murine reprogrammed fibroblasts: intact hormonal regulation, cardiac ion channel expression and development of contractility, Cell Physiol. Biochem. 24 (2009) 73–86.

[7] O Binah, K. Dolnikov, O. Sadan, M. Shilkrut, N. Zeevi-Levin, M. Amit, A. Danon, J. Itskovitz-Eldor, Functional and developmental properties of human embryonic stem cells-derived cardiomyocytes, J. Electrocardiol. 40 (2007) S192–S196.

[8] I. Kehat, D. Kenyagin-Karsenti, M. Snir, H. Segev, M. Amit, A. Gepstein, E. Livne, O. Binah, J. Itskovitz-Eldor, L. Gepstein, Human embryonic stem cells can differentiate into myocytes with structural and functional properties of cardiomyocytes, J. Clin. Invest. 108 (2001) 407–414.

[9] M. Pekkanen-Mattila, E. Kerkela, J.M. Tanskanen, M. Pietila, M. Pelto-Huikko, J. Hyttinen, H. Skottman, R. Suuronen, K. Aalto-Setala, Substantial variation in the cardiac differentiation of human embryonic stem cell lines derived and propagated under the same conditions – a comparison of multiple cell lines, Ann. Med. (2009) 1–15.

[10] L. Zwi, O. Caspi, G. Arbel, I. Huber, A. Gepstein, I.H. Park, L. Gepstein, Cardiomyocyte differentiation of human induced pluripotent stem cells, Circulation 120 (2009) 1513–1523.

[11] M. Pekkanen-Mattila, H. Chapman, E. Kerkela, R. Suuronen, H. Skottman, A.P. Koivisto, K. Aalto-Setala, Human embryonic stem cell-derived cardiomyocytes: demonstration of a portion of cardiac cells with fairly mature electrical phenotype, Exp. Biol. Med. (Maywood) 235 (2010) 522–530.

[12] C. Mummery, D. Ward-van Oostwaard, P. Doevendans, R. Spijker, S. van den Brink, R. Hassink, M. van der Heyden, T. Opthof, M. Pera, A.B. de la Riviere, R. Passier, L. Tertoolen, Differentiation of human embryonic stem cells to cardiomyocytes: role of coculture with visceral endoderm-like cells, Circulation 107 (2003) 2733–2740.

[13] H. Tokola, K. Salo, O. Vuolteenaho, H. Ruskoaho, Basal and acidic fibroblast growth factor-induced atrial natriuretic peptide gene expression and secretion is inhibited by staurosporine, Eur. J. Pharmacol. 267 (1994) 195–206.

[14] J. Pan, W.J. Tompkins, A real-time QRS detection algorithm, in: Biomedical Engineering, IEEE Transactions on BME-32, 1985, pp. 230–236.

[15] O.P. Hamill, A. Marty, E. Neher, B. Sakmann, F.J. Sigworth, Improved patch-clamp techniques for high-resolution current recording from cells and cell-free membrane patches, Pflugers Arch. 391 (1981) 85–100.

[16] S.R. Braam, L. Tertoolen, A. van de Stolpe, T. Meyer, R. Passier, C.L. Mummery, Prediction of drug-induced cardiotoxicity using human embryonic stem cell-derived cardiomyocytes, Stem Cell Res. 4 (2010) 107–116.

[17] K. Takahashi, K. Tanabe, M. Ohnuki, M. Narita, T. Ichisaka, K. Tomoda, S. Yamanaka, Induction of pluripotent stem cells from adult human fibroblasts by defined factors, Cell 131 (2007) 861–872.

[18] J. Yu, M.A. Vodyanik, K. Smuga-Otto, J. Antosiewicz-Bourget, J.L. Frane, S. Tian, J. Nie, G.A. Jonsdottir, V. Ruotti, R. Stewart, I.I. Slukvin, J.A. Thomson, Induced pluripotent stem cell lines derived from human somatic cells, Science 318 (2007) 1917–1920.

[19] A. Moretti, M. Bellin, A. Welling, C.B. Jung, J.T. Lam, L. Bott-Flugel, T. Dorn, A. Goedel, C. Hohnke, F. Hofmann, M. Seyfarth, D. Sinnecker, A. Schomig, K.L. Laugwitz, Patient-specific induced pluripotent stem-cell models for long-QT syndrome, N. Engl. J. Med. 363 (2010) 1397–1409.

[20] I.H. Park, N. Arora, H. Huo, N. Maherali, T. Ahfeldt, A. Shimamura, M.W. Lensch, C. Cowan, K. Hochedlinger, G.Q. Daley, Disease-specific induced pluripotent stem cells, Cell 134 (2008) 877–886.

[21] H. Liang, M. Matzkies, H. Schunkert, M. Tang, H. Bonnemeier, J. Hescheler, M. Reppel, Human and murine embryonic stem cell-derived cardiomyocytes serve together as a valuable model for drug safety screening, Cell Physiol. Biochem. 25 (2010) 459–466.

Disease Models & Mechanisms 5, 000-000 (2012) doi:10.1242/dmm.008409

Model for long QT syndrome type 2 using human iPS cells demonstrates arrhythmogenic characteristics in cell culture

Anna L. Lahti[1,2,*], Ville J. Kujala[1,2,*], Hugh Chapman[3], Ari-Pekka Koivisto[3], Mari Pekkanen-Mattila[1,2], Erja Kerkelä[1,‡], Jari Hyttinen[2,4], Kimmo Kontula[5], Heikki Swan[5], Bruce R. Conklin[6], Shinya Yamanaka[6,7], Olli Silvennoinen[1,2,8] and Katriina Aalto-Setälä[1,2,9,§]

SUMMARY

Long QT syndrome (LQTS) is caused by functional alterations in cardiac ion channels and is associated with prolonged cardiac repolarization time and increased risk of ventricular arrhythmias. Inherited type 2 LQTS (LQT2) and drug-induced LQTS both result from altered function of the hERG channel. We investigated whether the electrophysiological characteristics of LQT2 can be recapitulated in vitro using induced pluripotent stem cell (iPSC) technology. Spontaneously beating cardiomyocytes were differentiated from two iPSC lines derived from an individual with LQT2 carrying the R176W mutation in the *KCNH2* (*HERG*) gene. The individual had been asymptomatic except for occasional palpitations, but his sister and father had died suddenly at an early age. Electrophysiological properties of LQT2-specific cardiomyocytes were studied using microelectrode array and patch-clamp, and were compared with those of cardiomyocytes derived from control cells. The action potential duration of LQT2-specific cardiomyocytes was significantly longer than that of control cardiomyocytes, and the rapid delayed potassium channel (I_{Kr}) density of the LQT2 cardiomyocytes was significantly reduced. Additionally, LQT2-derived cardiac cells were more sensitive than controls to potentially arrhythmogenic drugs, including sotalol, and demonstrated arrhythmogenic electrical activity. Consistent with clinical observations, the LQT2 cardiomyocytes demonstrated a more pronounced inverse correlation between the beating rate and repolarization time compared with control cells. Prolonged action potential is present in LQT2-specific cardiomyocytes derived from a mutation carrier and arrhythmias can be triggered by a commonly used drug. Thus, the iPSC-derived, disease-specific cardiomyocytes could serve as an important platform to study pathophysiological mechanisms and drug sensitivity in LQT2.

INTRODUCTION

Signal propagation between cardiomyocytes is a very tightly regulated system. Mutations in ion channels involved in this system can cause electrical alterations that, in certain circumstances, such as during exercise or emotional stress, could trigger arrhythmias. Sudden death in a young healthy person can be the first devastating presentation of an underlying genetic disease. Long QT syndrome (LQTS) can either be genetic or acquired (e.g. drug-induced) in nature and is due to defective functioning of cardiac ion channels. LQTS is characterized by a prolonged cardiac repolarization phase resulting in a long QT interval in the surface electrocardiogram (ECG). The clinical symptoms of LQTS include palpitations, syncope, seizures and even sudden cardiac death. A special type of polymorphic ventricular tachycardia [torsade de pointes (TdP)] is associated with LQTS. Intriguingly, many mutation carriers are without any symptoms. A total of 12 congenital LQTS subtypes are presently known (Hedley et al., 2009). Two of these subtypes account for more than 90% of all genetically identified LQTS cases and both are due to defective functioning of potassium channels. LQTS type 1 (LQT1) is the most common subtype, resulting from mutations in the *KCNQ1* gene, which encodes the α-subunit of the slow component of the delayed rectifier potassium current (I_{Ks}) channel (Chiang and Roden, 2000). Individuals with LQT1 typically have symptoms during exercise (Schwartz, 2001; Roden, 2008). LQTS type 2 (LQT2) is due to defective functioning of the α-subunit of the rapid delayed potassium channel (I_{Kr}), encoded by the *KCNH2* [also known as human ether-a-go-go-related gene (*HERG*)] gene (Curran et al., 1995). Typically, individuals with LQT2 have clinical symptoms after abrupt auditory stimuli, often during sleep when the heart rate is slow (Schwartz, 2001; Roden, 2008). The acquired form of LQTS is also due to altered functioning of the same *KCNH2* ion channel.

Induced pluripotent stem cell (iPSC) technology (Takahashi et al., 2007; Yu et al., 2007) has revolutionized research on genetic

[1]Institute of Biomedical Technology, and [2]BioMediTech, University of Tampere, Biokatu 6-12, 33520 Tampere, Finland
[3]Department of In Vitro Pharmacology, Orion Pharma, Orion Corporation, Turku, Finland
[4]Department of Biomedical Engineering, Tampere University of Technology, Tampere, Finland
[5]Department of Medicine, University of Helsinki, Tukholmankatu 8 B, 5th and 6th floors, P.O. Box 20, 00014 Helsinki, Finland
[6]Gladstone Institute of Cardiovascular Disease and Department of Medicine, University of California, 1650 Owens Street, San Francisco, CA 94158, USA
[7]Center for iPS Cell Research and Application (CiRA), Kyoto University, 53 Kawahara-cho, Shogoin Yoshida, Sakyo-ku, Kyoto 606-8507, Japan
[8]Tampere University Hospital, Tampere, Finland
[9]Heart Center, Tampere University Hospital, Tampere, Finland
*These authors contributed equally to this work
‡Current address: Finnish Red Cross, Blood Service, Helsinki, Finland
§Author for correspondence (katriina.aalto-setala@uta.fi)

Received 30 June 2011; Accepted 20 October 2011

diseases. iPSCs can be generated from somatic cells of any individual and these pluripotent cells can be differentiated into the desired cell type. Accordingly, it is possible to create genotype-specific cell models with a correct functional intracellular environment. However, a major challenge in the iPSC approach is to reproduce the phenotype of the disease or the individual in iPSC-derived cells. An appropriate disease phenotype has been reproduced with iPSC technology from individuals with LQT1 (Moretti et al., 2010), LQT2 (Itzhaki et al., 2011; Matsa et al., 2011) and with Timothy syndrome (Yazawa et al., 2011). Considering non-cardiac disorders, a disease phenotype or pathogenesis in iPSC-derived models has been demonstrated only for a few neurological diseases (Lee and Studer, 2010) and for the LEOPARD syndrome (Carvajal-Vergara et al., 2010).

The penetrance of the clinical symptoms of LQTS is low and there is considerable variation in phenotypic expression even within families carrying the same mutation (Priori et al., 1999). In addition, it has been proposed that the population prevalence of milder LQTS mutations might be high, suggesting that the prevalence of latent or concealed LQTS, i.e. relatively asymptomatic individuals, is higher than currently anticipated (Marjamaa et al., 2009). For these reasons, LQTS is clinically very challenging. The previous LQT2 iPSC reports used individuals with severe symptoms and the severity of their symptoms was translated to the cardiomyocytes derived from the patient-specific iPSCs. However, a cell model for asymptomatic LQT2 mutation carriers would be valuable to help with clinical decisions about medical treatments and lifestyle restrictions for relatively asymptomatic patients.

A more thorough understanding of the molecular mechanisms underlying LQTS would be very helpful for the pharmaceutical industry. Drug-induced forms of LQTS often arise as a result of inhibition of the hERG channel gating, and is thus analogous to LQT2 (Hancox et al., 2008). These adverse cardiac effects have led to labeling restrictions on both cardiac and non-cardiac drugs as well as to withdrawal from the market (Roden, 2004). Currently, preclinical testing of new chemical entities (NCEs) for proarrhythmic potential relies on animal experiments and ectopic expression of individual ion channels in non-cardiac cells (Pollard et al., 2008). However, current models lack the relevant human physiological environment that might regulate or modify cellular responses (Pollard et al., 2008). Thus, some NCEs could be unnecessarily discarded in the preclinical phase, and others already in clinical use might in fact elicit adverse cardiac side effects. Functional cardiomyocytes derived from both symptomatic and, possibly even more importantly, asymptomatic LQTS individuals would add to and complement presently used models. These cell models would provide the relevant cellular milieu to study genetic and non-genetic interactions influencing the phenotype.

In the present study, we developed an in vitro cell model of LQT2. In contrast to the previous reports (Itzhaki et al., 2011; Matsa et al., 2011), we aimed at generating a model from cells of an individual with LQT2 without severe symptoms. To that end, iPSC lines were derived from a patient's fibroblasts carrying a mutation for LQT2. Although there is a family history of overt LQTS, this individual was asymptomatic except for occasional palpitations and his 12-lead ECG exhibited a heart-rate-corrected QT time (QTc) of 437 ms. This model for LQT2 provides an important platform to study the pathophysiology of LQT2 and to evaluate adverse cardiac effects of drugs with the potential to prolong the QT interval.

RESULTS

Patient characteristics

A skin biopsy was obtained from a 61-year-old man with a missense mutation in *KCNH2* causing an arginine-to-tryptophan substitution at position 176 (R176W, hERG-FinB; Fig. 1A). Although there is a family history of overt LQTS, this individual was asymptomatic except for occasional palpitations. His 12-lead ECG exhibited a QTc of 437 ms (Fig. 1B). His sister was diagnosed with LQTS having a QT(U)c interval of 550 ms (Fig. 1C), presence of palpitations and sudden death at the age of 32.

Characterization of iPSCs

Fibroblasts from an individual with LQT2 were infected with retroviruses encoding for *OCT4*, *SOX2*, *KLF4* and *MYC* to generate iPSCs. Morphologically, iPSC colonies exhibited characteristics similar to those of human embryonic stem cells (hESCs), with rounded shape and clear defined edges (Fig. 2A). Both LQT2-specific iPSC lines (UTA.00514.LQT2 and UTA.00525.LQT2) and control iPSC lines expressed endogenous pluripotent markers at the mRNA level, as shown by reverse transcriptase PCR (RT-PCR) (Fig. 2B). The protein expression of pluripotency genes was also demonstrated by immunocytochemical stainings (Fig. 2C) for further confirmation. By contrast, exogenous gene expression was turned off in all iPSC lines by passage six (Fig. 2B). Exogenous gene expression was not detected after cardiac differentiation, demonstrating that these genes were not reactivated in the process (data not shown). The generated iPSC lines were also analyzed for their karyotypes, which were all normal (Fig. 2D).

To confirm the pluripotency of our iPSC lines, an embryoid body (EB) formation assay was performed. The EB-derived cells from LQT2 iPSC and control iPSC lines all expressed markers from the three different embryonic lineages: endoderm, ectoderm and mesoderm (Fig. 2F). Pluripotency of the lines was further confirmed by teratoma formation. Teratomas were made from one LQT2-specific line (UTA.00525.LQT2) and two control lines (UTA.00112.hFF and UTA.01006.WT). In every case, tissues from all three germ layers were found in the teratomas (Fig. 2E).

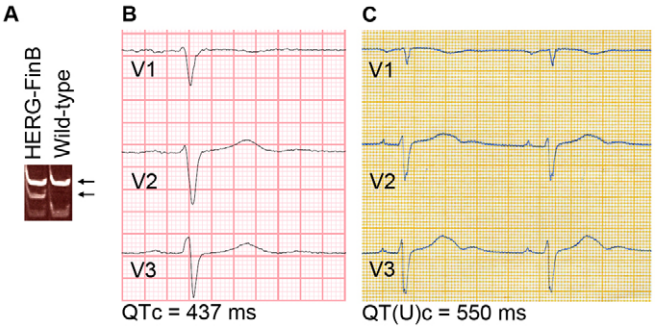

Fig. 1. Mutation and ECG analysis. (A) Mutation analysis confirmed the hERG-FinB mutation in the LQT2 iPSC line, which gave altered DNA cleavage by the *Sma*I restriction enzyme (lower arrow). (B,C) ECG from leads V1-V3 of the index patient, with a QTc of 437 ms (B), and from the patient's sister, with the presence of a U-wave following the T-wave; QT(U)c=550 ms.

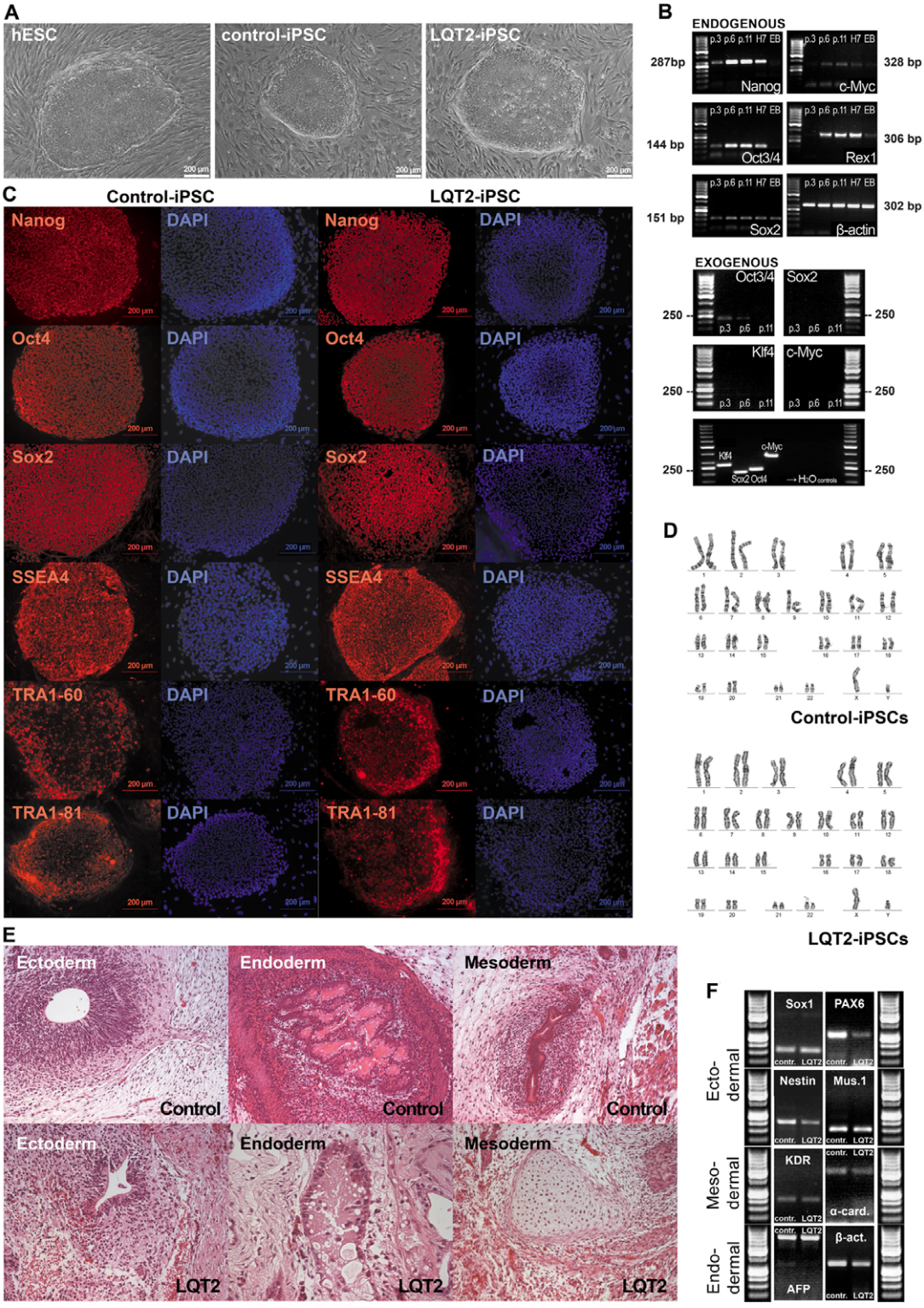

Fig. 2. Characterization of iPSCs. (A) Morphology of the iPSC colonies is similar to those of hESCs. The colonies are rather roundish and the edges are well defined and sharp, which is typical for a stem cell colony. (B) Expression of pluripotency markers in LQT2-specific iPSCs is shown by RT-PCR. All the endogenous pluripotency genes studied were turned on in iPSCs by passage 6 (top panel). As a positive control, they were also expressed in hESCs (H7). Expression of *Sox2* and very modest expression of *Rex1* and *Myc* was found also in EBs, which were used as a negative control. β-actin served as a loading control. None of the exogenous genes were expressed in iPSCs at passage 11. As a positive control, PCR was also done using the transfected plasmids as templates (bottom panel). RT-PCR results were similar for all the iPSC lines. (C) Immunocytochemical staining of the cells shows that pluripotency markers are expressed also at the protein level. The expression of Nanog, Oct3/4, Sox2, SSEA-4, TRA1-60 and TRA1-81 was similar in all iPSC lines and there were no differences between LQT2-specific and control lines. (D) Karyotypes of all the iPSC lines were analyzed and proved to be normal. (E) Teratomas were made from one LQT2-specific line and two control lines to further confirm the pluripotency of the lines. Tissues from all three germ layers were found in teratomas from every line. (F) EBs were also formed from all the lines to show the pluripotent differentiation capacity. The EB-derived cells from both LQT2-iPSC and all control iPSC lines expressed markers from the three embryonic germ layers.

Cardiomyocyte differentiation and characterization

LQT2-specific iPSCs, control iPSCs and hESCs differentiated into spontaneously beating cells. As shown by RT-PCR, these differentiated control and LQT2 cardiomyocytes expressed cardiac markers: troponin T (TNTT2), ventricular myosin light chain (MLC2V), atrial myosin light chain (MLC2A), connexin-43 (Cx-43), myosin heavy chain β (MHC-β; MYH7), HERG and GATA4 (Fig. 3B). The expression of cardiac troponin T, α-actinin and Cx-43 was also seen at the protein level as evidenced in Fig. 3A. The electrical properties of iPSC- and hESC-derived cardiomyocytes were also studied using microelectrode array (MEA; Fig. 3C,D). There were differences between control and LQT2-specific cells

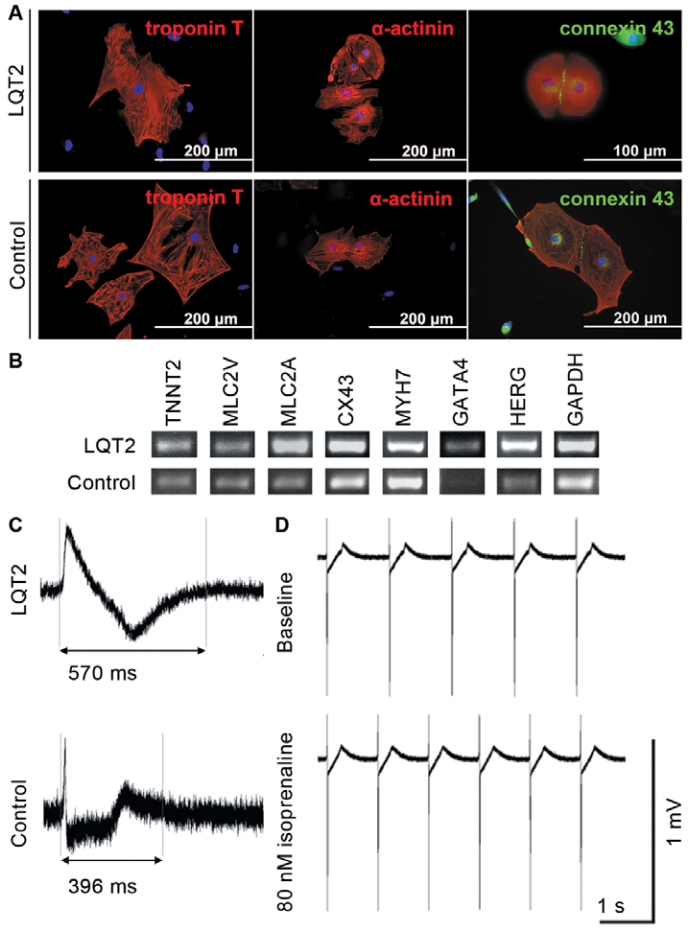

Fig. 3. The expression of cardiac markers in iPSC-derived cardiomyocytes and the electrical properties of the cells. (A) Immunocytochemical staining of different cardiac markers: troponin T and α-actinin are shown in red; green indicates connexin-43 and blue represents DAPI-staining for nuclei. The expression was similar in LQT2-specific and control cells, and there were no line-specific differences in the expression of cardiac proteins. (B) The expression of a larger repertoire of cardiac markers was also studied, with RT-PCR showing that the iPSC-derived cardiac cells manifest cardiac properties. *TNTT2*, *MLC2V*, *MLC2A*, *Cx-43*, *MYH7*, *GATA4* and *HERG* were present in the cells at the mRNA level. (C) Electrical properties of the cells were studied with MEA, which revealed the differences between LQT2-specific and control cells. FPD was significantly longer in LQT2-specific cardiomyocytes than in control cardiac cells. However, all lines evince the typical electrical properties of cardiomyocytes. (D) LQT2-specific cardiomyocytes showed increased chronotrophy when challenged with isoprenaline, a β-adrenergic agonist.

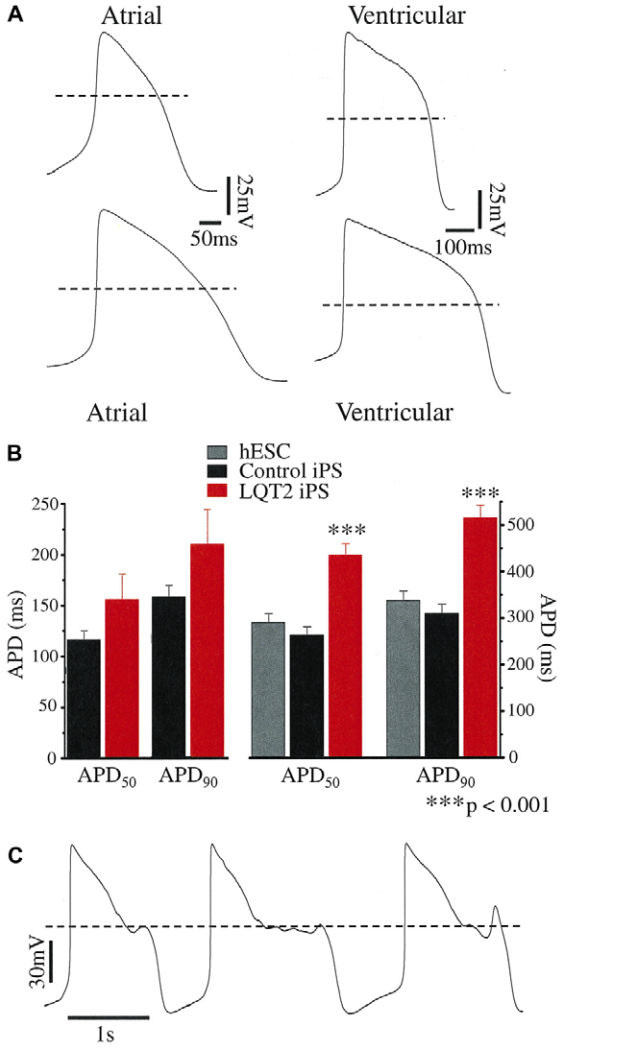

Fig. 4. Current-clamp recordings from human iPSC-derived cardiomyocytes. (A) Spontaneous APs from healthy control iPSC-derived (upper APs) and LQT2 patient-derived (lower APs) cardiomyocytes. The dashed line denotes 0 mV. (B) The action potential duration (APD) measured at 50% and 90% repolarization from the AP peak (APD_{50} and APD_{90}) of spontaneous atrial-like (n=5-6) and ventricular-like APs. For the latter, both the APD_{50} and APD_{90} of LQT2 patient-derived cardiomyocytes (n=13) were significantly prolonged compared with those of hESCs (n=7) or control-iPSC origin (n=11). (C) Spontaneous arrhythmogenic activity of an LQT2-iPSC-derived cardiomyocyte.

in their field potential durations (FPDs) (Fig. 3C), but both types showed increased chronotrophy when treated with isoprenaline, a β-adrenergic agonist (Fig. 3D), which is the anticipated response and indicates intact β-adrenergic signaling.

Electrophysiological properties of differentiated cardiomyocytes

The differentiation of both control and LQT2-specific iPSCs into cardiomyocyte subtypes was evident from the morphology of the spontaneous action potentials (APs) recorded with the patch-clamp technique. Two types of AP morphology were observed: ventricular-like, which displayed a distinct plateau phase; and atrial-like, which were triangular shaped (Fig. 4A). The AP properties of control-iPSC-derived cardiomyocytes were similar to those of other human ESC and iPSC studies (Table 1) (Gai et al., 2009; Yokoo et al., 2009; Zwi et al., 2009). For most AP parameters there was no significant difference between control and LQT2-iPSC-derived cardiomyocytes (P>0.05; Table 1). However, ventricular-like LQT2-iPSC-derived cardiomyocytes had significantly prolonged AP durations at 50% and 90% repolarization (APD_{50} and APD_{90}, respectively). The APD_{50} and APD_{90} of atrial-like LQT2-iPSC-derived cardiomyocytes, although prolonged, did not reach statistical significance. On the borderline of statistical significance was the slower AP frequency of ventricular-

Table 1. AP properties of atrial- and ventricular-like cardiomyocytes

	No. cells	Frequency (Hz)	APD_{50} (ms)	APD_{90} (ms)	dV/dt_{max} (V/second)	APA (mV)	MDP (mV)
Atrial-like							
Control	6	1.8±0.1	116.7±8.4	157.7±11.0	9.2±0.5	104.4±1.3	–65.6±0.6
LQT2	5	1.4±0.1	156.0±25.0	210.9±33.3	11.7±1.6	105.0±2.7	–65.4±1.4
Ventricular-like							
Control	13	1.2±0.1	264.7±15.0	314.4±17.6	26.8±6.3	113.2±2.4	–63.4±1.3
LQT2	16	0.9±0.1[a]	455.3±26.7[b]	538.0±28.5[b]	15.8±0.7	117.3±1.4	–62.4±0.9

AP properties of spontaneously beating human iPSC-derived cardiomyocytes. dV/dt_{max}, maximum rise of the AP upstroke; APA, AP amplitude; MDP, maximum diastolic potential. Mean values ± s.e.m. are shown. Comparison of control iPSC-CMs and LQT2 iPSC-CMs groups was performed with unpaired *t*-test with $P<0.05$ considered statistically significant.
[a]$P=0.05$; [b]$P<0.000005$. CMs, cardiomyocytes.

like LQT2-iPSC-derived cardiomyocytes; therefore, further analysis was restricted to a subset of cardiomyocytes to reduce the effect of any rate-dependent APD adaptation.

Both the APD_{50} and APD_{90} of LQT2-iPSC-derived ventricular-like cardiomyocytes were significantly prolonged compared with control-iPSC- and hESC-derived cardiomyocytes ($P<0.001$; Fig. 4A,B), at an AP frequency of about 1 Hz ($P=0.13$ between groups). The APD_{90} was 516.5±26.1 ms in LQT2-specific cardiomyocytes compared with 310.5±19.6 ms in control-iPSC-derived cardiomyocytes or 338.6±19.9 ms in hESC-derived cardiomyocytes. The APD_{90} did not differ significantly between cardiomyocytes from the two LQT2 iPSC lines (UTA.00514.LQT2 and UTA.00525.LQT2) or between hESC-derived cardiomyocytes and those of control iPSC origin. Collectively, these data indicate that the LQT2-iPSC-derived cardiomyocytes express the disease phenotype, characterized by a prolonged cardiac repolarization phase. Spontaneous arrhythmogenic activity was rare, early after depolarizations (EADs) were observed in only one of 20 LQT2-iPSC-derived cardiomyocytes studied (Fig. 4C) and in no recordings from control iPSC cardiomyocytes ($n=20$).

Ventricular-like cardiomyocytes were subjected to further investigations using voltage clamp (Fig. 5). Using the specific inhibitor E-4031, I_{Kr} was isolated (Fig. 5A) and its magnitude shown to be markedly reduced in LQT2 iPSC cardiomyocytes compared with that in control iPSC cardiomyocytes (Fig. 5B). Tail I_{Kr} density was significantly decreased, by 40-46%, after a depolarizing step to voltages from 0 to +40 mV ($P<0.01$; Fig. 5C). A similar reduction in tail I_{Kr} density (~40%) was seen in experiments when an alternative method, isotonic cesium conditions (Zhang, 2006), was used to isolate I_{Kr} from a different control and LQT2 iPSC line (supplementary

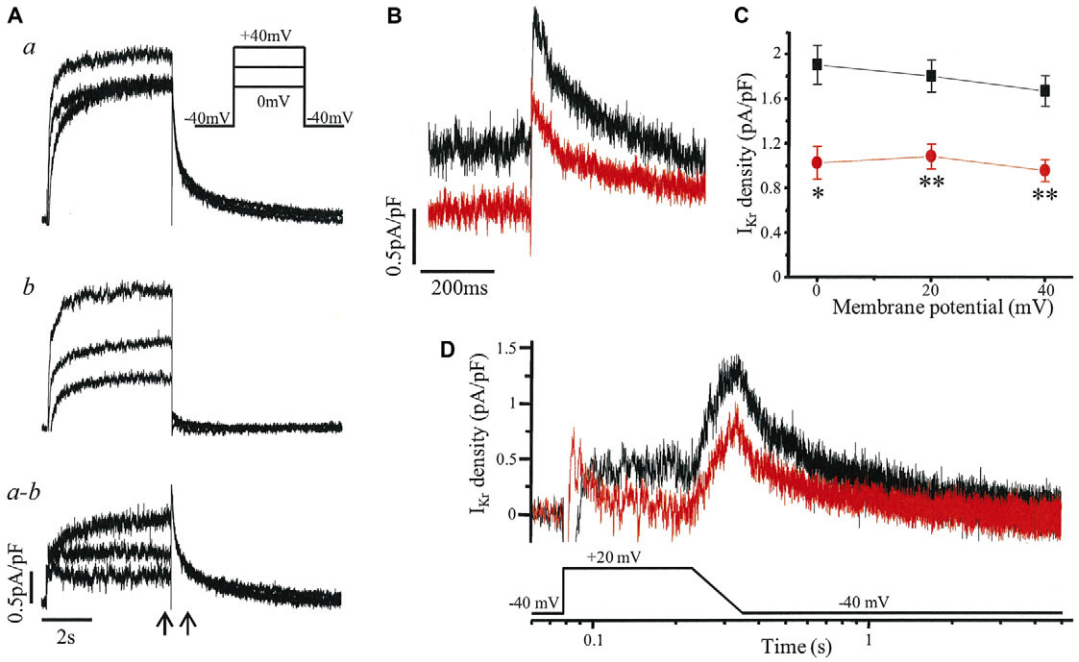

Fig. 5. I_{Kr} recorded from iPSC cardiomyocytes with a ventricular-like AP. (A) Example of the isolation of I_{Kr}. Whole-cell current, here from a control iPS cardiomyocyte, was recorded in the absence (*a*) and then presence of 1 µmol/l E-4031 (*b*), with I_{Kr} defined as the subtracted current (*a-b*), i.e. the E-4031-sensitive current. Current was evoked by a 5-second depolarization from a holding potential of –40 mV as shown in the inset. (B) I_{Kr} of a control iPS (black) and LQT2 iPS (red) cardiomyocyte evoked as in A with the time segment between the arrows expanded to show the peak tail currents on return to –40 mV following a step to +20 mV. (C) The peak tail I_{Kr} densities of control iPSC (black; $n=4$) and LQT2 iPSC (red; $n=5$) cardiomyocytes at membrane potentials from 0 to +40 mV were significantly different (*$P<0.01$, **$P<0.005$). (D) I_{Kr} currents of control iPSC (black) and LQT2 iPSC (red) cardiomyocytes evoked by a voltage protocol of step to +20 mV for 150 ms and ramp of 120 ms back to the –40 mV holding potential.

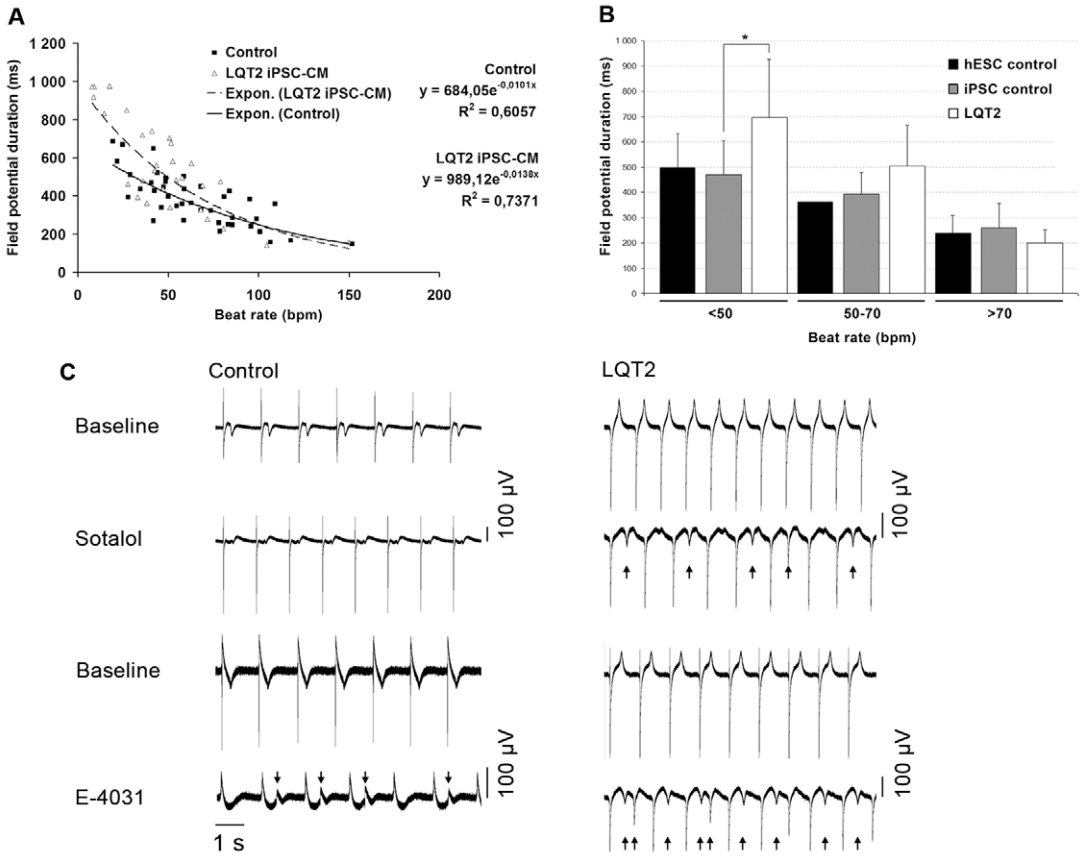

Fig. 6. FPD measured on MEA. (A) The effect of the beating rate on FPD in control and LQT2 cardiomyocytes (CMs). Control and LQT2 cardiomyocytes had a negative correlation with moderately high coefficients of determination (R^2). The exponential function gave the best fit as determined by R^2 between different fitting functions. The LQT2 cardiomyocytes had significantly more prolonged FPD compared with controls, especially at low beating frequencies, as determined by nonlinear regression analysis (P=0.0136). (B) At beating rates below 50 beats per minute (bpm), the FPD of LQT2 cardiomyocytes differed significantly from control cardiomyocytes (*P<0.05) as determined by t-test. (C) Drug responses of control and LQT2 cardiomyocytes. Sotalol (19 µmol/l) and E-4031 (500 nmol/l for LQT2-specific cells and 700 nmol/l for control cells) was administered to the cardiomyocyte aggregates derived from control iPSCs and LQT2 iPSCs. For both cell lines, baseline and drug conditions for sotalol and E-4031 are shown. Arrows mark the site of pharmacologically induced EADs. With 500 nmol/l E-4031 there were no EADs observed in control cells.

material Fig. S1). The reduction in resurgent I_{Kr} during repolarization was also demonstrated with the use of a step-ramp voltage protocol as a simplified version of a cardiac AP (Fig. 5D).

The in vitro cardiac FPD on MEA has been shown to correlate with QT interval properties in the ECG, and FPD recordings of beating cell aggregates give insight into the electrical function of myocardial tissue in vitro (Caspi et al., 2008). We observed a negative correlation between FPD and beating rate both in control cardiomyocytes and LQT2-specific cardiomyocytes (Fig. 6A,B). However, the LQT2 cardiomyocytes had a significantly prolonged FPD compared with controls, especially at low beating frequencies (P=0.014; Fig. 6A,B), as determined by nonlinear regression analysis. The two LQT2 iPSC lines behaved the same way and, thus, their data were combined, as were data from the three different control iPSC lines and hESC-derived cardiomyocytes, because they behaved similarly.

The inotropic response of the iPSC-derived cardiac cells was studied using isoprenaline. A panel of drugs with known QT-prolongation effects, including erythromycin, sotalol and cisapride, and a non-drug compound, E-4031, were investigated. The selective hERG blocker E-4031 increased arrhythmogenicity in control cardiac cells and even more frequently in LQT2 cardiomyocytes (Fig. 6C). Application of sotalol (0.8-19.4 µmol/l), an anti-arrhythmic drug with both β-blocker and class III activity, elicited arrhythmogenicity at the highest tested concentrations only in LQT2 cardiac cells (Fig. 6C). No increased arrhythmogenicity was observed with erythromycin (1.5-16 µmol/l) or cisapride (40-330 nmol/l) in control or LQT2 cardiac cells (data not shown). At baseline, no arrhythmogenicity was observed with control or LQT2 cardiac cells on MEA.

DISCUSSION

In this study we demonstrate that patient-specific iPSCs can be used to model a potentially lethal cardiac arrhythmic disease in vitro. The cells were differentiated into functional cardiomyocytes, which reproduced the phenotypic characteristics of LQT2, including a prolonged repolarization time and increased arrhythmogenicity. Furthermore, at slow beating rates, FPD (QT) was significantly more prolonged in LQT2 cardiomyocytes compared with control cells.

The R176W hERG mutation was reported to have the frequency of 0.5% in apparently healthy individuals (Ackerman et al., 2003) and, according to an epidemiological Finnish study, the mutation is present in about one of 400 Finns (Marjamaa et al., 2009). The majority of these individuals are completely asymptomatic and unaware of their carrier status. This mutation is one of the four founder mutations for LQTS in Finland and these mutations account for almost two-thirds of all established LQTS cases in the country (Fodstad et al., 2004). The QTc interval of LQT2 patients with the R176W mutation is reported to range from 386 to 569 ms, with a mean of 448 ms, whereas the mean for non-carriers was 416 ms (Fodstad et al., 2006). Furthermore, the mutation has also been identified in cases of sudden death (Tester and Ackerman, 2007; Tu et al., 2011). Although our patient had latent LQTS, his family did not. His younger sister died suddenly at the age of 32 when awakened by a telephone and his father died suddenly at the age of 40. The sister was documented to have abnormal QT intervals of up to 582 ms. The symptoms in this family, including palpitations, syncope, and sudden death due to abrupt auditory stimuli during sleep, were typical of LQT2 (Schwartz, 2001; Roden, 2008). In our study, the repolarization time was significantly prolonged in cultured LQT2-specific cardiac cells, compared with control cells, at low beating rates, and this is consistent with the clinical observation that, at slow beating rate, the QT interval is prolonged more in LQT2 patients compared with healthy individuals (Swan et al., 1999).

Although the underlying mechanism of R176W is presently unknown, when heterologously expressed, R176W reduces hERG tail current density by ~75%, although upon coexpression with wild type the difference in current densities was nullified (Fodstad et al., 2006). The decrease of ~43% in I_{Kr} density observed here in iPS cardiomyocytes from a heterozygous R176W individual might reflect the difference in cellular environment, e.g. the composition of the endogenous I_{Kr} channel, which includes both the ubiquitously in vitro expressed hERG1a subunit and hERG1b subunit with its alternatively spliced N-terminus, presence of accessory subunits and/or native interactions. However, it is also possible that this observed discrepancy results from a differential expression of the wild-type and mutant alleles in vitro versus in vivo. In both model systems, R176W does not display a dominant-negative effect, unlike the A614V hERG mutation (Nakajima et al., 1998). iPS cell lines with that particular mutation derived from a severely symptomatic LQT2 patient with recorded TdP have been generated (Itzhaki et al., 2011). This mutation resulted in a decrease in the activating I_{Kr} density of 72% with a depolarization step to 0 mV and of 64% in the tail current density following depolarization to +20 mV. Smaller reductions in these values (43% and 40%, respectively) were obtained for the R176W hERG mutation here. This difference in I_{Kr} reduction translates to the APD: at 1 Hz the ventricular-like LQT2 iPSC cardiomyocyte APD_{90} was 166% and ~200% of control for R176W and A614V, respectively, and in arrhythmogenicity, with EADs rarely observed here (~5%) but frequently (66%) in the report by Itzhaki and coworkers. Thus, the in vitro results obtained with iPSC cardiomyocytes seems to correspond to differences in expression of the disease, i.e. latent versus overt LQTS. Similarly, Matsa et al. demonstrated that the APD of both atrial-like and ventricular-like iPSC cardiomyocytes was significantly prolonged when derived from an LQT2 patient with episodes of syncope, seizures and TdP (Matsa et al., 2011). Although, in the study by Matsa et al., no spontaneous arrhythmicity was observed, such an effect could be induced pharmaceutically by isoprenalin.

One explanation for the genotype-phenotype discordance in LQTS is the repolarization reserve. This concept proposes that redundant mechanisms are available to bring about normal repolarization; therefore, to elicit the full-blown LQTS phenotype multiple hits might be required to sufficiently reduce the reserve (Roden, 2006). Such 'hits' might be the presence of compound mutations, polymorphisms, drug exposure, female gender, hypokalemia or other risk factors (Roden, 2006; Lehtonen et al., 2007). Evidence for the repolarization reserve and its genetic modulation comes from studies of individuals or first-degree relatives of individuals with drug-induced LQTS showing a prolongation of repolarization indices with pharmacological challenge (Kannankeril et al., 2005; Couderc et al., 2009). The unmasking of latent LQTS can occur accidentally (e.g. associated drug-induced TdP) (Lehtonen et al., 2007). In line with the repolarization reserve hypothesis and the clinical data, R176W LQT2 cardiac cells were more sensitive to drug effects that controls. The hERG-channel-specific blocker E-4031 induced arrhythmogenicity in both control and LQT2 cardiac cells, but sotalol induced arrhythmogenic behavior only in LQT2 cardiac cells. Sotalol has been used as a pharmacological challenge and is documented as inducing TdP in a patient carrying a hERG channel mutation (Lehtonen et al., 2007; Couderc et al., 2009). The concentrations of sotalol used in this study are similar to the effective free therapeutic plasma concentration range (1.8-14.7 μmol/l) (Redfern et al., 2003). Sotalol probably exacerbates the underlying defect, because the potency of sotalol towards hERG is similar between wild type and variant in transfected cells (Männikkö et al., 2010).

Comparison of single-cell recordings and MEA analysis and ECG findings of the patients revealed an interesting observation. Although single-cell recordings indicated major differences in repolarization time between control- and LQT2-derived cardiac cells (66% increase in AP_{90} in LQT2 cardiomyocytes), the corresponding differences measured using cell aggregates with the MEA technique were much more moderate (10-20%) and resembled differences in ECG in healthy individuals and LQTS patients (Fodstad et al., 2006). Similar observations can be found in the previously reported iPSC studies on LQTS. AP_{90} duration was reported to be increased by 50% in LQT1 cardiac cells compared with control cells, whereas the difference in ECG was only in the range of 10-15% (Moretti et al., 2010). In the studies with LQT2 cells, the repolarization times were greatly prolonged already at ECG level (50% or more) and similar differences were observed in their MEA recordings (50% difference between control and LQT2 cardiac cells) (Itzhaki et al., 2011; Matsa et al., 2011). However, in both of these studies, the AP_{90} duration was increased by 2- to 2.5-fold compared with control repolarization time. It is possible that cell-to-cell contacts in the syncytium result in compensatory mechanisms with a tendency to protect the repolarization system from major deviation from the normal conditions.

Our results on the abnormal electrophysiological properties and increased drug sensitivity of cardiac cells derived from an asymptomatic *KCNH2* R176W mutation carrier raise an important

issue about LQT2 and also a new challenge, as well as a possibility, for the pharmaceutical industry. LQT2 cell models for severely symptomatic patients (Itzhaki et al., 2011; Matsa et al., 2011) are most useful for studying the pathology of LQT2 and demonstrate in a convincing way that the phenotype of this syndrome can be reproduced in a cell culture model. Our results complement the previous research on LQT2-specific iPSC-derived cardiomyocytes by introducing a cell model for an asymptomatic mutation carrier. According to our findings, even these clinically asymptomatic individuals can possess the inherent electrophysiological abnormality in their cardiac cells. Taking advantage of this large resource of Finnish individuals with the same mutation, it might be possible to evaluate the electrophysiological properties and drug responses of cardiomyocytes from mutation carriers with and without symptoms, and thereby try to identify putative genetic or non-genetic modifiers of LQTS. These types of studies might also assist in the tailoring of individualized drug treatment of these patients. In the future, iPSC technology is likely to be increasingly exploited for drug development and safety studies.

In conclusion, iPSC-derived cardiomyocytes from an individual with LQT2 displayed the disease cardiac phenotype in cell culture conditions even though the individual was relatively asymptomatic. This model provides an additional platform to study the basic pathology of LQTS and to individualize drug treatment in a patient-specific manner. It also provides the means to explore the differences between clinical patients and mutation carriers and to scan the cardiac effects of different drugs on both.

METHODS

The study was approved by the ethical committee of Pirkanmaa Hospital District (R07080).

Cell culture

The LQT2 cells were derived from a 61-year-old man with an R176W mutation of *KCNH2* (hERG-FinB) (Fodstad et al., 2004). Primary fibroblasts from a skin biopsy were cultured under fibroblast culturing conditions: Dulbecco's Modified Eagle's Medium (DMEM) (Lonza, Basel, Switzerland) containing 10% fetal bovine serum (FBS) (Lonza), 2 mmol/l L-glutamine, 50 U/ml penicillin/streptomycin. 293FT cells (Invitrogen, Carlsbad, CA) were maintained similarly with 1% non-essential amino acids (NEAA) (Cambrex, East Rutherford, NJ). Plat-E (Cell Biolabs, San Diego, CA), irradiated SNL-76/7 (HPA Culture Collections, Salisbury, UK) and mouse embryonic fibroblast (MEF; Millipore, Billerica, MA) cells were cultured without antibiotics. iPSCs and hESCs were maintained in KSR medium: knockout (KO)-DMEM (Invitrogen) containing 20% KO serum replacement (KO-SR, Invitrogen), NEAA, L-glutamine, penicillin/streptomycin, 0.1 mmol/l 2-mercaptoethanol and 4 ng/ml basic fibroblast growth factor (bFGF; R&D Systems, Minneapolis, MN). H7 hESCs (WiCell Research Institute, Madison, WI) and iPSC lines FiPS 6-14 and UTA.00112.hFF (derived from foreskin fibroblasts), UTA.01006.WT and UTA.04602.WT (from adult skin fibroblasts) were used as controls.

Generation of iPSC lines

Patient-specific iPSC lines were established using lentivirus infection followed by retrovirus infection into the primary fibroblasts. The following cells, plasmids and reagents were used: 293FT cells, Plat-E cells, pLenti6/UbC/mSlc7a1 vector (Addgene, Cambridge, MA), ViraPower Packaging Mix (Invitrogen), Lipofectamine 2000 (Invitrogen), pMX retroviral vector (hOCT3/4, hSOX2, hKLF4 or hc-MYC; Addgene) and Fugene 6 (Roche Diagnostics, Mannheim, Germany). The protocol used has been described previously (Takahashi et al., 2007). Two LQT2-specific lines were established (UTA.00514.LQT2 and UTA.00525.LQT2) carrying the R176W mutation, which was confirmed by PCR as described previously (Fodstad et al., 2006). The FiPS 6-14 line was derived at the University of Helsinki (provided by Timo Otonkoski) (Rajala et al., 2010). Control iPSC lines from healthy individuals (UTA.01006.WT from a 36-year-old male and UTA.04602.WT from a 55-year-old female) and the UTA.00112.hFF line from human foreskin fibroblasts were established in the same way as the LQT2 lines.

RT-PCR

Total RNA was collected from the iPSC lines at passages 3, 6 and 11 and after cardiac differentiation. For positive pluripotency control, the H7 line was used. RNA from EBs was used as a negative control of pluripotency. RNA was purified with NucleoSpin RNA II kit (Macherey-Nagel, Düren, Germany) and cDNA conversion was performed with a high-capacity cDNA RT kit (Applied Biosystems, Carlsbad, CA). PCR was done with Dynazyme II (Finnzymes Oy, Espoo, Finland) using 1 µl of cDNA as a template and 2 µM primers. As positive controls for exogenous primers, PCR was also done using the transfected plasmids (hOCT3/4, hSOX2, hKLF4 and hc-MYC) as templates. PCR primers for iPSC characterization and detailed reaction conditions have been described previously (Takahashi et al., 2007). Primers for different germ layers and cardiac markers are presented in Table 2. β-actin and *GAPDH* were used as housekeeping controls.

Immunocytochemistry for pluripotency

iPSCs at passage 8 were fixed with 4% paraformaldehyde (Sigma-Aldrich) and stained with anti-OCT3/4 (1:400; R&D Systems), anti-tumor-related antigen (TRA)1-60 (1:200; Millipore), anti-SOX2, anti-NANOG, anti-stage-specific embryonic antigen (SSEA)4 and anti-TRA1-81 (all 1:200; from Santa Cruz Biotechnology, Santa Cruz, CA). The secondary antibodies (Invitrogen) were Alexa-Fluor-568-donkey-anti-goat-IgG, Alexa-Fluor-568-goat-anti-mouse-IgM or Alexa-Fluor-568-donkey-anti-mouse-IgG.

EB formation

EBs were cultured without feeder cells in EB medium (KO-DMEM with 20% FBS, NEAA, L-glutamine and penicillin/streptomycin) without bFGF for 5 weeks. RNA isolation and reverse transcription from EBs was performed as described above. The expression of markers characteristic of ectoderm, endoderm and mesoderm development in EBs was determined using RT-PCR (primers described in Table 2).

Mutation analysis

The hERG-FinB mutation was assayed with restriction enzyme analysis (Fodstad et al., 2006) by amplifying the genomic DNA with primers for *hERG* (forward: 5′-ACCACGTGCCTCTCCTCTC-3′, reverse: 5′-GTCGGGGTTGAGGCTGTG-3′) (reagents from Applied Biosystems) and digesting the amplified PCR product with

Table 2. Primers for RT-PCR of different germ layer markers and cardiac markers.

Gene	Primer F (5′-3′)	Primer R (5′-3′)	Size (bp)
Endodermal markers			
AFP	AGAACCTGTCACAAGCTGTG	GACAGCAAGCTGAGGATGTC	672
SOX17	CGCACGGAATTTGAACAGTA	CACACGTCAGGATAGTTGCAG	166
Mesodermal markers			
α-cardiactin	GGAGTTATGGTGGGTATGGGTC	AGTGGTGACAAAGGAGTAGCCA	486
KDR	GTGACCAACATGGAGTCGTG	TGCTTCACAGAAGACCATGC	218
Ectodermal markers			
SOX1	AAAGTCAAAACGAGGCGAGA	AAGTGCTTGGACCTGCCTTA	158
PAX6	AACAGACACAGCCCTCACAAACA	CGGGAACTTGAACTGGAACTGAC	274
Nestin	CAGCTGGCGCACCTCAAGATG	AGGGAAGTTGGGCTCAGGACTGG	208
Musashi 1	AGCTTCCCTCTCCCTCATTC	GAGACACCGGAGGATGGTAA	161
Cardiac markers			
TNTT2	ATCCCCGATGGAGAGAGAGT	TCTTCTTCTTTTCCCGCTCA	385
MLC2V	GGTGCTGAAGGCTGATTACGTT	TATTGGAACATGGCCTCTGGAT	382
MLC2A	GTCTTCCTCACGCTCTTTGG	GCCCCTCATTCCTCTTTCTC	269
Cx-43	TACCATGCGACCAGTGGTGCGCT	GAATTCTGGTTATCATCGGGGAA	293
MYH7	AGCTGGCCCAGCGGCTGCAGG	CTCCATCTTCTCGGCCTCCAGCT	443
GATA4	GACGGGTCACTATCTGTGCAAC	AGACATCGCACTGACTGAGAAC	474
HERG	GAACGCGGTGCTGAAGGGCT	AACTTGCGCTTGCGTTGCCG	527
Housekeeping control genes			
β-actin	GTCTTCCCCTCCATCGTG	GGGGTGTTGAAGGTCTCAAA	302
GAPDH	AGCCACATCGCTCAGACACC	GTACTCAGCGGCCAGCATCG	302

*Sma*I digestion enzyme (Fermentas GmbH, St Leon-Rot, Germany). The hERG-FinB mutation resulted in deletion of a *Sma*I-cleavage site. *Sma*I-cleaved PCR products were detected with gel electrophoresis: products for wild type were 182, 79, 46 and 23 bp and for R176W heterozygote 182, 125, 79, 46 and 23 bp long.

Karyotype analysis

Karyotypes of the cell lines were defined using standard G-banding chromosome analysis by a commercial company (Medix Laboratories, Espoo, Finland) according to standard procedure.

Teratoma formation

iPSCs were injected into nude mice under the testis capsule. Tumor samples were collected 8 weeks after injection and fixed with 4% paraformaldehyde. The sections were stained with hematoxylin and eosin.

Cardiac differentiation and characterization

Cardiomyocyte differentiation was carried out by co-culturing iPSCs and H7 hESCs with END-2 cells (a kind gift from Christine Mummery, Hubrecht Institute, Utrecht, The Netherlands). END-2 cells were cultured as described earlier (Mummery et al., 2003). The beating areas of the cell colonies were mechanically excised and treated with collagenase A (Roche Diagnostics) as described previously (Mummery et al., 2003). Seven days after dissociation, cells were fixed with 4% paraformaldehyde for immunostaining with anti-cardiac-troponin-T (1:2000; Abcam, Cambridge, MA), anti-α-actinin (1:1500; Sigma-Aldrich, St Louis, MO) and anti-connexin-43 (1:1000; Sigma-Aldrich).

Patch-clamp technique

APs were recorded from spontaneously beating dissociated cells using the perforated patch (by amphotericin) configuration of the patch-clamp technique with an Axopatch 200B amplifier (Molecular Devices, Sunnyvale, CA). A coverslip with the adhered cells was placed in the recording chamber and perfused with extracellular solution consisting of (in mmol/l) 143 NaCl, 4 KCl, 1.8 $CaCl_2$, 1.2 $MgCl_2$, 5 glucose, 10 HEPES (pH 7.4 with NaOH; osmolarity adjusted to 301±3 mOsm). Patch pipettes were pulled from borosilicate glass capillaries (Harvard Apparatus, Kent, UK) and had resistances of 1.5-3.5 MΩ when filled with a solution consisting of (in mmol/l): 122 K-gluconate, 30 KCl, 1 $MgCl_2$, 5 HEPES (pH 7.2 with KOH; osmolarity adjusted to 290±3 mOsm). The final concentration of amphotericin B (solubilized in dimethylsulfoxide) in the pipette was 0.24 mg/ml.

The data was filtered at 2 kHz, and digitized (Digidata 1322A; Molecular Devices) at 10 kHz; data acquisition and analysis was performed with pClamp 9.2 software (Molecular Devices). For some cardiomyocytes, voltage-clamp experiments were also performed to record I_{Kr}. Experiments were conducted at 36±1°C.

Field potential recordings

Field potentials of spontaneously beating cardiomyocyte aggregates were recorded with the MEA platform (Multi Channel Systems, Reutlingen, Germany) at 37°C. MEAs were hydrophilized with FBS for 30 minutes, washed with sterile water and coated with 0.1% gelatin for 1 hour. Cardiomyocyte aggregates were plated onto MEAs in EB medium. FPD and beating frequency were determined manually with AxoScope software (Molecular Devices).

TRANSLATIONAL IMPACT

Clinical issue

Long QT syndrome (LQTS) is a life-threatening cardiac disorder that predisposes individuals to ventricular arrhythmias and sudden death. The syndrome is characterized by a prolonged QT interval (detected by electrocardiography) and can be caused either by genetic defects or as a side effect of certain drugs. LQTS type 2 (LQT2) occurs owing to defective functioning of the hERG potassium channel, and is caused by mutations in the *KCNH2* gene (also known as *HERG*). The drug-induced form of LQTS also occurs owing to altered function of the hERG channel. Because prolongation of QT interval is one of the most common severe side effects of both cardiac and non-cardiac drugs, new drug candidates must be carefully tested for their effects on the hERG channel. However, physiological human cell models to test for this effect were not previously available. The clinical prevalence of LQTS is only ~1:5000, but its genetic prevalence has been estimated to be much higher (1:250 to 1:2000). Therefore, it is possible that asymptomatic carriers of LQTS-associated mutations are more susceptible to the side effect of certain medications, and are at risk of developing severe symptoms in certain settings.

Results

This study investigates whether an LQTS-related phenotype can be detected in an in vitro model based on cells from an asymptomatic carrier of an LQT2-associated *KCNH2* mutation. The authors generate patient-specific induced pluripotent stem cells (iPSCs) from an asymptomatic individual and differentiate them into functional cardiac cells. These cells recapitulate the phenotypic characteristics of LQT2 in vitro, including prolonged repolarization time and increased arrhythmogenicity. Additionally, at slow beating rates, cardiomyocyte aggregates derived from these iPSCs present prolonged field potential duration (QT) compared with control cells. These results are in line with clinical findings that individuals with LQT2 usually display symptoms when heart rate is slow. These results indicate that electrophysiological abnormalities can be detected in iPSC-derived cardiac cells, even when derived from asymptomatic carriers of *KCNH2* mutations.

Implications and future directions

This in vitro model of LQT2 offers a new system with which to evaluate electrophysiological properties and drug responses of cardiomyocytes from *KCNH2* mutation carriers with and without LQTS symptoms. In addition, the model provides a platform from which to study the basic pathology of LQTS and to identify genetic and non-genetic modifiers that can be considered in designing and developing medications to treat distinct patient groups. In addition, the model provides the means to analyze the cardiac side effects of different drugs in carriers of LQTS-associated mutations.

Isoprenaline (Isuprel; Hospira, Lake Forest, IL), D,L-sotalol (Sigma), erythromycin (Abbott, IL), cisapride (Sigma) and E-4031 (Alomone Labs, Jerusalem, Israel) were diluted in 5% FBS containing EB medium for drug tests. Baseline conditions as well as drug effects were recorded for 2 minutes after a 2-minute stabilization period. Baseline FPDs were measured from 43 control cardiomyocyte aggregates and 30 LQT2 cardiomyocyte aggregates.

Statistical methods

Data are given as mean ± s.e.m. or s.d. Comparison of patch-clamp data between LQT2-iPSC and control-iPSC cardiomyocytes was performed using Student's *t*-test for independent data. One-way analysis of variance followed by Tukey test was used for comparison of multiple groups. The I_{Kr} data was assessed using Student's *t*-test for independent data. The difference in FPDs between different populations of spontaneously beating cardiomyocyte aggregates was determined by nonlinear regression analysis using R software. The difference in FPDs between populations when categorized according to beating frequencies was determined by *t*-test with SPSS software (IBM).

ACKNOWLEDGEMENTS

We thank Merja Lehtinen and Henna Venäläinen for technical support, Christine Mummery for providing END-2 cells, Timo Otonkoski for sharing his knowledge, Annukka Lahtinen for help in the LQTS genotyping of the iPSC lines, Heini Huhtala for help on statistical analysis, and Kenta Nakamura, Chris Schlieve and the Gladstone Stem Cell Core for advice and reagents. We also thank Takayuki Tanaka for help in setting up our iPSC system.

COMPETING INTERESTS

The authors declare that they do not have any competing or financial interests.

AUTHOR CONTRIBUTIONS

A.L.L. was involved in iPS cell generation and analysis, cardiomyocyte differentiation and characterization, figure preparation, and writing the manuscript. V.J.K. performed MEA experiments and analysis, wrote parts of the manuscript, was involved in editing the manuscript, and was involved in figure preparation. H.C. designed and performed all patch-clamp experiments and analysis. A.-P.K. provided expertise in electrophysiology. M.P.-M. was involved in cardiac differentiation and cardiomyocyte analysis. E.K. planned and performed cardiac cell differentiation experiments. J.H. designed the MEA experiments. K.K. provided genetic expertise and provided genotyped patients. H.S. provided genetic and cardiological expertise on LQTS. B.R.C. helped design the study. S.Y. provided expertise in iPSC technology. O.S. helped design the study and analyze the results. K.A.-S. was leader of the group, and was involved in the planning and evaluation of the results, and finalizing the manuscript.

FUNDING

This work was supported by the Academy of Finland [grant number 126888]; the Finnish Foundation for Cardiovascular Research; Pirkanmaa Hospital District (EVO); the Finnish Cultural Foundation; Biocenter Finland; and the Sigrid Juselius Foundation.

SUPPLEMENTARY MATERIAL

Supplementary material for this article is available at
http://dmm.biologists.org/lookup/suppl/doi:10.1242/dmm.008409/-/DC1

REFERENCES

Ackerman, M. J., Tester, D. J., Jones, G. S., Will, M. L., Burrow, C. R. and Curran, M. E. (2003). Ethnic differences in cardiac potassium channel variants: implications for genetic susceptibility to sudden cardiac death and genetic testing for congenital long QT syndrome. *Mayo Clin. Proc.* **78**, 1479-1487.

Carvajal-Vergara, X., Sevilla, A., D'Souza, S. L., Ang, Y.-S., Schaniel, C., Lee, D.-F., Yang, L., Kaplan, A. D., Adler, E. D., Rozov, R. et al. (2010). Patient-specific induced pluripotent stem-cell-derived models of LEOPARD syndrome. *Nature* **465**, 808-812.

Caspi, O., Itzhaki, I., Arbel, G., Kehat, I., Gepstien, A., Huber, I., Satin, J. and Gepstein, L. (2008). In vitro electrophysiological drug testing using human embryonic stem cell derived cardiomyocytes. *Stem Cells Dev.* **18**, 161-172.

Chiang, C.-E. and Roden, D. M. (2000). The long QT syndromes: genetic basis and clinical implications. *J. Am. Coll. Cardiol.* **36**, 1-12.

Couderc, J.-P., Kaab, S., Hinterseer, M., McNitt, S., Xia, X., Fossa, A., Beckmann, B. M., Polonsky, S. and Zareba, W. (2009). Baseline values and sotalol-induced changes of ventricular repolarization duration, heterogeneity, and instability in patients with a history of drug-induced torsades de pointes. *J. Clin. Pharmacol.* **49**, 6-16.

Curran, M. E., Splawski, I., Timothy, K. W., Vincen, G. M., Green, E. D. and Keating, M. T. (1995). A molecular basis for cardiac arrhythmia: HERG mutations cause long QT syndrome. *Cell* **80**, 795-803.

Fodstad, H., Swan, H., Laitinen, P., Piippo, K., Paavonen, K., Viitasalo, M., Toivonen, L. and Kontula, K. (2004). Four potassium channel mutations account for 73% of the genetic spectrum underlying long-QT syndrome (LQTS) and provide evidence for a strong founder effect in Finland. *Ann. Med.* **36 Suppl. 1**, 53-63.

Fodstad, H., Bendahhou, S., Rougier, J. S., Laitinen-Forsblom, P. J., Barhanin, J., Abriel, H., Schild, L., Kontula, K. and Swan, H. (2006). Molecular characterization of two founder mutations causing long QT syndrome and identification of compound heterozygous patients. *Ann. Med.* **38**, 294-304.

Gai, H., Leung, E. L.-H., Costantino, P. D., Aguila, J. R., Nguyen, D. M., Fink, L. M., Ward, D. C. and Ma, Y. (2009). Generation and characterization of functional cardiomyocytes using induced pluripotent stem cells derived from human fibroblasts. *Cell Biol. Int.* **33**, 1184-1193.

Hancox, J. C., McPate, M. J., El Harchi, A. and Zhang, Y. H. (2008). The hERG potassium channel and hERG screening for drug-induced torsades de pointes. *Pharmacol. Ther.* **119**, 118-132.

Hedley, P. L., Jørgensen, P., Schlamowitz, S., Wangari, R., Moolman-Smook, J., Brink, P. A., Kanters, J. K., Corfield, V. A. and Christiansen, M. (2009). The genetic basis of long QT and short QT syndromes: a mutation update. *Hum. Mutat.* **30**, 1486-1511.

Itzhaki, I., Maizels, L., Huber, I., Zwi-Dantsis, L., Caspi, O., Winterstern, A., Feldman, O., Gepstein, A., Arbel, G., Hammerman, H. et al. (2011). Modelling the long QT syndrome with induced pluripotent stem cells. *Nature* **471**, 225-229.

Kannankeril, P. J., Roden, D. M., Norris, K. J., Whalen, S. P., George, J. A. L. and Murray, K. T. (2005). Genetic susceptibility to acquired long QT syndrome: Pharmacologic challenge in first-degree relatives. *Heart Rhythm* **2**, 134-140.

Lee, G. and Studer, L. (2010). Induced pluripotent stem cell technology for the study of human disease. *Nat. Meth.* **7**, 25-27.

Lehtonen, A., Fodstad, H., Laitinen-Forsblom, P., Toivonen, L., Kontula, K. and Swan, H. (2007). Further evidence of inherited long QT syndrome gene mutations in antiarrhythmic drug-associated torsades de pointes. *Heart Rhythm* **4**, 603-607.

Männikkö, R., Overend, G., Perrey, C., Gavaghan, C. L., Valentin, J. P., Morten, J., Armstrong, M. and Pollard, C. E. (2010). Pharmacological and electrophysiological characterization of nine, single nucleotide polymorphisms of the hERG-encoded potassium channel. *Br. J. Pharmacol.* **159**, 102-114.

Marjamaa, A., Salomaa, V., Newton-Cheh, C., Porthan, K., Reunanen, A., Karanko, H., Jula, A., Lahermo, P. i., Väänänen, H., Toivonen, L. et al. (2009). High prevalence of four long QT syndrome founder mutations in the Finnish population. *Ann. Med.* **41**, 234-240.

Matsa, E., Rajamohan, D., Dick, E., Young, L., Mellor, I., Staniforth, A. and Denning, C. (2011). Drug evaluation in cardiomyocytes derived from human induced pluripotent stem cells carrying a long QT syndrome type 2 mutation. *Eur. Heart J.* **32**, 952-962.

Moretti, A., Bellin, M., Welling, A., Jung, C. B., Lam, J. T., Bott-Flügel, L., Dorn, T., Goedel, A., Höhnke, C., Hofmann, F. et al. (2010). Patient-specific induced pluripotent stem-cell models for long-QT syndrome. *N. Engl. J. Med.* **363**, 1397-1409.

Mummery, C., Ward-van Oostwaard, D., Doevendans, P., Spijker, R., van den Brink, S., Hassink, R., van der Heyden, M., Opthof, T., Pera, M., de la Riviere, A. B. et al. (2003). Differentiation of human embryonic stem cells to cardiomyocytes: role of coculture with visceral endoderm-like cells. *Circulation* **107**, 2733-2740.

Nakajima, T., Furukawa, T., Tanaka, T., Katayama, Y., Nagai, R., Nakamura, Y. and Hiraoka, M. (1998). Novel mechanism of HERG current suppression in LQT2: shift in voltage dependence of HERG inactivation. *Circ. Res.* **83**, 415-422.

Pollard, C. E., Valentin, J. P. and Hammond, T. G. (2008). Strategies to reduce the risk of drug-induced QT interval prolongation: a pharmaceutical company perspective. *Br. J. Pharmacol.* **154**, 1538-1543.

Priori, S., Napolitano, C. and Schwartz, P. (1999). Low penetrance in the long-QT syndrome. *Circulation* **99**, 529-533.

Rajala, K., Lindroos, B., Hussein, S. M., Lappalainen, R. S., Pekkanen-Mattila, M., Inzunza, J., Rozell, B., Miettinen, S., Narkilahti, S., Kerkelä, E. et al. (2010). A defined and xeno-free culture method enabling the establishment of clinical-grade human embryonic, induced pluripotent and adipose stem cells. *PLoS ONE* **5**, e10246.

Redfern, W. S., Carlsson, L., Davis, A. S., Lynch, W. G., MacKenzie, I., Palethorpe, S., Siegl, P. K. S., Strang, I., Sullivan, A. T., Wallis, R. et al. (2003). Relationships between preclinical cardiac electrophysiology, clinical QT interval prolongation and torsade de pointes for a broad range of drugs: evidence for a provisional safety margin in drug development. *Cardiovasc. Res.* **58**, 32-45.

Roden, D. M. (2004). Drug-Induced Prolongation of the QT Interval. *N. Engl. J. Med.* **350**, 1013-1022.

Roden, D. M. (2006). Long QT syndrome: reduced repolarization reserve and the genetic link. *J. Int. Med.* **259**, 59-69.

Roden, D. M. (2008). Long-QT Syndrome. *N. Engl. J. Med.* **358**, 169-176.

Schwartz, P. J. (2001). Genotype-phenotype correlation in the long-QT syndrome: gene-specific triggers for life-threatening arrhythmias. *Circulation* **103**, 89-95.

Swan, H., Viitasalo, M., Piippo, K., Laitinen, P., Kontula, K. and Toivonen, L. (1999). Sinus node function and ventricular repolarization during exercise stress test in long QT syndrome patients with KvLQT1 and HERG potassium channel defects. *J. Am. Coll. Cardiol.* **34**, 823-829.

Takahashi, K., Tanabe, K., Ohnuki, M., Narita, M., Ichisaka, T., Tomoda, K. and Yamanaka, S. (2007). Induction of pluripotent stem cells from adult human fibroblasts by defined factors. *Cell* **131**, 861-872.

Tester, D. J. and Ackerman, M. J. (2007). Postmortem long QT syndrome genetic testing for sudden unexplained death in the young. *J. Am. Coll. Cardiol.* **49**, 240-246.

Tu, E., Bagnall, R. D., Duflou, J. and Semsarian, C. (2011). Post-mortem review and genetic analysis of sudden unexpected death in epilepsy (SUDEP) cases. *Brain Pathol.* **21**, 201-208.

Yazawa, M., Hsueh, B., Jia, X., Pasca, A. M., Bernstein, J. A., Hallmayer, J. and Dolmetsch, R. E. (2011). Using induced pluripotent stem cells to investigate cardiac phenotypes in Timothy syndrome. *Nature* **471**, 230-234.

Yokoo, N., Baba, S., Kaichi, S., Niwa, A., Mima, T., Doi, H., Yamanaka, S., Nakahata, T. and Heike, T. (2009). The effects of cardioactive drugs on cardiomyocytes derived from human induced pluripotent stem cells. *Biochem. Biophys. Res. Commun.* **387**, 482-488.

Yu, J., Vodyanik, M. A., Smuga-Otto, K., Antosiewicz-Bourget, J., Frane, J. L., Tian, S., Nie, J., Jonsdottir, G. A., Ruotti, V., Stewart, R. et al. (2007). Induced pluripotent stem cell lines derived from human somatic cells. *Science* **318**, 1917-1920.

Zhang, S. (2006). Isolation and characterization of IKr in cardiac myocytes by Cs+ permeation. *Am. J. Physiol. Heart Circ. Physiol.* **290**, H1038-H1049.

Zwi, L., Caspi, O., Arbel, G., Huber, I., Gepstein, A., Park, I.-H. and Gepstein, L. (2009). Cardiomyocyte differentiation of human induced pluripotent stem cells. *Circulation* **120**, 1513-1523.

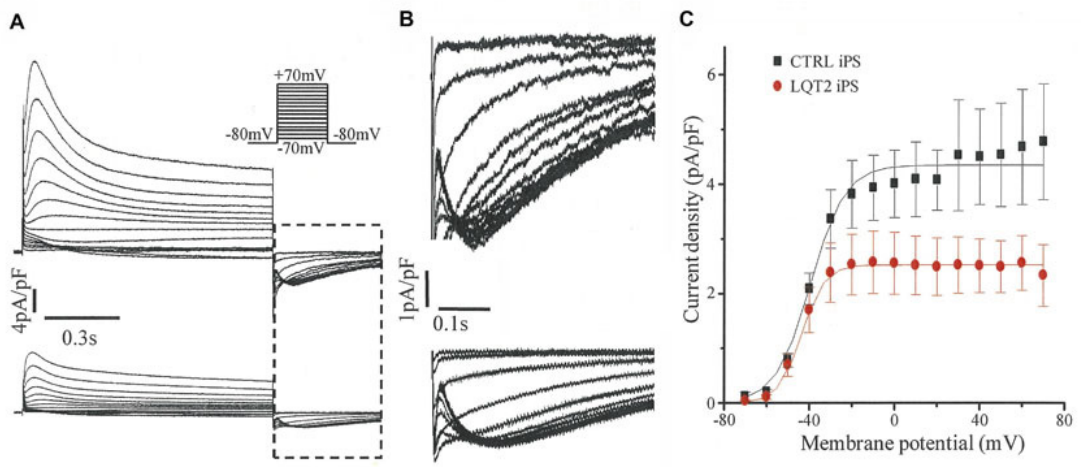

Supplementary figure 1. IKr recorded from iPSC-cardiomyocytes using cesium method. Membrane currents of cardiomyocytes derived from the control and LQT2 cell lines were measured in the conventional whole-cell configuration at room temperature using an Axopatch 200B amplifier and pClamp 9.2 software (Molecular Devices, Sunnyvale, CA, USA). The extracellular solution used in these recordings contained (in mmol/L) 135 CsCl, 1 MgCl2, 10 glucose, 10 HEPES and 10 µmol/L nifedipine (pH 7.4 with CsOH; osmolarity adjusted to 301±3 mOsm). The recording pipettes were filled with a solution containing (in mmol/L): 135 CsCl, 1 MgCl2, 10 EGTA, 10 HEPES (pH 7.2 with CsOH; osmolarity adjusted to 290±3 mOsm). A & B: Whole-cell currents evoked from control (above) and LQT2 (below) human iPS derived cardiomyocytes by 1s depolarizing steps (from −70 to +70 mV). The boxed section of A, the repolarization to the holding potential of −80 mV, is expanded in B to show the inward tail currents. C: The voltage-dependence of activation of the Cs+ current. Tail current amplitudes were divided by the capacitance value (Cs) to give the tail current density which was plotted against the depolarizing voltage. Fitting of a Boltzmann function to the activation curves gave half-maximum activation voltages and slope factors of −39.5±1.5 and 8.1±1.3 mV for control (n=3) and −43.5±1.0 and 5.8±0.3 mV for LQT2 iPS cardiomyocytes (n=4; P>0.05). These values are similar to those obtained with hERG expressing HEK cells and rabbit ventricular myocytes, however the current densities are smaller (Zhang, 2006). The tail current density of control and LQT2 iPS cardiomyocytes after a depolarizing step to +20 mV was respectively 4.1±0.6 pA/pF (n=3) and 2.5±0.5 pA/pF (n=4; P>0.05).